University of Zurich[UZH]

Assessing Potential Ink Disease Distribution in Sweet Chestnut Forests in Switzerland. A Remote Sensing Approach

GEO 511 Master's Thesis

Author
Lisa Zumbrunn
19-922-772

Supervised by
Prof. Dr. Alexander Damm
Dr. Lars Waser (lars.waser@wsl.ch)
Dr. Simone Prospero (simone.prospero@wsl.ch)

Faculty representative
Prof. Dr. Alexander Damm

20.01.2025
Department of Geography, University of Zurich

Acknowledgments

Over the past few months, I have had the valuable opportunity to gain insight into the field of research, facilitated by the context of my chosen Master's specialisation in Remote Sensing. I would like to give my thanks the two institutions that made this possible for me, the University of Zürich and the Swiss Federal Institute for Forest, Snow and Landscape Research.

My sincere thanks is directed to my supervisors, Dr. Lars Waser, Dr. Simone Prospero and Prof. Dr. Alexander Damm-Reiser. Your support and expertise in any regards to my questions was fundamental for this work and I am fortunate to have benefited from your in-depth knowledge and insightful feedback.

I would like to express my special thanks to Tiziana Koch, who provided me with a high-quality dataset of pre-processed Sentinel-2 data, as well as additional resources such as an R Script and the *Tree Species Map of Switzerland*, all of which were fundamental to the completion of this thesis. Furthermore, the support in any kind of questions and feedback to my methodology was of large value for my work.

Abstract

This Master's thesis evaluates the use of Sentinel-2 and sampled tree data, combined with machine learning techniques, for monitoring sweet chestnut trees *(Castanea sativa)* showing visual symptoms of ink disease in the Canton of Ticino, Switzerland. The study addresses two main research questions: How to assess the spatial distribution of diseased trees using Sentinel-2 data and sampled tree data (Research Question 1), and which features are indicative of the disease and how they can be extracted (Research Question 2). Especially the study area's diverse topography, characterised by steep slopes and mixed forest types, presents challenges not yet addressed in the existing literature. The thesis provides detailed insight into the approach of training a Random Forest classifier by using preprocessed Sentinel-2 data from 2017 to 2023, exceeding the standard quality of freely available Level-2A products. The study develops a feature selection method that combines Recursive Feature Elimination with Leave-Location-Out Cross-Validation and includes a pre-assessment of the values of the original Sentinel-2 bands and eight selected vegetation indices using visual and statistical methods. The resulting classification model achieved an overall accuracy of 86.7%, but nonetheless has some weaknesses to discuss. While with remote sensing data alone, one cannot directly detect ink disease, it offers valuable insights for identifying areas with potential phytosanitary issues, supporting subsequent field validation. With this, the thesis highlights the importance of collaborative work within the field of research and encourages the use of combined methods to better understand the distribution and progression of ink disease in Switzerland.

Contents

List of Figures

List of Tables

Acronyms

C

CCI Chlorophyll Carotenoid Index
CIre Chlorophyll Index Red-Edge
CRS Coordinate Reference System
CSV Comma-separated Values
CV Cross-Validation

D

DN Digital Number
DSM Digital Surface Model

E

EPSG European Petroleum Survey Group Geodesy
ESA European Space Agency
ESRI Environmental Systems Research Institute
ETRS European Terrestrial Reference System
EU European Union
EVI Enhanced Vegetation Index

F

FN False Negatives
FORCE Framework for Operational Radiometric Correction for Environmental monitoring
FP False Positives

G

GMES Global Monitoring for Environment and Security
GNDVI Green Normalised Vegetation Index

I

ID Identifier

L

LAEA Lambert Azimuthal Equal Area
LiDAR Light Detection and Ranging
LLO CV Leave-Location-Out Cross-Validation

M

ML Machine Learning

N

NDVI Normalised Difference Vegetation Index
NDVIre Normalised Difference Vegetation Red-Edge Index
NDWI Normalised Difference Wetness Index
NFI Swiss National Forest Inventory
NIR Near-Infrared

O

OA Overall Accuracy

R

RE Red Edge
RF Random Forest
RFE Recursive Feature Elimination
RQ Research Question
RS Remote Sensing

S

SAR Synthetic Aperture Radar
SAVI Soil-Adjusted Vegetation Index
SWIR Short-Wave Infrared

T

TP True Positives

U

UAV Unmanned Aerial Vehicle

V

VHM Vegetation Height Model
VI Vegetation Index

W

WSL Swiss Federal Institute for Forest, Snow and Landscape Research

Chapter 1

Introduction

The sweet chestnut (*Castanea sativa* Mill.) forests of Ticino are characteristic for the region on the southern side of the Swiss Alps. The cultivation of the species has a long-standing tradition in this area and is marked with serving multiple purposes for humans, including food production, timber, and landscape management (Krebs et al., 2012). However, since the 1990s, a noticeable increase in tree mortality has been observed, which has been partly attributed to a re-emergence of ink disease caused by the invasive species *P. cinnamomi* Rand and *P. x cambivora* (Petri) Buism. (Prospero et al., 2023). These pathogens attack the root systems of sweet chestnut trees, leading to a decline in tree vitality and, finally to the death of the tree (Jung et al., 2018). Visual symptoms as reduced foliage and nut production, smaller, yellowish coloured leaves and dark, flame shaped lesions on the root collar with a typical root rot are indicative of the disease (Prospero et al., 2023).

To assess the impact and current distribution of ink disease in southern Switzerland's sweet chestnut forests, the Swiss Federal Institute for Forest, Snow and Landscape Research (WSL) has been conducting research since 2013 (Prospero et al., 2023). The investigations include surveys based on forest service data, field sampling and laboratory analyses. Despite these efforts, a comprehensive overview of the disease's distribution in southern Switzerland remains unavailable (Prospero et al., 2023). This leads to Remote Sensing (RS), which has evolved into an important tool for various Earth observation tasks, including detecting land use change, disaster management, ocean and urban observation, as well as forest monitoring (Fu et al., 2024). Different types of platforms provide data targeted to specific needs, for example Unmanned Aerial Vehicle (UAV)s enable precise data collection for specific locations and times, while satellite-derived images allow continuous, long-term monitoring over large areas (Matyukira & Mhangara, 2024). For example, European Space Agency (ESA)'s Sentinel-2 mission provides a consistent source of global data with high spatial resolution (ranging from 10x10 m to 60x60 m pixels) and a revisit time of two to five days, depending on the location on Earth. Since its launch in 2015, Sentinel-2 data has been freely available (Molnár & Király, 2024). The development of specialised Vegetation Index (VI)s has further enhanced the ability to quantitatively assess the health and productivity of vegetation, enabling accurate monitoring of forest conditions (Matyukira & Mhangara, 2024). Combined with the fast development of Machine Learning (ML) techniques within the last years, the use of such high-dimensional (regarding spatial, temporal and spectral dimensions) and therefore processing-intensive RS data has opened up new possibilities to assess forest areas on large scale within short time (Torres et al., 2021). Latest research,

conducted in southern European countries showed the suitability of RS combined with ML methods to monitor the health of sweet chestnut trees on a landscape scale (see Marques et al., 2019; Pádua et al., 2020; Sebastiani et al., 2024). A current lack in research is the examination of such an approach in regions with topographical and landscape characteristics similar to those of southern Switzerland. Furthermore, there is an increasing demand on long-term studies that can provide better insights into the progression of ink disease (Jung et al., 2018).

The aim of this thesis was to develop a straight-forward approach for monitoring sweet chestnut trees that show visual symptoms of ink disease in Ticino by using Sentinel-2 time series data and field-sampled tree data. Thus, by implementing a Random Forest (RF) model to classify the condition of trees as either non-symptomatic or symptomatic over multiple years, enabling to monitor the potential disease spread over time. In the literature, the use of Sentinel-2 data to train a RF model is a common and effective approach for forest monitoring, demonstrating strong potential for classification tasks. The method has provided promising results in several studies, as demonstrated by Alonso et al. (2020), Guzmán Q. et al. (2023), Molnár and Király (2024), Rösch et al. (2022), and Sebastiani et al. (2024).

The thesis was conducted in collaboration with the WSL, which provides valuable knowledge from a previous pilot project, as well as data used within this work (see Prospero et al., 2023). The thesis focuses on the region of the Canton of Ticino with three selected focus sites for detailed analysis.

To gain a deeper understanding of the data characteristics, an initial step of this work was to analyse the spectral information provided by Sentinel-2 time series data with both original bands and VIs. Furthermore, a feature selection method was applied prior to set up a RF model. The following questions will guide the investigation within this thesis:

RQ1: How can the current spatial distribution of diseased sweet chestnut (*Castanea sativa*) in Ticino be assessed by using freely available remote sensing data and sampled tree data?

RQ2: What features are indicative for such an assessment and how can they be extracted?

The following chapters will present the approach to addressing these questions, beginning with an introductory chapter that gives the context for the research. This will be followed by a comprehensive section about the methods, already highlighting some challenges and the considerations behind the chosen approaches also with reference to existing literature. The results will be presented in a consistent structure by first showing outcomes of the feature analysis, then the feature selection and finally the results of the RS classification. The results will be discussed, with particular attention given to the challenges and limitations of this work. The conclusion will summarise the key findings and suggest future direction for research, outlining the potential applications and relevance of this work in terms of monitoring forest areas by using Sentinel-2 data.

Chapter 2

Research Context

2.1 Sweet Chestnut in the Canton of Ticino, Switzerland

The tradition of cultivating sweet chestnut trees dates back to the Roman Age, when humans discovered the diverse utility of the species as a source of food (nuts) and valuable timber and provider of important ecosystem services (e.g., soil erosion control) (Prospero et al., 2023). The species, known for its exceptional longevity, brought a wide range of use and played a central role in the agricultural and forestry systems of southern Europe, including the Canton of Ticino (Krebs et al., 2012). Over time, the cultivation of sweet chestnut evolved from intensive monoculture systems to more mixed, naturally regenerated forests, starting in 1950, when the management of chestnut stands gradually stopped (Heiniger & Conedera, 1994).

With the introduction of alternating staple foods as for example maize and potatoes as well as changing climatic conditions, a first decline in sweet chestnut areas began. This decline accelerated during the 20th century with upcoming diseases and pests, including ink disease (caused by *Phytophthora* spp.), chestnut blight (*Cryphonectria parasitica*), and the Asian chestnut gall wasp (*Dryocosmus kuriphilus*) (Conedera et al., 2021).

Nowadays, higher temperatures resulting from changing climate conditions favour the tree's growth beyond its traditional range, particularly in northern regions of Europe, where the species is increasingly promoted as a climate- and drought-resistant alternative for forest management systems (Freitas et al., 2021). Nevertheless, there are also critical voices against the promotion of sweet chestnut due to its vulnerability to several invasive pathogens and pests. Changing climate conditions, in particular higher winter temperatures, lead to better conditions for thermophilic pathogens that may threaten the European stands of sweet chestnut. Conedera et al. (2021) state that the chestnut tree is not inherently future-proof, regarding increasing occurences of drought and rising temperatures. Especially such environments pose the best conditions for the thermophilic pathogens that cause ink disease. This highlights the need to assess the impact of ink disease on sweet chestnut stands in Switzerland in order to develop a sustainable long-term forest management strategy for the country (Conedera et al., 2021).

Sweet chestnut in the Canton of Ticino region typically grow at lower elevations, ranging from 300 to about 1,000 m a.s.l. (Krebs et al., 2012). The species prefers acidic to neutral soils and is less suited to soils dominated by limestone, which are prevalent in the northern

part of the canton (see section 2.3). The species occurs predominantly in the flat areas of southern Ticino and in the valleys throughout the whole canton, where it favours sunny, well-exposed locations and is sensitive to shade (see fig. 2.1) (Scapozza & Ambrosi, 2021). In terms of phenology, sweet chestnut trees bloom late compared with other species, abundantly from May to June, with fruits ripening by the end of October (Kälin et al., 2005).

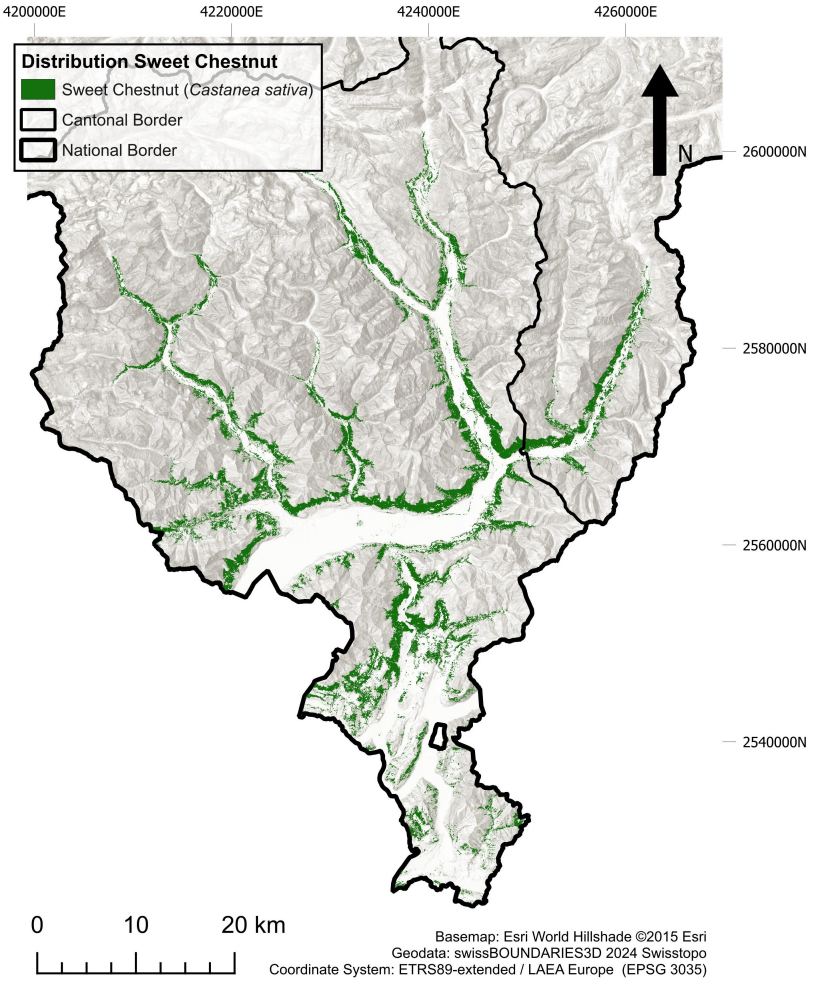

Figure 2.1: **Distribution of sweet chestnut in the Canton of Ticino and the Val Bregaglia, Switzerland.** The map is based on the *Tree Species Map of Switzerland* (Koch et al., 2024a) with additional refinement focus exclusively on areas below 900 m a.s.l. It highlights regions where the sweet chestnut is the dominant tree species.

2.2 Ink Disease

Ink disease is one of the most severe biotic threats for sweet chestnut. The first occurrence of the disease in Europe dates back to 1838 in Portugal after which it was reported also in Spain, Italy and France. With the appearance of the chestnut blight (*Cryphonectria parasitica*) in the 20th century, the threat of ink disease gained less attention after 1930 (Vannini & Vettraino, 2001). The causal agent of ink disease are two *Phytophthora* species, namely *P. x cambivora*, and todays' main agent, the more aggressive *P. cinnamomi* (Marzocchi et al., 2024). The pathogens spread by zoospores which can reach a plant's root by actively swimming through the films of water in soil pores (Prospero et al., 2023). Especially events such as heavy rain during the growing season and disrupted soil structure due to cultivation practices favour its spread (Cardillo et al., 2018).

(a) (b)

Figure 2.2: **Typical symptoms of ink disease.** Dark necrotic bark lesion at the root collar (a) is the main symptom of ink disease and can lead to further visible signs on trees, such as less foliage (b). Image sources (a) and (b): © Phytopathology WSL, unpublished, 2019.

The main symptom of ink disease is root rot, and as a consequence less foliage, reduced nut production or outgrowth of thin branches due to more light in the reduced canopy cover (see fig. 2.2b). Further symptoms at the tree base are dark coloured cortical lesions which become visible after removing the bark (see fig. 2.2a) (Prospero et al., 2023). The pathogens trigger two possible courses of the disease: Either a tree dies rapidly, frequently within a

growing season, or lasts in a general state of declining vitality over many years (Prospero et al., 2023). The conditions leading to either one or the other course of the disease rest still unknown and are currently a subject of research. Especially the observed coexistence between the pathogens and the chestnut tree over decades is a current focus to investigate. The observed survival of chestnut stands in former areas affected by ink disease suggests the possibility of creating a balanced system between the pathogen and sweet chestnut trees (Marzocchi et al., 2024). After decades of limited spread, the disease began to re-establish itself in the 1990s (Prospero et al., 2023). Presumed reasons for this re-emergence of the disease are the changing climate conditions, in particular the warmer winters which lead to better survival conditions for thermophilic species. Further, increasing drought events weaken the vitality of the trees and make them more susceptible to pathogens (Jung et al., 2018).

Despite ongoing research into ink disease and its spread, effective control of the disease remains a significant challenge (see Frascella et al., 2022; Prospero et al., 2013). Since water is one of the main vector favouring the spread of the pathogen, to mitigate the local spread of ink disease specialists recommend the implementation of a controlled water management in soil (Turchetti & Maresi, 2000). Additionally, the possibility of a biological control is currently being explored. By integrating biological isolates into plant systems, the *Phytophthora* species should be suppressed (Frascella et al., 2022).

The first official report of ink disease in Switzerland was in 1943. With considerably rising infection rates and more affected trees occurring in northern regions of Europe, research at a national level was initiated (Prospero et al., 2023). A recent study examining the distribution of ink disease in southern Switzerland by laboratory analysis confirmed the presence of *P. cinnamomi* in 20 stands, while *P. x cambivora* was detected in seven stands. Additionally, three other pathogen species were identified. However, the two mentioned *Phytophthora* species, *P. cinnamomi* and *P. x cambivora*, remain the predominant pathogens in this region of Switzerland (Prospero et al., 2023).

2.3 Study Area

The study area of this thesis comprises the Canton of Ticino, which is in southern Switzerland, ranging from Chiasso in the south (45°49'N 9°1'E) to the Piz Gaglianera in the north (46°37'N 8°57'E) (see fig. 2.3). The area is characterised by a broad range of topographic and climatic conditions. Northern regions are influenced by its proximity to the Swiss Alps, having rough climatic conditions, and a valley shaped landscape with steep, rocky slopes, ranging up to over 3,000 m a.s.l. From Bellinzona and further south, the region is influenced by a more mediterranean climate, predominantly in the area around Lago Maggiore. Also, the valleys widen towards the border with Italy and topography gets flatter. Depending on the steepness of the valleys, the number of sunny hours per year ranges from 1,400 in the northern parts with high rock faces to over 2,000 in the flatter, southern Locarno region (Scapozza & Ambrosi, 2021). About half of the total surface of the Canton of Ticino (total surface: 2,812 km^2 (Ustat, 2024)) is covered by forests, which is the highest cantonal forest cover percentage

in Switzerland (Galfetti, 2020). In the lowlands, a mean annual precipitation of 1,855 mm and a mild climate with a mean annual temperature of 12.9 °C (MeteoSwiss, 2024) favour the growth of sweet chestnut, which shapes the landscape of the valleys of the Ticino. Other broadleaf species as deciduous oak (*Quercus spp.*), small-leaved lime (*Tilia cordata*), wild cherry (*Prunus avium*), black alder (*Alnus glutinosa*), maple (*Acer spp.*), and ash (*Fraxinus spp.*) are further part of the landscape, resulting in wide areas of mixed forest (De Angelis et al., 2015).

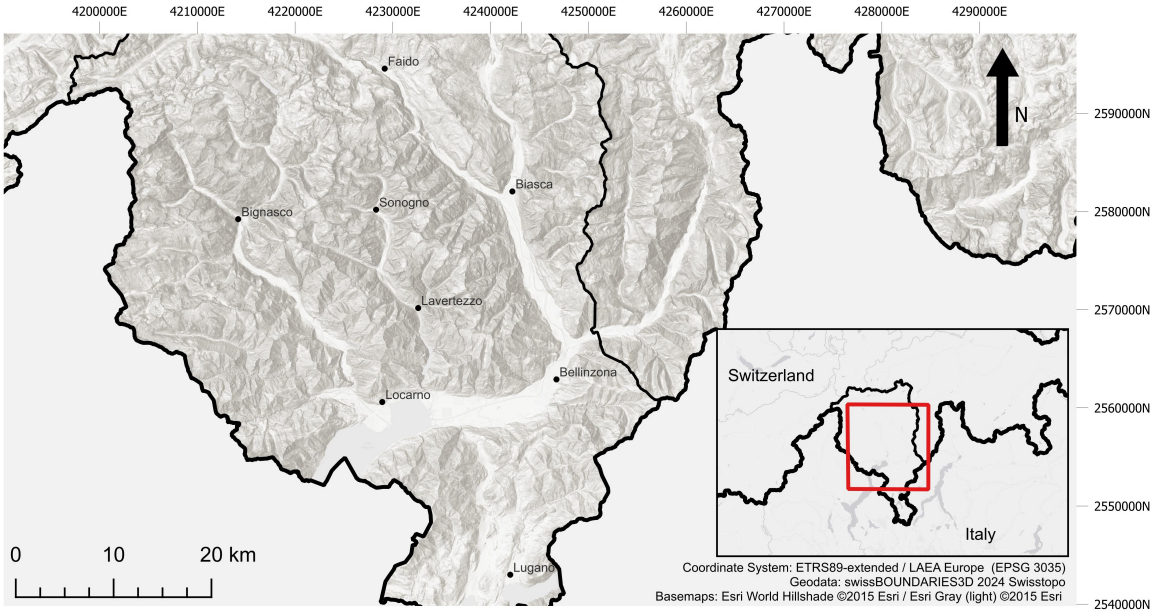

Figure 2.3: **The Canton of Ticino as the study area.** The study area is characterised by a diverse landscape, with the Alps to the north and flatter regions to the south. The mild climatic conditions in the lower zones, in particular, favour the growth of sweet chestnuts.

2.4 Focus Sites

To enable a detailed evaluation of the classification approach developed in this thesis, three focus sites were selected for further analysis (see fig. 2.4). The sites were chosen to represent a diverse range of locations with different characteristics, allowing for an assessment of the classification results under different topographic and sylvicultural conditions. At each site, the classified forest area covers approximately 48.0 ha, enabling a direct comparison of the quantified classification results. For the purposes of this classification, the criterion for considering an area as forest cover was that at least 60% of the vegetation within a selected pixel exceeded 3 m in height (see section 4.3). The following sites were selected for further classification:

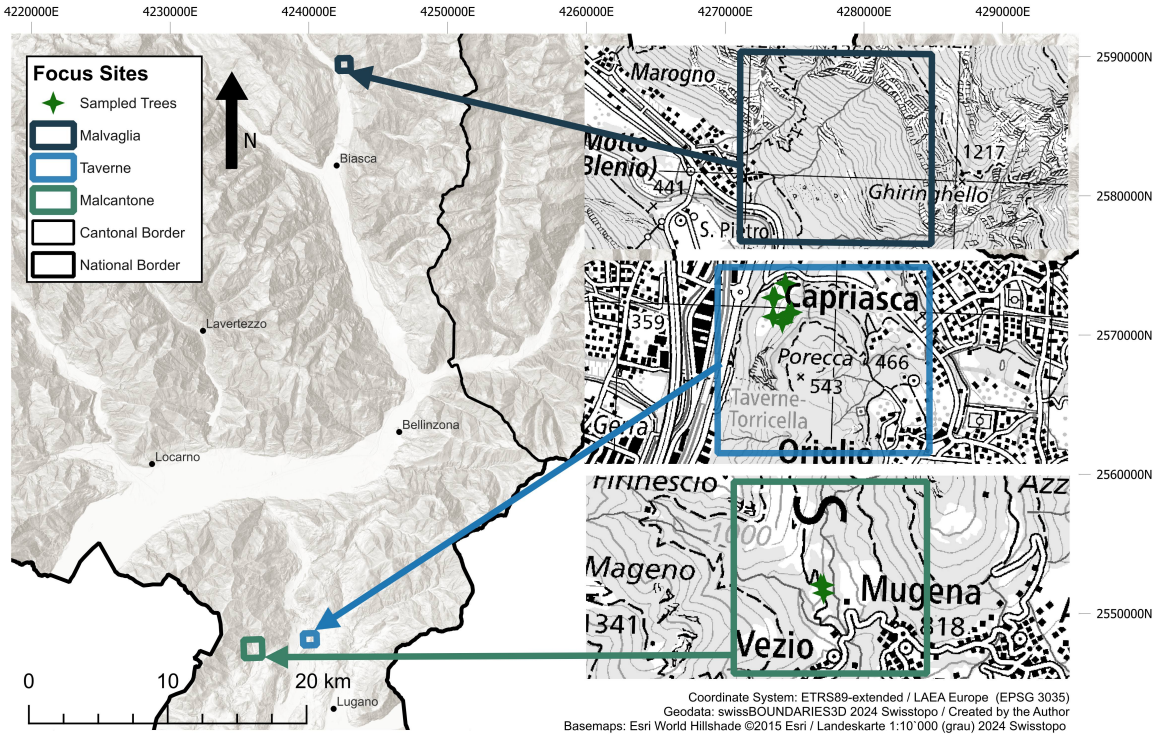

Figure 2.4: **Focus sites of Malvaglia, Taverne and Malcantone.** The three sites were selected to enable a detailed evaluation of the classification approach for sweet chestnut trees, representing a range of conditions across different regions within the Canton of Ticino.

The **Malvaglia** focus site spans the two municipalities of Serravalle and Acquarossa, located in the Val Blenio (coordinates of the centre of the site: 46°25'N 8°58'E). The site covers a total area of approximately 83.0 ha and includes 48.7 ha designated as forest which consists mainly of non-managed, old sweet chestnut coppice stands. The elevation within the focus site ranges from 417 to 1,355 m a.s.l., resulting in a landscape characterised by significant topographical variation, including a steep, south-facing slope. At the base of the forest area lies the cantonal road that connects the Lukmanier Pass to Biasca, running parallel to the Brenno river. The site includes no assessed areas of non-symptomatic and symptomatic sweet chestnut trees, ensuring its remoteness from training samples used later in this work.

The **Taverne** focus site extends over the neighbouring municipalities of Torricella-Taverne, Lamone, Origlio and Ponte Capriasca which are located north of Lugano (coordinates of the centre of the site: 46°4'N 8°58'E). The site covers a total of 84.3 ha, of which 47.6 ha are forests dominated by sweet chestnut. The elevation within the site ranges from 330 to 580 m a.s.l. The forest extends over a mountain base with slopes to the west, north and east, with agricultural fields at its base, adjacent to an industrial zone and railroad tracks. The site includes sampled trees of non-symptomatic and symptomatic sweet chestnut trees that have been used later in this work.

The third focus site of **Malcantone** lies within the municipality of Alto Malcantone to the north-west of Lugano (coordinates of the centre of the site: 46°3'N 8°53'E) and covers a total area of 157.6 ha, of which 44.8 ha are defined as forest. The elevation ranges from 706 to 1,291 m a.s.l. As the other focus sites, the forest at this site is dominated by sweet chestnut which grows in form of old fruit orchards (well-spaced, big trees). The forest area is not directly connected to inhabited zones and is accessible via secondary roads. The site included sampled trees of non-symptomatic and symptomatic sweet chestnut trees that have been used for this work.

Chapter 3

Data

3.1 Sampled Tree Data

The original dataset used for this thesis consists of 251 sweet chestnut trees, sampled from selected stands in the Canton of Ticino and Grisons by the Phytopathology group of the WSL (see appendix A). According to Prospero (2022), the sites were selected based on the presence of symptoms potentially due to ink disease. Sampling and tree assessment were performed in 2013, 2019, 2020 and 2023, and included information about the name of the sites, its approximate coordinates (spatial accuracy of 10 m), the visual health condition of the trees (categorised as either "non-symptomatic" or "symptomatic"), and the results of testing for *P. x cambivora* and *P. cinnamomi* (positive or negative) in the tree rhizosphere. For assessing the presence of the pathogens, five chestnut trees with symptoms of ink disease were sampled from overall symptomatic looking sectors, five non-symptomatic trees were sampled within the same sector, and five non-symptomatic trees were sampled from a nearby healthy-looking forest area. Some stands were re-sampled after initial sampling. For each selected tree, soil samples were collected from the rhizosphere at a maximum distance of 1.5 m from the trunk and a depth of 5–15 cm (see fig. 3.1). Samples were analysed in the laboratory of WSL using the baiting approach. This method involves the use of healthy rhododendron leaves as baits for *Phytophthora* species (Prospero, 2022). With this procedure, *P. x cambivora* and *P. cinnamomi* were isolated from the rhizosphere of 151 out of the 251 chestnut trees sampled.

(a) (b)

Figure 3.1: **Tree sampling for ink disease at the focus site of Taverne (Torricella-Taverne). Screenshot of institutional internal map showing sampled trees (a) and image of soil sample extraction (b).** Soil samples were collected from dead or dying sweet chestnut trees (b) and on a regular 50x50 m grid at five sampling times (November 2023, February 2024, May 2024, August 2024, November 2024). Samples are either identified as positive over all samplings (red), positive over some samplings (orange) or negative over samplings (green) in regard to the presence of *P. cinnamomi* (a). Image source (a): © Phytopathology WSL (Basemap: Google, Imagery ©2024 Airbus, CNES / Airbus, Maxar Technologies), unpublished, 2024. Image source (b): Created by the author, 2024.

3.2 Sentinel-2 Data

For this thesis, already preprocessed Sentinel-2 time series from March 2017 to December 2023 from Koch et al. (2024b) have been used. These data exceed the standard quality of freely available Level-2A products, as they include additional corrections and cloud masking. The processing was conducted by using the Framework for Operational Radiometric Correction for Environmental monitoring (FORCE) software (Frantz, 2019) whose pipeline includes semi-automated download of available Sentinel-2 Level-1C data via API and data processing such as atmospheric correction, cloud masking, reprojection and gridding. Further, the spatial resolution of the raster data was resampled to an overall resolution of 10x10 m. Final products are Level-2 data cubes in Geo Tiff format, accompanied with meta data (Frantz, 2019). The data cubes, as displayed in fig. 3.2, are structured on a 30x30 km grid, allowing individual grid cells to be easily accessed for analysis.

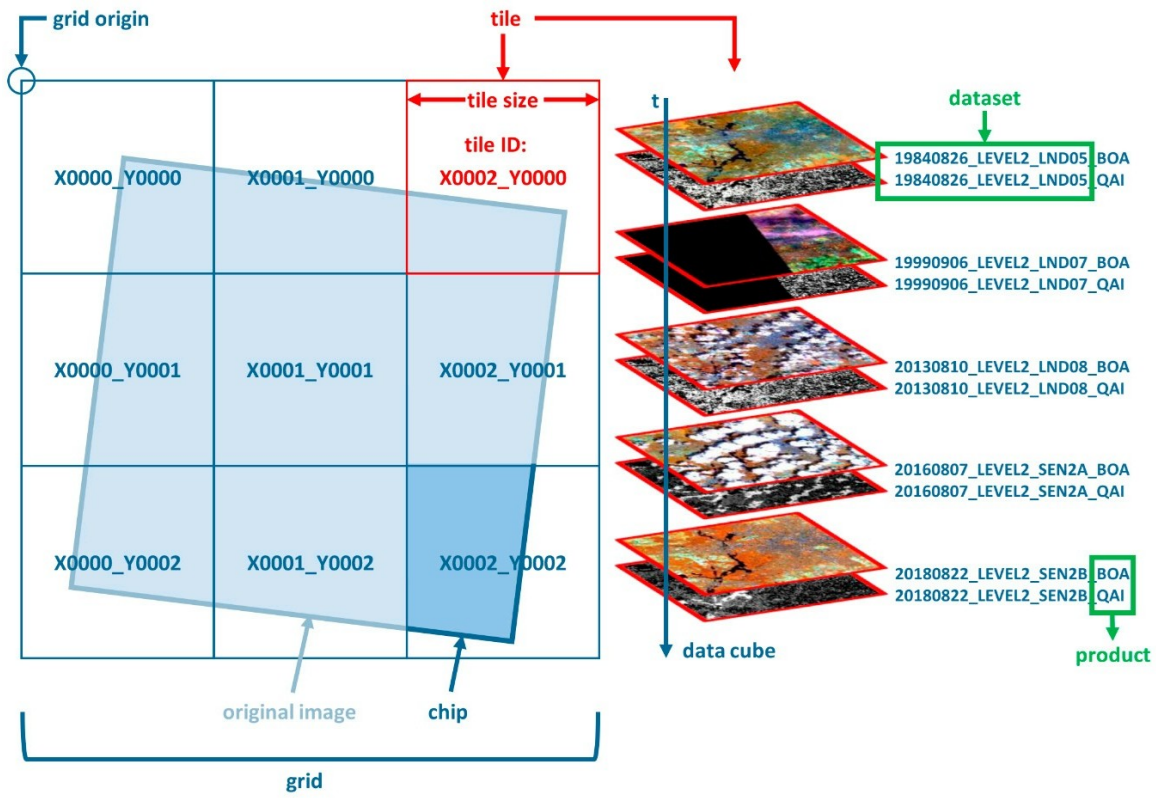

Figure 3.2: **Structure of the Sentinel-2 data processed with FORCE.** The Sentinel-2 images used in this thesis exceed the standard Level-2A quality of freely available images. The processed data cubes allow for easy access to individual grid cells for detailed analysis. Image source: Frantz (2019).

Spectral and temporal information about the trees was derived using preprocessed Sentinel-2 time series between 2017 and 2023, combined with the sampled tree dataset. The Sentinel-2 mission is part of the Copernicus Programme, developed by the ESA in collaboration with the European Union (EU) (Phiri et al., 2020). It aims to provide continuous, multispectral satellite data for specialized application in land cover mapping, for monitoring climate change and for disaster management. Starting in 1998 under the name Global Monitoring for Environment and Security (GMES), the ESA and EU reintroduced the programme under the name "Copernicus" in 2014 (Jutz & Milagro-Pérez, 2020). The Sentinel-2 constellation consists of satellite composites, complementing each other with a revisit time of five days at the equator. Sentinel-2A has been launched in 2015, since 2017 Sentinel-2B is additionally providing data from an altitude of 789 km on a global level (Jutz & Milagro-Pérez, 2020). Since September 2024, a third satellite, Sentinel-2C, has started its operations and will soon complete the mission by providing continuous, long-term data over several years (ESA, 2024). Sentinel-2 data is freely available, which enables its use for a broad audience. The images

comprise 13 bands, with spatial resolutions ranging from 10 to 60 m, and a spectral range that includes visible, Near-Infrared (NIR), and Short-Wave Infrared (SWIR) bands and are available in quality levels ranging from Level 1B to Level 2A (Phiri et al., 2020). The data provides an appropriate base for this thesis, as the mission is specifically developed to supply imagery for time-series landcover analysis, including forest monitoring (Molnár & Király, 2024).

The data used within this thesis are flagged Level-2 time series for spectral bands and VIs, including all available images with land surface information within the given time period. Additional smoothed or interpolated data was not considered, as this would most likely have reduced the effect of spectral values to distinguish between non-symptomatic and symptomatic sweet chestnut trees. Within this thesis, a collection of eight preprocessed bands (see table 3.1) and eight VIs from which five were already provided were used (see table 3.2). Three additional VIs were calculated that have been proven to be beneficial for forest classifications. The given Coordinate Reference System (CRS) of the data is European Terrestrial Reference System (ETRS)89-extended / Lambert Azimuthal Equal Area (LAEA) Europe (European Petroleum Survey Group Geodesy (EPSG) 3035) which is used as the base CRS for all spatial data within this thesis.

Table 3.1: **Sentinel-2 bands used in this thesis, derived from data preprocessed with FORCE.** Source: Molnár and Király (2024).

Band Name	**Abbreviation**	**Band Number**	**Central Wavelength [nm]**	**Spatial Resolution [m]**
Blue	BLU	B2	490 nm	10 m
Green	GRN	B3	560 nm	10 m
Red	RED	B4	665 nm	10 m
Red-Edge 1	RE1	B5	705 nm	20 m
Red-Edge 3	RE3	B7	783 nm	20 m
Near-Infrared	NIR	B8	842 nm	10 m
Short-Wave Infrared 1	SW1	B11	1610 nm	20 m
Short-Wave Infrared 3	SW2	B12	2186 nm	20 m

Table 3.2: **Vegetation indices.** The selection of eight vegetation indices was used in this thesis.

Index Name	Abbreviation	Source
Chlorophyll Carotenoid Index	CCI	Gamon et al. (2016)
Chlorophyll Index Red-Edge	CIre	Gitelson et al. (2003)
Normalised Difference Wetness Index	NDWI	Gao (1996)
Normalised Difference Vegetation Index	NDVI	Tucker (1979)
Enhanced Vegetation Index	EVI	Huete et al. (2002)
Soil-Adjusted Vegetation Index	SAVI	Huete (1988)
Green Normalised Vegetation Index	GNDVI	Gitelson and Merzlyak (1997)
Normalised Difference Vegetation Red-Edge Index	NDVIre	Gitelson and Merzlyak (1994)

3.3 Auxiliary Data

To select areas where sweet chestnut is the predominant species for defining the regions for classification, the *Tree Species Map of Switzerland* from Koch et al. (2024a) was used. The map provides information on the dominant tree species in forested areas, derived from Sentinel-2 time series data and represented as a raster layer with a spatial resolution of 10 m. It is important to note that the validation of the *Tree Species Map* by using independent data is not yet conducted (Koch et al., 2024a).

The training areas for RF classification (see section 4.3) were further refined with help of the *swissTLM3D* dataset, which includes nationwide landscape features of natural and artificial origin, and further name data stored as vector data (Swisstopo, 2024c). This dataset was used to exclude street segments, as well as to clip the training areas only to land cover classes specifically associated with forested regions. To clip all data sets to the extent of the Canton of Ticino, the *swissBOUNDARIES3D* dataset was used, which consists of vector files indicating the administrative boundaries within Switzerland and Liechtenstein (Swisstopo, 2024a). For further visual assessment of trees within forest areas, digital orthophotos from Swisstopo (2024b)'s textitSWISSIMAGE datasets were used. The orthophoto mosaics have a spatial resolution of 10 cm in plain areas (e.g., southern Ticino) and 25 cm in alpine regions (e.g., northern Ticino) and were acquired in 2021, respectively 2022, for the targeted regions within this thesis (Swisstopo, 2022).

For the refinement of the classification dataset, only pixels below 900 m a.s.l. were considered, provided they were covered by at least 60% vegetation with a height larger than 3 m (resulting in a canopy closure of at least 60%). These criteria ensured that only relevant forest areas were included in the analysis. The selection was facilitated by using the *Digital Surface Model (DSM)* (Swisstopo, 2023) and the *Vegetation Height Model (VHM)* (Ginzler, 2021) for Switzerland, which is a product of the Swiss National Forest Inventory (NFI).

Chapter 4

Methods

4.1 Overview Workflow

The general workflow elaborated to provide a structured approach to addressing the Research Question (RQ)s stated in this thesis is illustrated in fig. 4.1. To monitor diseased sweet chestnut trees, a RF model was used to classify predefined forest areas into non-symptomatic and symptomatic class. The potential input features for model training were monthly calculated median values from June to September, derived from Sentinel-2 time series data within a period from 2017 to 2023.

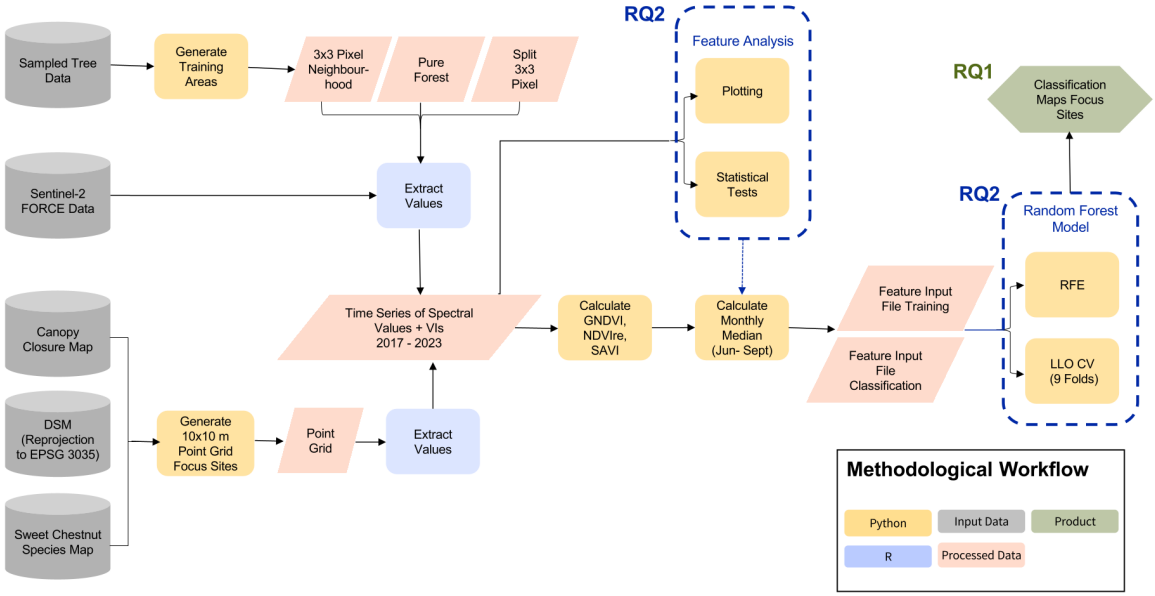

Figure 4.1: **Overview of the methodological approach elaborated for the analysis of the research questions of this thesis, as stated in chapter 1.** An in-depth analysis of the input features provides insights into the data's characteristics, facilitating the selection of specific features (RQ2) for training the RF model to classify the selected areas within the focus sites (RQ1).

Training samples were generated by creating a 10x10 m grid based on point-sampled tree data. One of the outputs of this thesis are classification maps for the three focus sites Malvaglia, Taverne and Malcantone (see section 2.4), derived from the trained RF model. The pixels for classification were defined using a *DSM*, the *Tree Species Map of Switzerland*, and a self-generated canopy closure map. These maps were used to limit the focus sites to only those with sweet chestnut and a threshold canopy closure, which is described in section 4.3. In addition to the spectral band values from the Sentinel-2 time series, various VIs were considered as potential input features for the RF model. To find the optimal combination and number of features from a total number of 64 input features, Recursive Feature Elimination (RFE) and Leave-Location-Out Cross-Validation (LLO CV) were applied within the RF framework (see section 4.6). Prior to the final feature selection, a comprehensive analysis of all available spectral bands and VIs was conducted. This involved visual assessment of time series plots and boxplots, as well as statistical analysis to obtain quantitative insights into the characteristics of the features (see section 4.5).

4.2 Generating Training Sample Areas

The sampled areas used for training the RF model are crucial to the quality and robustness of the model's output. A three step approach was carried out to ensure representative and reliable training data for the model. The sampled tree data, described in section 3.1 served as a basis for generating the training areas. Samples from the year 2013 were excluded, as Sentinel-2 data from the given dataset for value extraction are available only since 2017 (Koch et al., 2024b). The final dataset consisted of 95 sampled trees. Extracting values directly from the given point coordinates would have been misleading, as these points approximate the actual tested tree locations with an error up to 10 m, which involved the risk of selecting a wrong tree's values. Therefore, three successive methods to generate reliable training areas were analysed and tested for their performance within the RF model, as visualised in fig. 4.2 and described in the following paragraphs. In general, the raster grid of the preprocessed Sentinel-2 data was used as the base grid for all methods. The grid consists of cells with a size of 10x10 m in the ETRS89-extended / LAEA Europe (EPSG 3035) projection each.

3x3 Pixel Neighbourhood Approach The first approach involved creating a 3x3 pixel (30x30 m) neighbourhood around each tree's coordinate, with the central pixel representing the tree's approximate location. This method aimed to mitigate possible discrepancies in the labeled measurement locations. A Python script was used to intersect the provided tree coordinates with the Sentinel-2 data raster grid. Each central pixel was identified and expanded to include the neighbouring eight pixels, as the sampled tree's coordinates were only given with an accuracy of 10 m. The resulting squares therefore had an area of 30x30 m (900 m^2) each. The complete dataset of generated squares was then stored as Environmental Systems Research Institute (ESRI) shapefiles to enable efficient data management with several attributes used to define the characteristics of each area (ESRI, 1998).

This method was a preliminary approach to generate training areas based on the given tested tree's coordinates and had limitations. The created areas often contained more than only trees, as for example other land cover types such as streets, rocks or meadows. As the tree sampling was conducted manually, the sampled trees were frequently located in easily accessible areas near roads. This resulted in partly impure training areas which were not fully covered by tree areas. Additionally, some areas overlapped as certain trees were sampled within a 30 m radius of one another (see fig. 4.2, left).

Figure 4.2: **Overview of the step-wise approach for generating training areas.** The first approach involved creating 30x30 m areas surrounding the sampled trees (left), followed by the second approach which aimed to exclude street segments and non-vegetated land cover (middle). The final approach subdivided the areas into smaller 10x10 m sections (right).

Pure Forest 3x3 Pixel Neighbourhood Approach A second approach involved clipping the 3x3 pixel areas by removing parts that did not contain forest cover. This refinement was necessary, as the input data for the RF model should represent the purest possible forest areas. To achieve this, street segments from the *swissTLM3D* dataset were buffered by a diameter of 3 m and further used to remove street areas from the underlying training areas within QGIS (version 3.34.0). The same procedure was applied by using a preprocessed land cover classification shapefile, also derived from the *swissTLM3D* dataset. Subsequently, manual adjustments were made on each training area through visual assessment with help of the *SWISSIMAGE* orthophotos. These refinements were to exclude additional non-forest areas from the training areas. As a result, the dataset included training areas with the original 3x3 pixel size of 900 m^2, as well as areas consisting of smaller parts of the original size (see fig. 4.2, middle).

Split 3x3 Pixel Approach The third approach to generating the training areas for the RF model based on the previous methods described in this chapter. As there was only a

total amount of 95 sampled trees from the years 2017 to 2023 and the RF model performed poorly on the testing data, the final decision was made to artificially increase the number of training samples. The previously refined 3x3 pixel areas were subdivided into nine smaller squares, each measuring 10x10 m. The partitioning of the original 3x3 pixel areas was conducted with a Python script, which considered the original preprocessed Sentinel-2 raster structure. To ensure the purity of the subdivided training samples, squares that did not fully cover forest areas were clipped and duplicates were excluded (see fig. 4.2, right). This method resulted in a significant increase in the total number of training samples, enhancing the dataset from 95 to 541 samples. However, since the original tree sample was located only in the central pixel of the subdivided areas, the health status of each 10x10 m area was reassessed. Using the *SWISSIMAGE* orthophotos from 2021 and 2022, each square was visually assessed and if necessary, reclassified in either non-symptomatic or symptomatic test areas. Any changes to the labels were recorded, and the assessment year was updated to reflect the monitoring year of the orthophotos, ensuring consistency in subsequent value extraction steps. Additional pixel areas were added to the data set by visual analysis of the *SWISSIMAGE* data to ensure a balanced representation of both non-symptomatic and symptomatic samples.

4.3 Defining Classification Areas

In addition to defining the training areas, the pixels to be classified had to be generated. In general, the task is given for a canton-wide evaluation of the existing sweet chestnut tree stands. As a classification across the whole of Ticino would have gone beyond the scope of this thesis, three focus sites were selected to undergo a classification. To facilitate the identification of sweet chestnut stands within the given sites, the *Tree Species Map of Switzerland* was used as a reference. Areas where sweet chestnut was identified as the predominant species were extracted from the raster file and clipped to the extent of the Canton of Ticino using the data from *swissBOUNDARIES3D* shapefiles. To consider only areas located below or equal to 900 m a.s.l., the resulting map was further clipped by using the *DSM* in raster format. Before the reduction of the extent based on the chosen thresholds, the data was reprojected from LV95 LN02 (EPSG 2056) to ETRS89-extended / LAEA Europe (EPSG 3035) to ensure spatial consistency. These preparatory steps were performed within QGIS (version 3.34.0), resulting in a clipped raster file representing areas of predominantly sweet chestnut below 900 m a.s.l, from which the three focus sites were extracted.

These three focus sites were subsequently split into 10x10 m squares, corresponding to the grid size of the Sentinel-2 data. To optimise computational efficiency for later value extraction, a point layer representing the centroids of each 10x10 m square was generated in Python. Thus, by iterating over each pixel in the raster and assigning an Identifier (ID) to each point to ensure unique point labeling.

To consider potential mixed pixels at forest edges or within widely spaced trees, the classification areas were further refined using canopy closure as a parameter. This measure

was calculated by using the *VHM* and represents the proportion of vegetation that is higher than 3 m for each square. Squares with less than 60% canopy closure were excluded from the area to be classified. This additional refinement was also performed in QGIS (version 3.34.0).

4.4 Features Derived from Sentinel-2

Performing a classification with a RF model requires features that indicate specific values, which are then used for both training and classification (Dobrinić et al., 2022). In the context of this thesis, the representative values were the Digital Number (DN)s of Sentinel-2 measurements of the original bands, as well as of VIs, as they target specific information about the condition of plants (Xiong et al., 2023). The DN unit represents the raw pixel values derived by Sentinel-2 which can be converted to reflectance values by division of 10,000 (Reflectance = DN/10,000) (EU, 2022). These DNs were extracted from the preprocessed data cubes using an existing R script from Koch (2023), originally developed for value extraction of point layers. Only few adaptations were required to modify the script for the purpose of this thesis, enabling the extraction of area-wise values instead of point-wise values. The script reads an ESRI point shapefile and generates a Comma-separated Values (CSV) table for each band, containing a matrix with point locations as rows and daily dates between the 1st of January 2017 and 31st of December 2023. The final output is for each band and VI the CSV file containing the extracted DNs over the whole time range. For extracting DNs for the pixels within the focus sites to be classified, the original R script for point extraction was adapted and applied to the spatial extent of the selected areas.

4.5 Pre-assessment of Spectral Bands and Vegetation Indices

Before the selection of possible input features for training the RF model (see detailed approach in section 4.6), an in-depth analysis of the original Sentinel-2 bands and VI was performed to better understand the spectral characteristics of non-symptomatic and symptomatic trees, as well as to understand the dynamics of feature selection for the RF model. In the following section, the chosen VIs are introduced and described in detail, highlighting their primary characteristics.

4.5.1 Introduction Spectral Bands and Vegetation Indices

Greenness Indices Normalised Difference Vegetation Index (NDVI) and Enhanced Vegetation Index (EVI) are both sensitive to changes in chlorophyll content, but EVI is more responsive in densely vegetated areas (Liu et al., 2024). Given that the study area included both sparse and dense forests, the use of these two VIs aimed to provide specific insights into the physiological state of the vegetation across varying conditions. A further chlorophyll index is the Green Normalised Vegetation Index (GNDVI), which is a commonly used VI for vegetation mapping and disease detection. Several studies indicated GNDVI as one of the

most important features for such assessments since it displays water and nitrogen uptake of a plant and therefore indicates phytosanitary characteristics (see Marques et al., 2019; Mohammadpour et al., 2022; Molnár & Király, 2024; Pádua et al., 2020; Sebastiani et al., 2024; Xiong et al., 2023).

To consider the presence of sparsely covered areas within the study area, where lower foliage on diseased chestnut trees may expose the soil, the Soil-Adjusted Vegetation Index (SAVI) was chosen. SAVI has the advantage of a soil adjustment factor, allowing for better handling of variations in soil brightness (Mohammadpour et al., 2022).

Literature often indicates the Red Edge (RE) bands to be particularly important for health detection, as they lie in the spectral range between the red and the NIR band, where the reflectance difference of healthy vegetation is the largest (see Boiarskii & Hasegawa, 2019; Dobrinić et al., 2022; Pádua et al., 2020; Sebastiani et al., 2024; Tan et al., 2024). Therefore, the Normalised Difference Vegetation Red-Edge Index (NDVIre) was selected to consider specifically the RE1 band within an index. Since the wavelengths of the RE1 band are less prone to oversaturation by the upper canopy, they enable an accurate detection of even small variations in chlorophyll content of a plant's leaves, making them particularly useful for the early detection of plant stress (Boiarskii & Hasegawa, 2019).

Chlorophyll and Carotenoid Indices Additionally, the chlorophyll, respectively carotenoid-specific VIs Chlorophyll Carotenoid Index (CCI), and Chlorophyll Index Red-Edge (CIre) were considered to provide a better insight into the sampled trees' characteristics. The CCI is an index originally developed for evergreen trees, as it is able to estimate vegetation dynamics over the whole season by measuring the ratio between the chlorophyll content and carotenoid pigments (Gamon et al., 2016). Especially in winter, the chlorophyll content in plants is reduced, while the amount of carotenoid pigments increases. This gives the opportunity to gain insights into plants over the whole year, which are difficult to detect with VIs such as the NDVI (Gamon et al., 2016). Regarding the deciduous sweet chestnut trees, the index served to focus on specifically the behaviour of carotenoids within a tree, which may contribute to detect symptomatic trees. Additionally, the Clre has been used which indicates chlorophyll content. This index has the advantage of being insensitive to the saturation effect. Therefore, unlike traditional VIs that typically use the red and NIR bands, this index is calculated using the RE band (Helfenstein et al., 2022).

Water Content Indices Besides these mainly chlorophyll focused VIs, the Normalised Difference Wetness Index (NDWI) was used to detect the water content within the trees' leaves or canopy and with this focusing on another possible proxy for symptomatic trees. The NDWI calculates the ratio between the green and the NIR-band, as the green band has high and the NIR-band low reflectance values for vegetation containing water (Viana et al., 2019).

4.5.2 Visual Analysis

A statistical and visual analysis of the time-series data was conducted to gain a deeper understanding of the available spectral bands and VIs and their behaviour over time. These preliminary examinations were essential to obtain insights into the data's characteristics. For the analysis, monthly medians, means and standard deviations were calculated (see appendix B). By generalising the available values on a monthly basis, this approach facilitated the identification of consistent patterns across the spectral values and selected VIs. Plots were made by using Python and the standard library `matplotlib`.

4.5.3 Statistical Analysis

Besides the visual analysis by generating plots of the data, a preliminary assessment of the spectral bands and VIs was performed based on statistical tests and calculations. This to provide further insight into the relationships between the sampled trees and the spectral bands and VIs and to explore them by quantitative means. The statistical tests were performed for each month over the entire time period from March 2017 to December 2023, allowing an evaluation of the spectral features on a monthly basis. These tests aimed to identify significant differences between non-symptomatic and symptomatic trees for each band and VI. This approach was chosen to provide a general overview of which bands and VIs showed consistent differences between non-symptomatic and symptomatic trees, without being influenced by any potential temporal trends. The following section outlines the statistical tests performed:

Mann-Whitney U Test: Test on Data Distribution A first approach to evaluate the given training data was a Mann-Whitney U test to assess eventual statistical differences between the available training data parameters. The dataset, covering the period from March 2017 to December 2023, includes measurements from both non-symptomatic and symptomatic chestnut trees. To evaluate the differences between these two classes, a Mann-Whitney U, respectively two-sided t-test was conducted with each selected combination of data. For each month and each spectral band or VI, the null hypothesis (H0) was tested, which assumes the distribution of non-symptomatic and symptomatic trees to be equal. Specifically, this means that there is no significant difference in their rank-based values. The alternative hypothesis (Ha) suggests a significant difference between the distribution of the two data sets (Nachar, 2008).

Bands and VIs from the compared classes showing significant p-values ($p < 0.05$) were interpreted as especially favourable candidates for inclusion in the RF model. The choice between the non-parametric Mann-Whitney U test and the parametric t-test was made after conducting a previous Shapiro-Wilk test which verifies whether the data follows a normal distribution or not (Shapiro & Wilk, 1965). The statistical analyses were performed in Python using the `scipy` package (version 1.14.0).

Cliff's Delta: Calculation of Effect Size After the Mann-Whitney U, respectively the two-sided t-test, the effect size was calculated to provide a quantified insight into the differences in the classes of specific bands and VIs. For each combination of the monthly bands or VIs, Cliff's Delta was calculated to assess the practical significance of the differences between the classes. The measure evaluates the whole range of data for each class. It quantifies the proportion of the non-overlapping area between the two distributions, resulting in a value between -1 and 1, whereas a value of 0 indicates that none of the classes has statistically exceeding values over the other (Macbeth et al., 2010). The resulting effect sizes are often categorised as negligible, small, medium and large, but have to be taken with care, as their meaning may vary depending on the characteristics of the data (Meissel & Yao, 2024). Within this work, the interpretation of Cliff's Delta is based on the definition outlined by Meissel and Yao (2024) which considers the absolute values of the measure. An overview of the categories is presented in table 4.1.

Table 4.1: **Interpretation of Cliff's Delta effect sizes based on absolute values.** Source: Meissel and Yao (2024)

Interpretation	**Cliff's Delta**
Negligible	< 0.15
Small	0.15
Medium	0.33
Large	0.47

As the preprocessed Sentinel-2 data is generally of non-parametric nature, the measure is suitable to assess specific months and bands, respectively VIs that show the greatest differences between the two selected classes. Such statistical methods further enable to provide information about the relative importance of these months and bands, respectively VIs to characterise the health condition of sweet chestnut trees. It is recommended by literature as a complementary evaluation besides feature selection methods (Granitto et al., 2006). The calculation of Cliff's Delta was executed within Python by using the `cliffs_delta` package (version 1.0.0) (Ernst, 2021).

4.6 Feature Selection and Model Training

The multiple values derived from the time series had to be bundled to single values as input for RF. For this thesis, the median values calculated for the months of June, July, August, and September of each year from 2017 to 2023 were used to characterise each training area, resulting in a total of 64 possible input features. These specific months were chosen, as they cover the growing season of sweet chestnut. During this period, the trees' photochemical processes are most active, making differences between non-symptomatic and symptomatic

trees most evident (Sebastiani et al., 2024). An overview of all 64 available input features is given in table 4.2.

Table 4.2: **Overview of available input features for Random Forest model training and classification.** Monthly calculated median values from June to September for each year from 2017 to 2023.

Band / Index	June	July	August	September
Blue	BLU_month6	BLU_month7	BLU_month8	BLU_month9
Green	GRN_month6	GRN_month7	GRN_month8	GRN_month9
Red	RED_month6	RED_month7	RED_month8	RED_month9
Red-edge 1	RE1_month6	RE1_month7	RE1_month8	RE1_month9
Red-edge 3	RE3_month6	RE3_month7	RE3_month8	RE3_month9
Near-Infrared	NIR_month6	NIR_month7	NIR_month8	NIR_month9
Short Wave Infrared 1	SW1_month6	SW1_month7	SW1_month8	SW1_month9
Short Wave Infrared 2	SW2_month6	SW2_month7	SW2_month8	SW2_month9
CCI	CCI_month6	CCI_month7	CCI_month8	CCI_month9
CIre	CIre_month6	CIre_month7	CIre_month8	CIre_month9
NDWI	NDWI_month6	NDWI_month7	NDWI_month8	NDWI_month9
NDVI	NDVI_month6	NDVI_month7	NDVI_month8	NDVI_month9
EVI	EVI_month6	EVI_month7	EVI_month8	EVI_month9
SAVI	SAVI_month6	SAVI_month7	SAVI_month8	SAVI_month9
GNDVI	GNDVI_month6	GNDVI_month7	GNDVI_month8	GNDVI_month9
NDVIre	NDVIre_month6	NDVIre_month7	NDVIre_month8	NDVIre_month9

In the following section, the methodologies for finding the optimal number of input features and identifying the specific combination of features for training the final RF model will be presented. Additionally, the approaches for testing and validating model performance will be explained in detail. Before providing a detailed description of the implementation of the selected methods in section 4.6.4 and section 4.6.5, this chapter will begin with a theoretical introduction to the three key approaches chosen for this thesis: the RF model, RFE, and LLO CV.

As previously described, the retrieved Sentinel-2 band values and selected VIs were given as possible input features for the RF classification task within this thesis, which targets the classification of forest areas into either symptomatic or non-symptomatic tree cover. As the literature states, the use of a large number of input features can lead to issues such as feature redundancy and correlation (Dobrinić et al., 2022). Especially when features are indicating similar characteristics of the target classification, this can negatively affect the model's performance (Pudjihartono et al., 2022). To mitigate the risk of overfitting,

a selection of specific features was conducted to identify the most important variables for classification (see section 4.6). While existing literature proposes specific bands and VIs for vegetation related topics, the choice of input features should be adapted to the specific context of this thesis. Thus, as recommendations of features to use for such a model vary between different research setups and study areas (see e.g., Pádua et al., 2020; Sebastiani et al., 2024; Yu et al., 2021).

4.6.1 Random Forest Model

RF (Breiman, 2001) is a ML classification algorithm based on the principle of decision trees. The ensemble classifier works by using the concept of bagging, also known as bootstrap

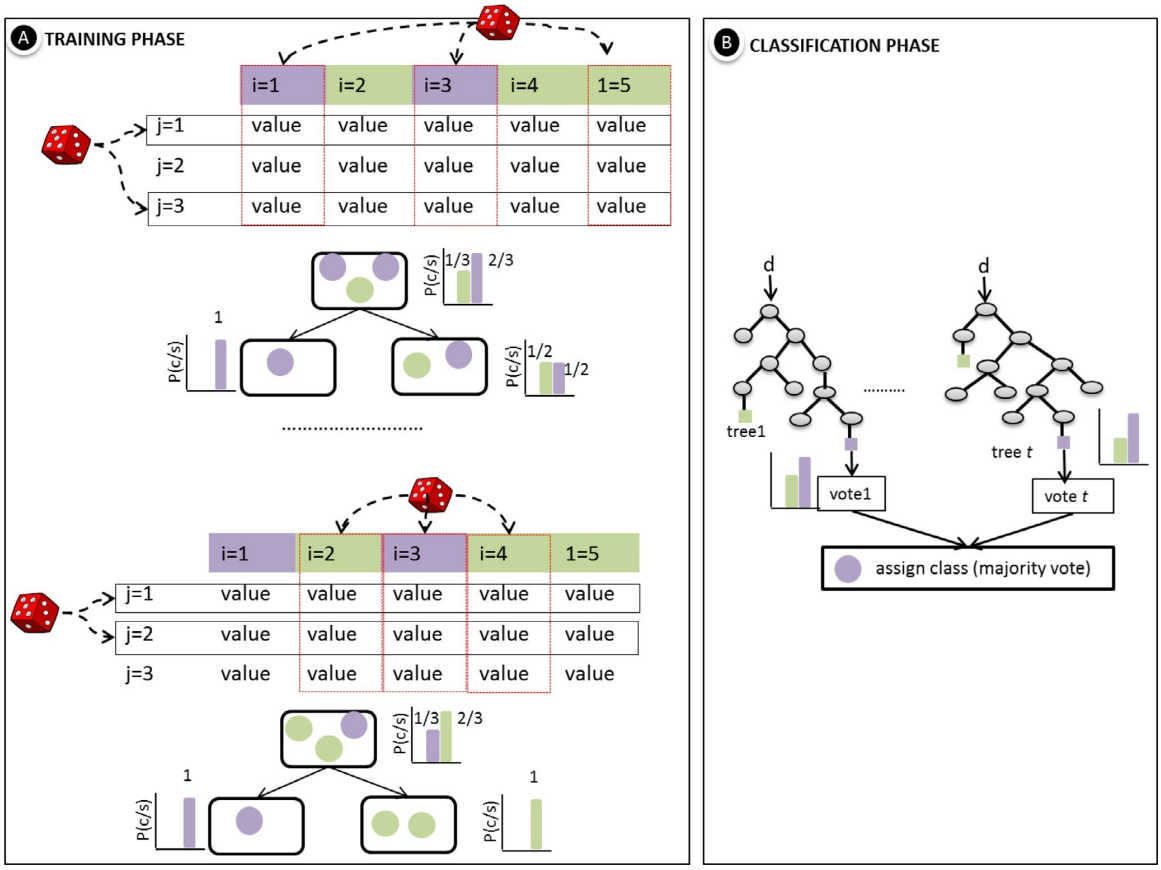

Figure 4.3: **Principle of Random Forest approach.** RF is a ML approach which is based on the principle of decision trees. During the training process, given samples (j) having given input features (i) are used to assign characteristics to distinguished classes by using decision trees. During classification, a new data input (d) is assigned to one of the classes according to the majority vote from the results of several decision trees. Image source: Reprinted from Belgiu and Drăguţ (2016), Copyright 2016, with permission from Elsevier, licensed through Copyright Clearance Center's RightsLink® service.

aggregation. The bagging approach works by taking randomly chosen subsets of given training data and constructing several decision trees to define a sample's class or predict a sample's value. Due to the specific, known choice of input data, RF is a supervised classification method. Two main parameters are used to adapt a model's performance: The number of trees (*ntrees*) determines how many trees are generated with randomly chosen subsets of the given data and has 500 as a default value, and the number of variables (*Mtry*) is the number of features considered for splitting at each node. This is crucial for balancing a model's performance and computational time. *Mtry* is generally chosen by calculating the square root of all bands within the model. Taking a randomly chosen subset of samples and of variables for building decision trees reduces the risk of overfitting, as the subsets provide a variability of characteristics. As visualised in fig. 4.3, RF takes the majority of decisions of each tree for a final decision in classification tasks, while for regression, it averages the outputs of the individual decision trees (Belgiu & Drăguţ, 2016). Besides the advantage of reduced risk of overfitting, RF can deal with high dimensional data and extract the most important features for model training. This is an especially important characteristic for typically high-dimensional RS images and saves time-consuming feature selection in advance (Mohammadpour et al., 2022).

Since the training data is crucial for the classifier's output, some requirements need to be considered. Training samples should be statistically independent and should represent their classes as well as possible. For image data, samples therefore have to be as pure as possible. Additionally, the training samples should be balanced between classes, as RF tends to favour the classes with more instances in the dataset. Also, the number of training samples should be adapted to the number of variables and the size of the study area. Literature suggests that training samples should cover around 0.25% of the whole study area and that samples should be equally distributed, as RF is sensitive to spatial autocorrelation (Belgiu & Drăguţ, 2016).

Due to the advantages discussed in this chapter, as well as the general long-term experience with its application and stable classification results mentioned in the literature, the RF algorithm was the selected approach for the classification of non-symptomatic and symptomatic trees within this thesis.

4.6.2 Recursive Feature Elimination

RFE is a well-established method in classification tasks to enhance a model's performance to identify the most relevant features while eliminating those that are less important (Brungard et al., 2015). This technique has been recommended in literature that approaches similar applications, such as monitoring the health status of trees (see Brungard et al., 2015; Dobrinić et al., 2022; Pádua et al., 2020). RFE works in an iterative way, by ranking features based on their contribution to the model's classification accuracy which is displayed by the feature importances. In each iteration, the least important feature is removed. The number of iterations depends on the final number of features to keep for model training and can be chosen by the user (Granitto et al., 2006). The RF model itself serves as an estimator of feature importances during this process, allowing RFE to evaluate the impact of each feature

in relation to the model's overall performance (Granitto et al., 2006).

For this thesis, the approach was particularly important regarding the objective of identifying key indicators for detecting symptomatic sweet chestnut trees. Even if RF is well-known to handle multicollinear data, feature selection mitigates the risk of correlation, which could arise from using the whole set of 64 available input features (Dobrinić et al., 2022). Especially regarding the presence of multiple greenness and chlorophyll VIs selected for this thesis, correlation was a very likely effect to consider. Further, RFE helps to reduce noise and enhances the interpretability of feature importances (Granitto et al., 2006). Thus, the input feature set was refined to ensure that the model concentrated on the relevant predictors, aiming to provide better insights into the most important features for classification.

4.6.3 Leave-Location-Out Cross-Validation

Improving a model's performance and analysing its accuracy are key parts of applying ML methods. In this thesis, the validation method used for the RF model was a LLO CV, which aimed to generalise the process as effectively as possible (Meyer et al., 2018). Traditional CV assumes that data sets are independent and separates reference data into two subsets: One part is used for training the model, a second part is used for validating its performance and testing for prediction errors. This separation of the data ensures an independent evaluation of a model's performance without autocorrelating data (Karasiak et al., 2021). However, the input data in this thesis was closely tied to geographical and topographical factors. A missing consideration of the spatial dependence of data could have led to biased validation scores with overestimation of a model's performance (Pohjankukka et al., 2020).

Pohjankukka et al. (2020) describe the key point of such a spatial Cross-Validation (CV) as making sure that "the training data set only contains data points that are at least a certain spatial or temporal distance away from the test data set". The key concept of this evaluation method is to iteratively test the model's performance by excluding one fold for testing while using the remaining folds for training, leaving out each fold once for testing (Valavi et al., 2018). Therefore, LLO CV was selected to better assess the model's performance within the specific spatial context of the thesis. This approach was expected to lead to higher error estimates, as classification was tested on unknown locations (Meyer et al., 2018).

4.6.4 Implementation: Evaluation of Feature Combinations and Random Forest Model Performance

After the theoretical introduction of RF, RFE and LLO CV, it follows the description of the practical implementation of these methods within the thesis. The approach is a step-by-step method which first aims to find the best feature combination as input for training the RF model. Therefore, ten feature combinations were built for different numbers of features (ranging from 6 to 23) by using RFE. Furthermore, the 180 resulting feature combinations were validated with LLO CV. The feature combination achieving the highest mean accuracy score was used for training the final RF model, which at the end was tested (see fig. 4.4). The detailed validation and testing method is described in the following section 4.6.5.

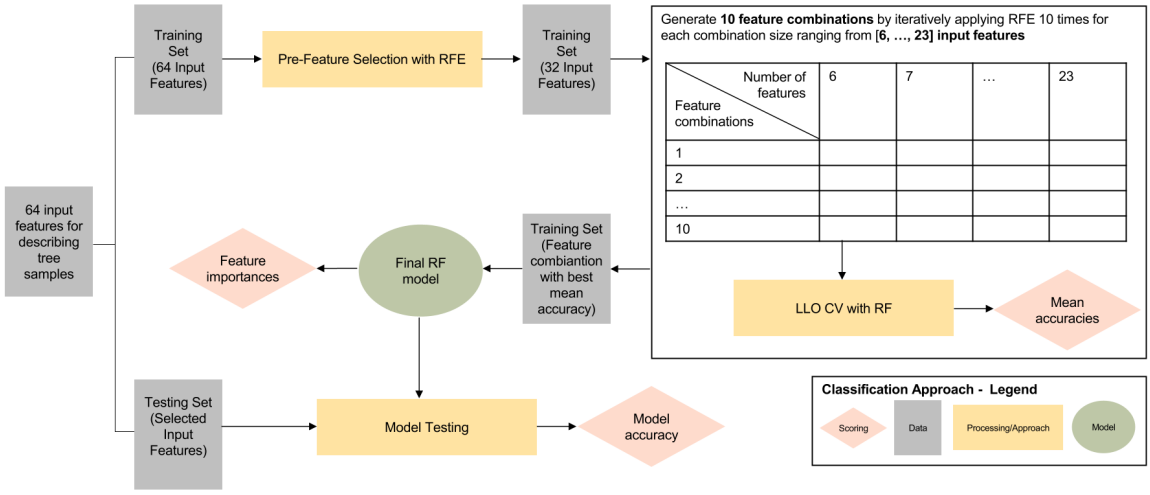

Figure 4.4: **Classification approach with Recursive Feature Elimination, Leave-Location-Out Cross-Validation, and Random Forest.** For different numbers of features [6, ..., 23] features) ten feature combinations were generated using RFE. The resulting 180 feature combinations were then validated using LLO CV. The feature combination that achieved the highest mean accuracy was selected for training the RF model.

To find the optimal number of features as well as the best combination of input features, RFE was implemented in combination with the RF model framework. A pre-assessment of features was conducted by evaluating the feature importances, which were obtained by training a RF model using all 64 available input features. This initial analysis allowed for the exclusion of half of the features (32 features), as an evaluation of the whole set would have been computationally and time intensive.

After the analysis followed an iterative RFE approach, which tested on the classification performance for different number of features and different feature combinations. Specifically, for each feature count between 6 and 23, ten distinct feature combinations were generated by using different random seeds to get variability between the combinations. To assess the performance of each combination, LLO CV was employed, and the resulting accuracy scores were stored. The feature combination that achieved the highest mean accuracy across all combinations was selected for use in training the final RF classifier. To ensure an effective choice, this process has been executed several times, showing consistent results. The procedure has been executed within a Python script by using the `scikit-learn` package (version 1.5.1) and the basic packages `random`, `pandas`, `collections` and `numpy`. The implementation is publicly available on GitHub (see Zumbrunn, 2025).

For training the RF model, default parameters were used on a number of trees ($ntrees$) = 100 and the number of features to consider when splitting the model ($Mtry$) = 5 (square root of features as upper boundary). The classifications were made on a yearly basis over the period from 2017 to 2023.

4.6.5 Implementation: Model Training and Testing

Before evaluating the feature combinations and training the RF model, the sampled tree data was partitioned into spatial folds through a manual selection process. Nine spatial folds, displayed in fig. 4.5, were created by visually interpreting the distribution of clustered trees. The selection of the number of folds is based on the spatial distribution of samples across the study area. To ensure spatial independence and avoid autocorrelation among samples, a minimum distance of 3.4 km between each fold was ensured. Each fold represents a distinct spatial region within the study area of the Canton of Ticino, with sizes ranging from 17 to 135 samples. This uneven sample distribution was considered when assessing model performance, as it may affect the accuracy across different folds.

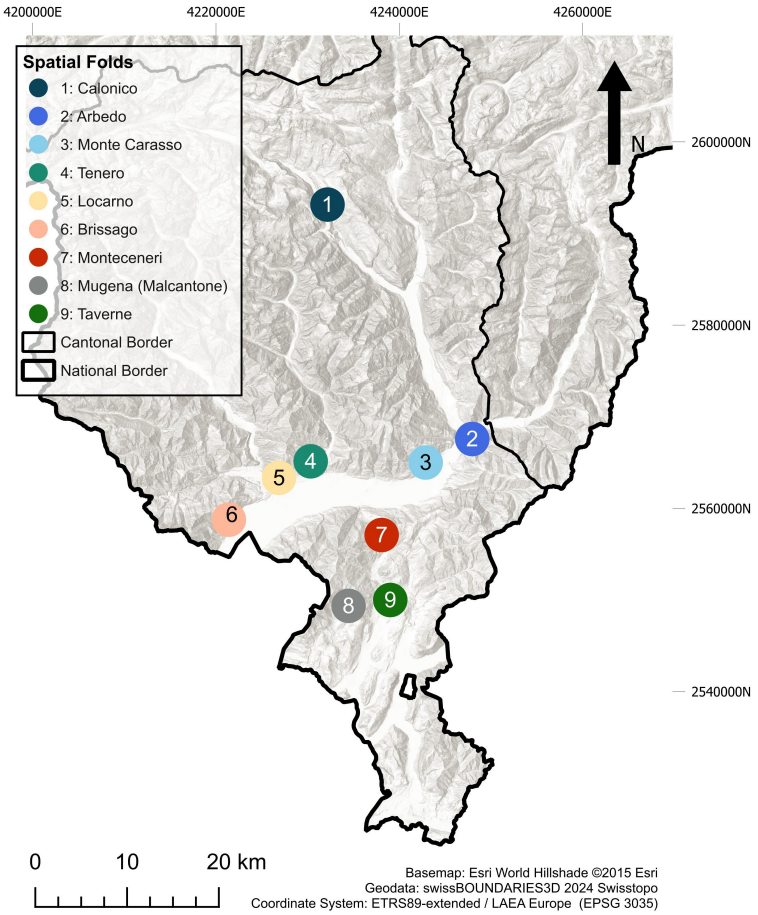

Figure 4.5: **Overview of the nine spatial folds for Leave-Location-Out Cross-Validation.** The manually selected folds ensure a minimum distance of 3.4 km between each fold. The sample sizes of tested sweet chestnut trees within a fold range from 17 to 135.

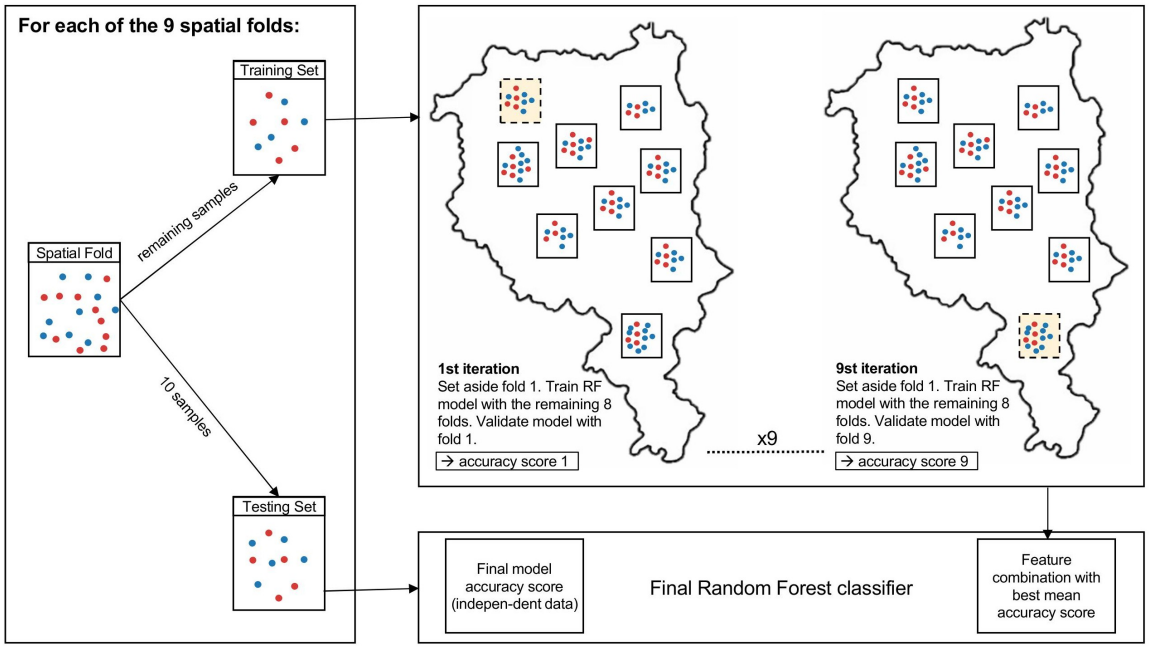

Figure 4.6: **Principle of Leave-Location-Out Cross-Validation** Other than traditional CV, LLO CV takes into account spatial dependence. The data is divided into spatial folds, ensuring a minimum distance between neighbouring folds. In each iteration, one fold is held out from the training process and used for validation. This procedure is repeated until every fold has been used once for validation.

Before conducting the LLO CV, the entire dataset was divided into a training set and a testing set. The testing set consisted of ten samples from each fold, the remaining samples from each fold were included in the training set. As visualised in fig. 4.6, LLO CV is part of the Python based evaluation of feature combinations and was executed in nine iterations. In each iteration, one fold of the training data was held out as a validation set, while the remaining eight folds were combined to train the model. The mean accuracy across all nine iterations was used to evaluate the performance of each feature combination, which was then compared to other combinations.

Once the final RF model was trained using the selected input features, its performance was evaluated using the testing set. This set consists of the total number of 90 held out samples (ten from each fold) and was not used within the feature selection process and the training phase. Instead, it was reserved to assess the final model's classification accuracy by comparing its predictions with the known labels of the samples.

The accuracy metrics used in this thesis include the precision, recall, and F1 score for each class, as well as the Overall Accuracy (OA). Precision is defined as the ratio of True Positives (TP) to the sum of TP and False Positives (FP) for each class:

$$precision = \frac{\mathrm{TP}}{\mathrm{TP} + \mathrm{FP}}$$

(Tatbul et al., 2018). This metric reflects the model's ability to correctly identify positive samples while avoiding false positives. Recall measures the proportion of actual positive samples that are correctly labelled as positive by the model. It is calculated as the ratio of TP to the sum of TP and False Negatives (FN) for each class:

$$recall = \frac{\text{TP}}{\text{TP} + \text{FN}}$$

(Tatbul et al., 2018). The F1 score provides a balanced evaluation of precision and recall, combining them using the following formula:

$$F_1 = 2 \times \frac{\text{precision} \times \text{recall}}{\text{precision} + \text{recall}}$$

(Dobrinić et al., 2022). Lastly, the OA of the model is calculated as the ratio of correctly classified samples (TP) to the total number of samples across both classes and serves as an overall measure of classification performance:

$$OA = \frac{\text{TP (over both classes)}}{\text{total number of samples (over both classes)}}$$

(Rösch et al., 2022).

Chapter 5

Results

5.1 Visual Analysis of Time Series and Boxplots

In general, the visual assessment of the individual bands and VIs aimed to give first insight into the data's characteristics. By plotting the data, certain trends and effects became more perceptible over time and are described next.

A comparative analysis of the plotted time series representing monthly means and additionally calculated standard deviations for the classes of non-symptomatic and symptomatic trees over the whole study area revealed that data contains the presence of outliers. The large effect of an outlier was particularly evident for the month of December 2017: High DN values were measured for bands on the 18th of December 2017 and lead to an overestimated mean value for both classes of non-symptomatic and symptomatic trees (see fig. 5.1). Less apparent was the outlier in the plotted VI values (see fig. 5.2).

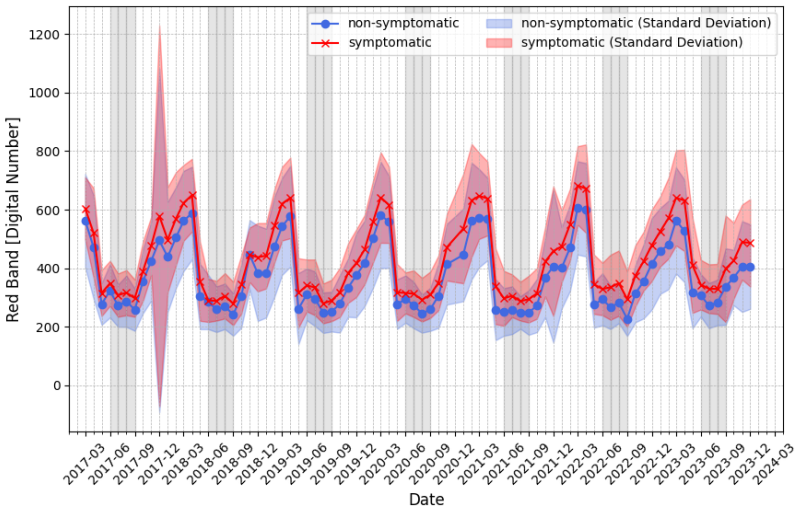

Figure 5.1: **Time series of monthly mean values for the Sentinel-2 red band.** Classified into non-symptomatic (blue) and symptomatic (red) sweet chestnut tree classes from 2017 to 2023. Intra-seasonal months (June to September) for the species are highlighted in grey. The plotted mean values, particularly those derived from the original bands, reveal the presence of outliers in the data.

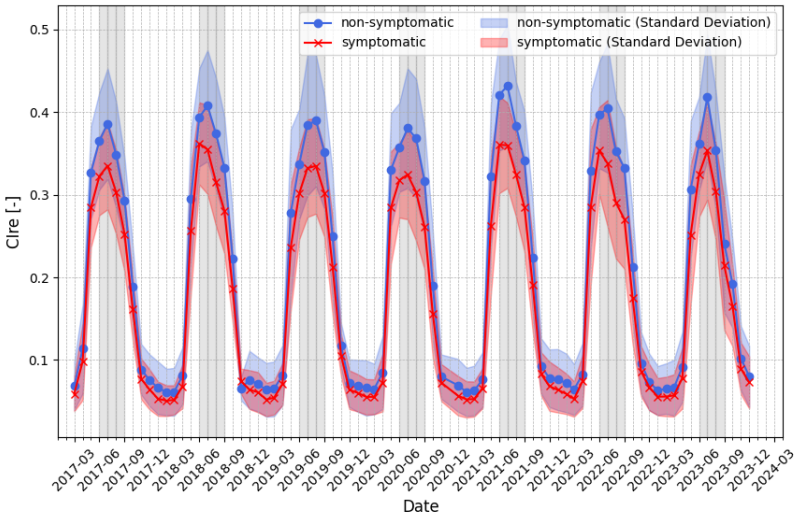

Figure 5.2: **Time series of monthly mean values for the Chlorophyll Index Red-Edge.** Classified into non-symptomatic (blue) and symptomatic (red) sweet chestnut tree classes from 2017 to 2023. Intra-seasonal months (June to September) for the species are highlighted in grey. Outliers in the VIs are less prominent compared to those in the original bands.

To reduce this observed occurrence of outliers, the metric was changed from monthly mean and standard deviation values to monthly calculated median values for the given classes. The plotted values showed consistent differences in the curves from at least June to September of every observed year. Notably, certain bands and VIs exhibited differences between classes even throughout the whole year. In general, the spectral band DNs for symptomatic trees were higher than those for non-symptomatic trees (see e.g., the pattern of the red band in fig. 5.3, except for the NIR and the RE3 band, where non-symptomatic trees displayed higher values. The VIs showed higher ratios for non-symptomatic trees than those for symptomatic trees. This is visually represented by the CIre in fig. 5.4. Particularly during the growing season, non-symptomatic trees consistently showed elevated values compared to symptomatic trees.

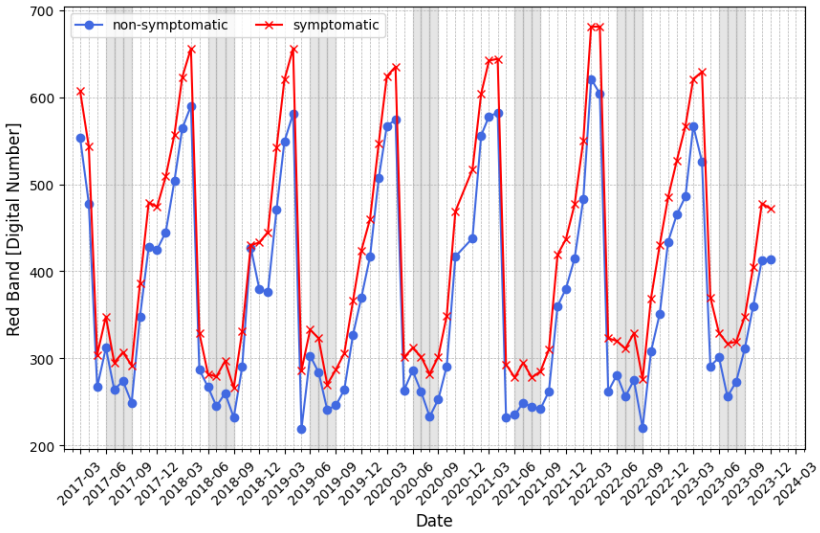

Figure 5.3: **Time series of monthly median values for the Sentinel-2 red band.** Classified into non-symptomatic (blue) and symptomatic (red) sweet chestnut tree classes from 2017 to 2023. Intra-seasonal months (June to September) for the species are highlighted in grey. In general, the spectral band DNs for symptomatic trees were higher than those for non-symptomatic trees.

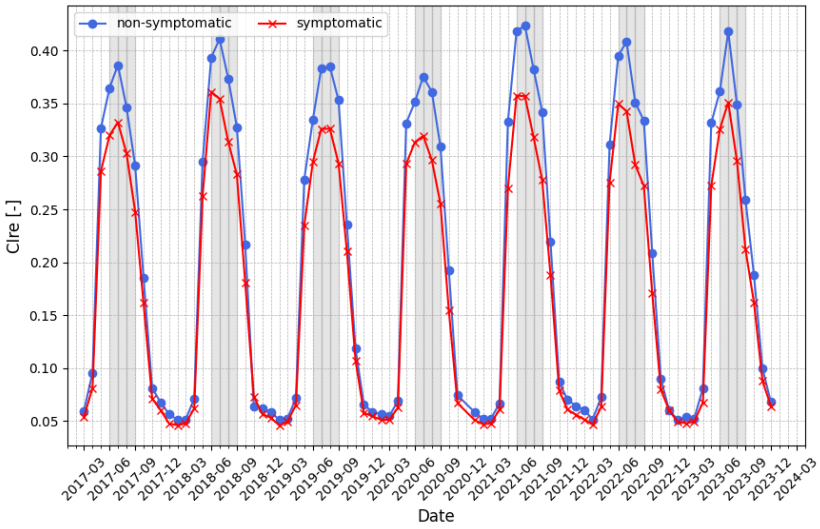

Figure 5.4: **Time series of monthly median values for the Chlorophyll Index Red-Edge.** Classified into non-symptomatic (blue) and symptomatic (red) sweet chestnut tree classes from 2017 to 2023. Intra-seasonal months (June to September) for the species are highlighted in grey. The VI show a consistent difference in the curves of the non-symptomatic and symptomatic classes between June to September across all years.

Besides an examination of the values generalised over the whole study area, additional class- and month-wise median values were calculated for each of the spatial folds. This examination revealed a spatial dependence in the measurements. While the medians calculated across all samples of the study area showed a general trend, no consistent overall structure or pattern became visible within the plots of fold-separated monthly medians. Data availability in general varied between the spatial folds and particularly in the winter months, the range of the median values varied across different spatial folds. When adding the trendlines, it became apparent that there is no visual distinction between trajectories of the two classes over all spatial folds. The slopes of the trendlines remained approximately stable over most years, resulting in a constant distance between them (see fig. 5.5). Only one spatial fold showed slopes differing between the non-symptomatic and symptomatic classes over the years: In Locarno, the difference between the classified values diverged over time. Taking the CIre values over seven years as an example, a clear decrease was observed for the symptomatic trees, while the trendline for the non-symptomatic trees showed a slight increase (see fig. 5.6). The trees were tested in 2019, when the decrease of CIre values for symptomatic trees could already be observed but getting lower for the following five years. When comparing the *SWISSIMAGE* data between the year 2012 and 2020 an increase in symptomatic trees could be observed. The trendlines of the remaining folds and VIs behaved in the same way as the shown example of the CIre.

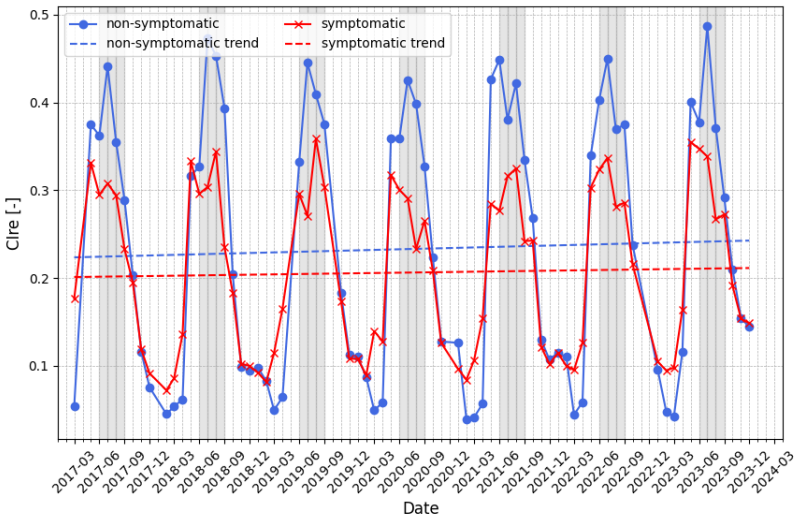

Figure 5.5: **Time series of monthly median values for the Chlorophyll Index Red-Edge in the area of Taverne.** Classified into non-symptomatic (blue) and symptomatic (red) sweet chestnut tree classes from 2017 to 2023. Intra-seasonal months (June to September) of the species are highlighted in grey. With the exception of the Locarno site fig. 5.6, the difference in the slopes of the trendlines for the median values between non-symptomatic and symptomatic trees remained almost constant over the seven years of observation.

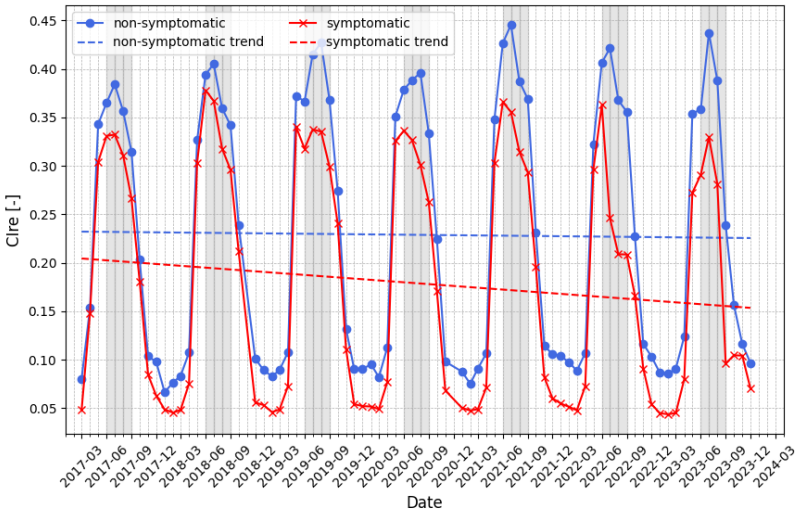

Figure 5.6: **Time series of monthly median values for the Chlorophyll Index Red-Edge in the area of Locarno.** Classified into non-symptomatic (blue) and symptomatic (red) sweet chestnut tree classes from 2017 to 2023. Intra-seasonal months (June to September) of the species are highlighted in grey. While the values for the non-symptomatic class remained constant over the seven years of observation, the values for the symptomatic class decreased over the same period.

In general, the boxplots of the monthly medians per band and VI further consolidated the findings from the time series analysis. A class-wise plotting of all samples showed different medians per class, with one class constantly having higher values than the other. The visualised distribution of individual measurements revealed considerable overlap in the data point ranges for both classes. In general, while in summer months, the differences between classes become more apparent (see fig. 5.7), the winter months showed smaller variance in data, as the trees are in a general state of reduced phytoactivity (see fig. 5.8).

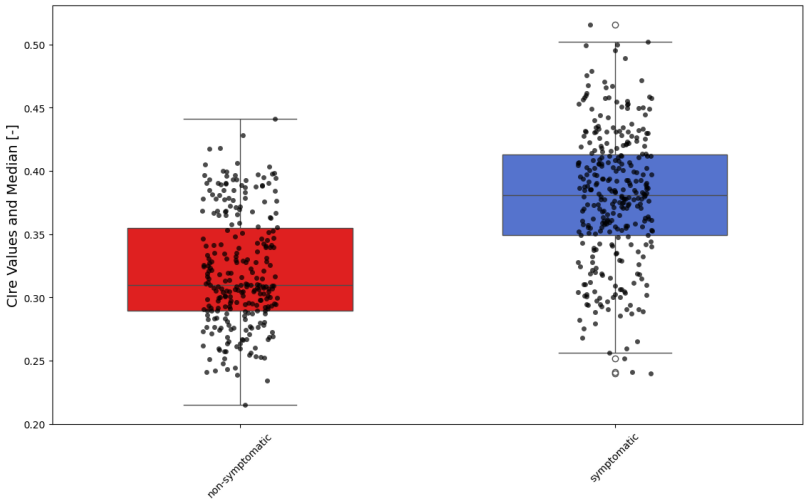

Figure 5.7: **Boxplots of monthly median values for the Chlorophyll Index Red-Edge for August 2021.** Classified into non-symptomatic (blue) and symptomatic (red) sweet chestnut tree classes. To improve readability, data points are randomly jittered along the x-axis within each class. In summer months, the differences between classes become more apparent.

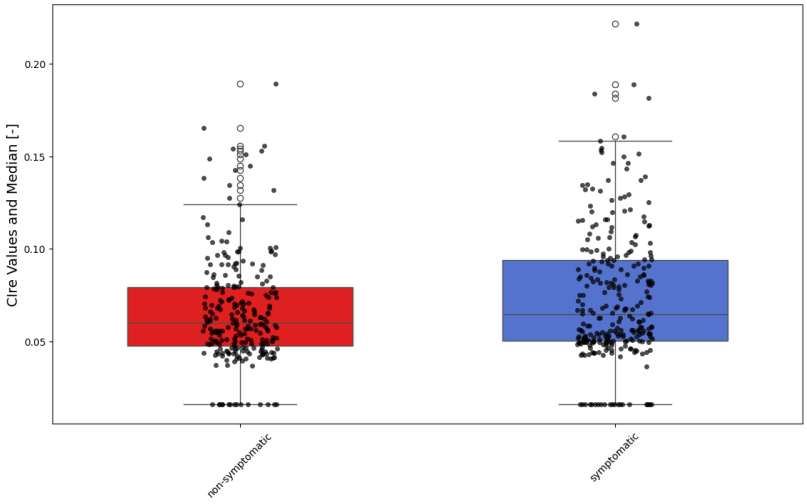

Figure 5.8: **Boxplots of monthly median values for the Chlorophyll Index Red-Edge for December 2021.** Classified into non-symptomatic (blue) and symptomatic (red) sweet chestnut tree classes. To improve readability, data points are randomly jittered along the x-axis within each class. Winter months generally exhibit smaller variance due to reduced phytoactivity.

5.2 Statistical Analysis of Features

Mann-Whitney U Test for Feature Assessment The Mann-Whitney U Test was conducted on a total of 1,296 band, respectively VI per month and year combinations to assess statistically significant differences between the measurements' distribution of non-symptomatic and symptomatic tree classes. The analysis revealed that 94.5% of these combinations show statistically significant differences, as indicated by p-values below 0.05. The total occurrences of "no difference"-combinations for each band or VI showed slight variability among the different features examined. Notably, the GNDVI and NDVIre consistently showed statistically significant differences between the two target classes (starting from March 2017 to December 2023), followed by several bands and VIs. In contrast, the EVI as well as the NIR and RE3 bands showed up to 15 instances of no statistically significant differences (see fig. 5.9). This evaluation provided a first impression into relevant features used for the RF input, highlighting differences between selected months and bands and VIs.

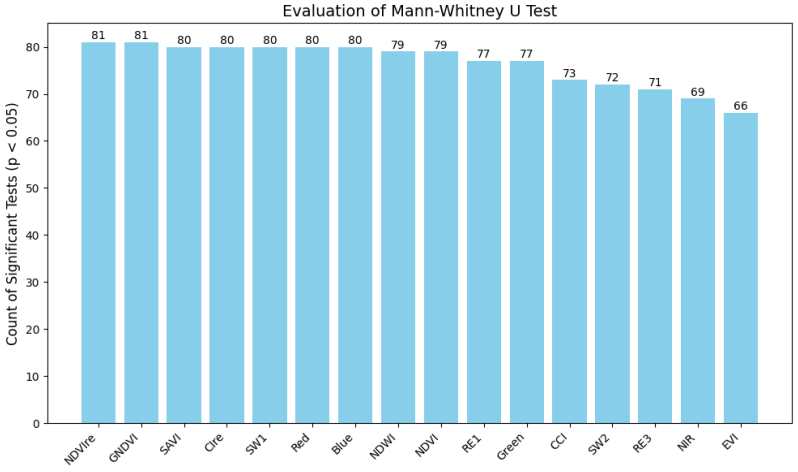

Figure 5.9: **Results of Mann-Whitney U tests.** The figure shows the number of occurrences where statistically significant differences (p-value < 0.05) were found between the distributions of measurements for each band, month and year combination. NDVIre and GNDVI consistently showed statistically significant differences between the two target classes, with a total of 81 significant results across twelve months over seven years (excluded are January 2017, February 2017, and December 2020 due to missing median values).

Cliff's Delta – Effect Size For further quantifying the magnitude of the difference in measurement distribution between classes, Cliff's Delta sizes were calculated for each band and index per month and year combination. Among the total combinations analysed, 6.9% exhibited absolute values greater than or equal to 0.47, indicating a large effect size when comparing the data of the two classes on a monthly base. To be noted is that 93.3% of these large effect sizes could be observed within the seasonal data for the months of June to

September, which is positive in regard to considering these values as input for training the RF model.

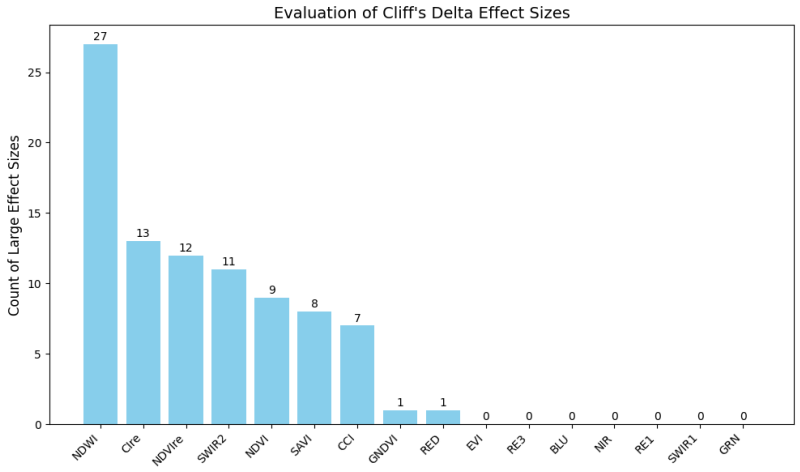

Figure 5.10: **Results of calculation of Cliff's Delta.** Represented is the number of occurrences where combinations of band, month, and year have large effect sizes (absolute values of Cliff's Delta ≥ 0.47). The NDWI shows the highest number of large effect sizes, with 27 occurrences across all month- and year-combinations, followed by CIre (13 occurrences), NDVIre (12 occurrences), SW2 (11 occurrences), and NDVI (9 occurrences).

A band-wise evaluation of the measure provided additional insights into the features. The NDWI showed to have the most occurences of large effect size by far, as 27 instances of the absolute Cliff's Delta values above or equal to 0.47 were recorded (see fig. 5.10). They were followed by several chlorophyll VIs as well as the SW2 band with occurrences ranging between eleven and 13 each. These findings suggested that these features were likely to be significant contributors to the classification tasks undertaken by the RF model. On the other side, the red, green, blue, SW1, NIR, and both RE bands, as well as the EVI showed to have no or one occurrence with large effect sizes, which was notable for further feature extraction.

5.3 Evaluation of Feature Combinations

A combined use of RFE, LLO CV and RF model was used to find the optimal feature combination in terms of both the number of features and specific input features. The selection of seven distinct features achieved the highest mean accuracy of 77.3%, along with the highest maximal accuracy of 81.2%, as observed during the LLO CV across all feature combinations. Notably, the accuracy showed a distinct peak at the number of seven features. With increasing count of features, the mean accuracies from the LLO CV decreased and stabilised between 19 and 23 features at a mean accuracy of approximately 73.0% to 73.0% (see fig. 5.11).

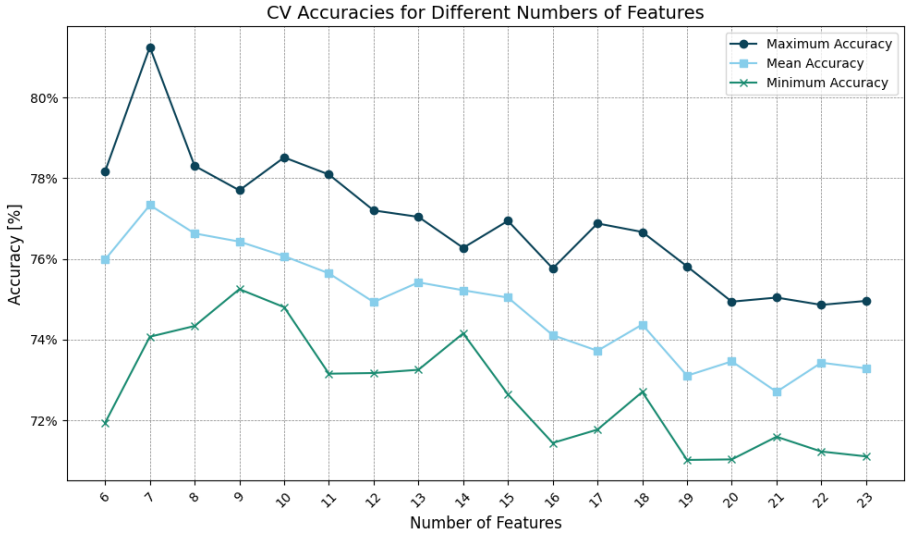

Figure 5.11: **Leave-Location-Out Cross-Validation accuracies for different numbers and combinations of input features.** The maximum, mean and minimum LLO CV accuracies were calculated to assess the performance of ten feature combinations, with the number of features ranging from six to 23. The final RF model was trained using a combination of seven input features, which achieved the highest accuracy of 81.2%.

The specific feature combination selected for further RF application is presented in table 5.1. The CIre, NDWI and the SW2 band appeared for two months each (CIre for August and September, NDWI for June and September, and SW2 for June and August) while the NDVIre index appeared for the month of August. Therefore, these stated VIs and the band were selected three times for the month of August and twice for each of June and September. The final model achieved an OA of 86.7%, with the non-symptomatic class having higher F1 and recall scores, while the symptomatic class achieved a higher precision score (see table 5.2). Therefore, the RF model is more effective at classifying non-symptomatic pixels, while it shows fewer misclassification for the symptomatic class (Tan et al., 2024).

Table 5.3 shows the output of the LLO CV for the final set of features. The accuracy values ranged from 53.1% for the spatial fold 1, which had 45 samples that remained for training the model, to 95.2% for the spatial fold 9, which had 21 remaining samples after the having been split into testing and training sets.

Table 5.1: **Feature importances of the seven features selected for training the final Random Forest model.** The feature importances range from 11.0% to 20.8%.

Feature Label	**Feature Importance (Final Model)**
CIre_month8	20.8%
NDVIre_month8	17.4%
SW2_month6	13.6%
CIre_month9	13.0%
NDWI_month9	12.9%
SW2_month8	11.3%
NDWI_month6	11.0%

Table 5.2: **Class-wise F1, precision and recall score for the final Random Forest model.** Accuracies calculated for non-symptomatic and symptomatic classified pixels.

	non-symptomatic	**symptomatic**
F1	88.9%	83.3%
Precision	85.7%	88.2%
Recall	92.3%	79.0%

Table 5.3: **Leave-Location-Out Cross-Validation accuracies of each spatial fold.** The variance in accuracy scores is large, as the number of training samples across the spatial folds differs to a large extent.

Nr.	**Label**	**Nr. of Training Samples**	**LLO CV-Accuracy**
1	Calonico	45	53.1%
2	Arbedo	48	70.5%
3	Monte Carasso	27	84.0%
4	Tenero	34	90.5%
5	Locarno	125	81.6%
6	Brissago	101	94.7%
7	Monteceneri	43	81.3%
8	Mugena (Malcantone)	7	57.1%
9	Taverne	21	95.2%

5.4 Classification

As described in section 4.3, areas predominantly covered by sweet chestnut forest within the focus sites were divided into 10x10 m pixels for further classification using the trained RF model. The classification results for these pixels are presented in the following sections:

Table 5.4: **Classification result of the Malvaglia focus site.** $n = 4,866$ pixels in total were classified. The column labelled with "2017-2023" indicates the n and % of pixels that kept the same labelled class over all the seven years. From the total n of classified pixels of the Malvaglia focus site, 32.9% showed this consistency.

Malvaglia		**2017**	**2018**	**2019**	**2020**	**2021**	**2022**	**2023**	**2017-2023**
Non-symptomatic	[n]	3,977	3,143	3,819	3,539	3,939	4,109	2,192	1,423
	[%]	81.7%	64.6%	78.5%	72.7%	80.9%	84.4%	45.0%	88.9%
Symptomatic	[n]	889	1,723	1,047	1,327	927	757	2,674	178
	[%]	18.3%	35.4%	21.5%	27.3%	19.1%	15.6%	55.0%	11.1%

Malvaglia For the focus site Malvaglia, 4,866 pixels were classified into non-symptomatic and symptomatic class with the trained RF model. The proportion for each class varied over the seven observed years, with a range between 15.6% and 55.0% for symptomatic pixels and 45.0% and 84.4% for the non-symptomatic pixels (see table 5.4). The highest proportion of symptomatic pixels, which was observed in 2023, followed the lowest proportion of symptomatic pixels in 2022. A clear pattern or evolution of symptomatic pixels could not be seen from the data. 32.9% of the pixels had the same class label over the seven years, of which 88.9% were of the non-symptomatic class and 11.1% of the symptomatic class. The spatial analysis shows an above-average number of pixels along watercourses being classified as symptomatic (see fig. 5.12). Two streams that divide the whole focus site into three vertical zones could be recognized in the classification pattern, especially from 2018 to 2022 and in 2023. Furthermore, it became apparent that the lower part of the focus site was generally more affected by symptomatic classified pixels over the entire period, while the higher part of the focus site showed predominantly non-symptomatic areas, with exception of the watercourses. Particularly prominent was the classification in 2023 which results in the lower part of the slope showing symptomatic signs over the entire focus site.

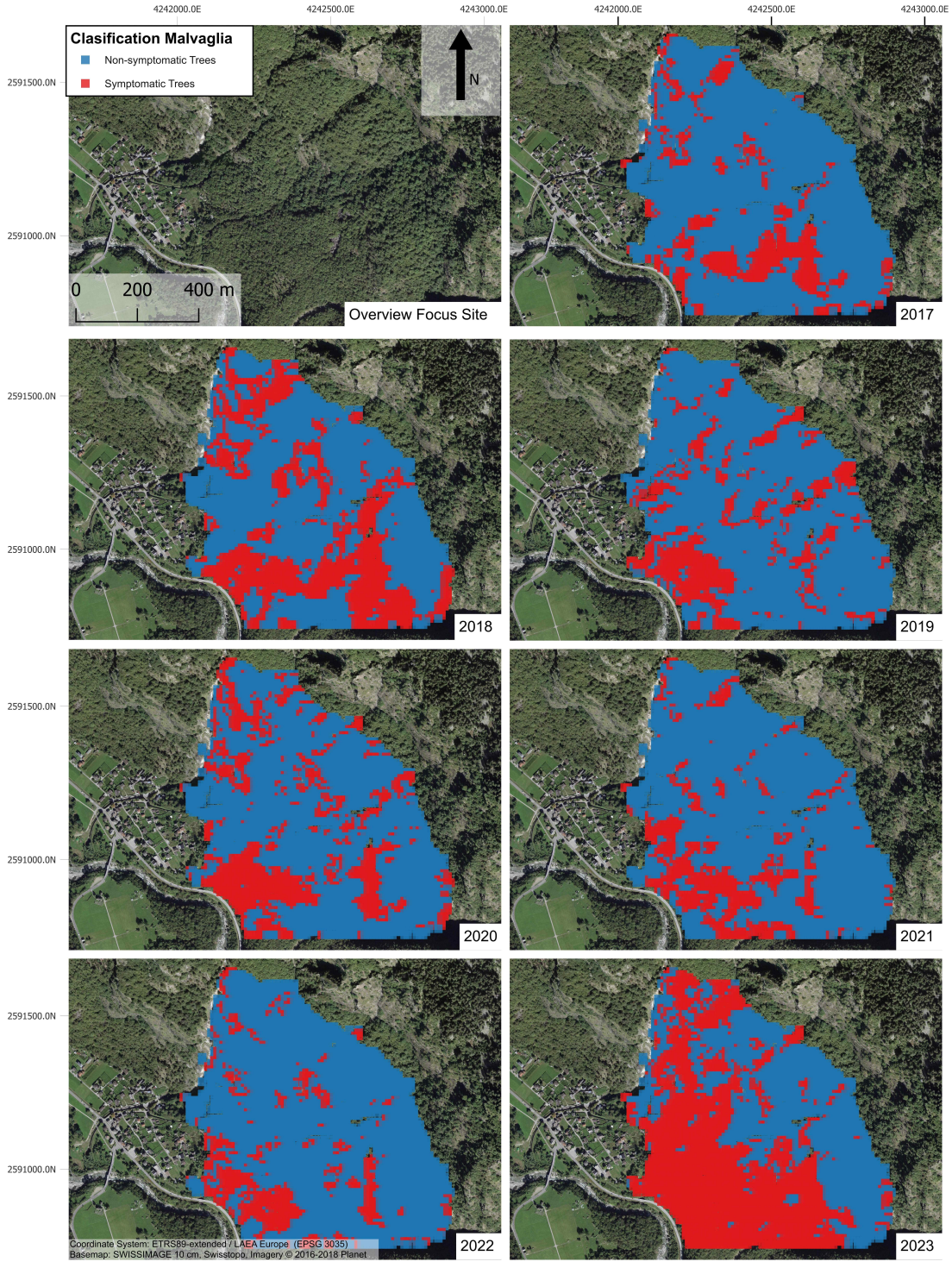

Figure 5.12: **Classification of sweet chestnut for the focus site Malvaglia.** Selected pixels from the focus site of Malvaglia were classified as either symptomatic (red) or non-symptomatic (blue) for each year from 2017 to 2023. A core area of symptomatic pixels was observed in the lower part of the site. Additionally, two streams that divide the site into three vertical zones were observed in the classification pattern.

Table 5.5: **Classification result of the Taverne focus site.** $n = 4,758$ pixels in total were classified. The column labelled with "2017-2023" indicates the n and % of pixels that kept the same labelled class over all the seven years. From the total n of classified pixels of the Taverne focus site, 25.8% showed this consistency.

Taverne		**2017**	**2018**	**2019**	**2020**	**2021**	**2022**	**2023**	**2017-2023**
Non-symptomatic	[n]	2,068	3,297	4,164	2,441	3,792	2,101	1,987	1,027
	[%]	43.5%	69.3%	87.5%	51.3%	79.7%	44.2%	41.8%	83.7%
Symptomatic	[n]	2,690	1,461	594	2,317	966	2,657	2,771	200
	[%]	56.5%	30.7%	12.5%	48.7%	20.3%	55.8%	58.2%	16.3%

Taverne The classification for the focus site Taverne included 4,758 pixels. The proportion per class varied among years, from a minimal proportion of 12.5% of symptomatic pixels to a maximal proportion of 58.2% for symptomatic pixels (see table 5.5). As for the focus site Malvaglia, the maximal proportion occured in 2023, whereas the minimal proportion was observed in 2019. For three of the seven observed years, the proportion of symptomatic classified pixels was over 50%, which is a high rate compared to the other two focus sites. 25.8% of the pixels had the same class label over the seven years, while 83.7% of them were of non-symptomatic class and 16.3% of symptomatic class. As for the focus site Malvaglia, no clear pattern of evolution of the symptomatic class could be detected for the focus site Taverne. The visual assessment revealed that the distribution of non-symptomatic and symptomatic pixels changed from year to year and did not show any consistent development (see fig. 5.13). In 2017, 2020, 2022, and 2023, the spatial spread of symptomatic classified pixels was significantly greater than in other years. A clear separation into non-symptomatic and symptomatic regions was not possible in any of the years, as the classes were evenly distributed over the entire foot of the mountain. Even if the focus site Taverne included several streams, there was no clear clustering of symptomatic pixels along the watercourses, in contrast to what was observed in the focus site Malvaglia.

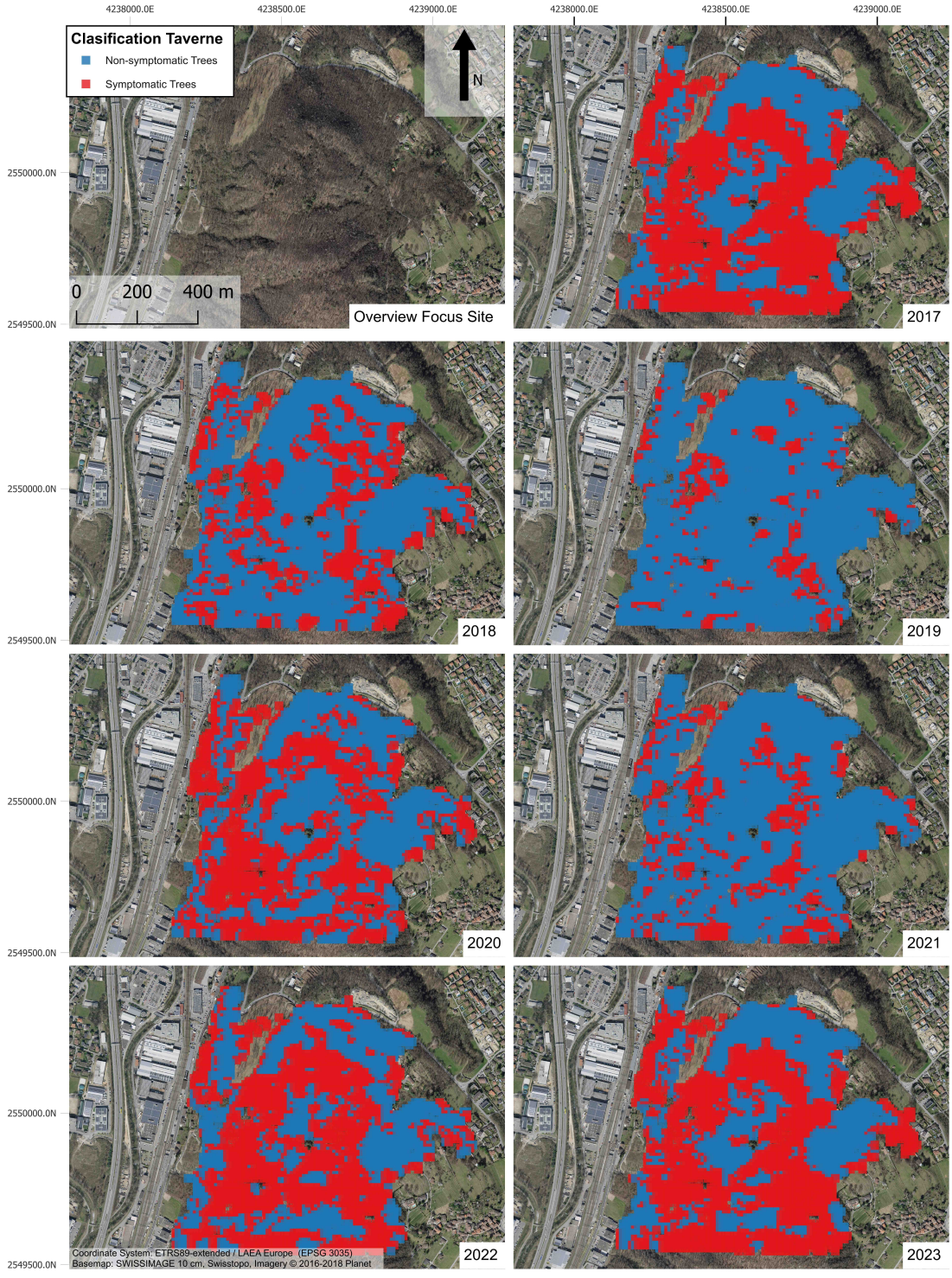

Figure 5.13: **Classification of sweet chestnut for the focus site Taverne.** Selected pixels from the focus site of Taverne were classified as either symptomatic (red) or non-symptomatic (blue) for each year from 2017 to 2023. A clear separation into class regions was not possible in any of the years, as they were evenly distributed along the entire foot of the mountain.

Table 5.6: **Classification result of the Malcantone focus site.** $n = 4,483$ pixels in total were classified. The column labelled with "2017-2023" indicates the n and % of pixels that kept the same labelled class over all the seven years. From the total n of classified pixels of the Malcantone focus site, 44.4% showed this consistency.

Malcantone		**2017**	**2018**	**2019**	**2020**	**2021**	**2022**	**2023**	**2017-2023**
Non-symptomatic	[n]	2,424	3,380	4,209	3,864	3,698	3,036	3,122	1,847
	[%]	54.1%	75.4%	93.9%	86.2%	82.5%	67.7%	69.6%	92.7%
Symptomatic	[n]	2,059	1,103	274	619	785	1,447	1,361	145
	[%]	45.9%	24.6%	6.1%	13.8%	17.5%	32.3%	30.4%	7.3%

Malcantone The classified targets for the focus site Malcantone included a total of 4,483 pixels of which the symptomatic class ranged from 6.1% in 2019 to 45.9% in 2017 (see table 5.6). About 44.4% of the classified areas had the same labels over all seven years, of which 92.7% belonged to the non-symptomatic class and 7.3% to the symptomatic class. Although a clear pattern of evolution of the labeled classes could not be seen, the general proportion of symptomatic classified pixels was smaller compared to the other two focus sites. A visual assessment of the classification result showed that in general, pixels in the valleys and the south-western facing slope were mostly classified as symptomatic, while the eastern facing slope was mainly classified as non-symptomatic over all seven years (see fig. 5.14). The valleys as well as the south-western facing slope included several watercourses that converge in a stream towards the inhabited zone of Vezio and Mugena. The general pattern of the distribution of non-symptomatic and symptomatic pixels remains more or less the same over the years, with a higher presence of symptomatic pixels in 2017 and 2018, a decreased presence between 2019 and 2021 and in the last two years of the analysis again an increased presence of symptomatic pixels.

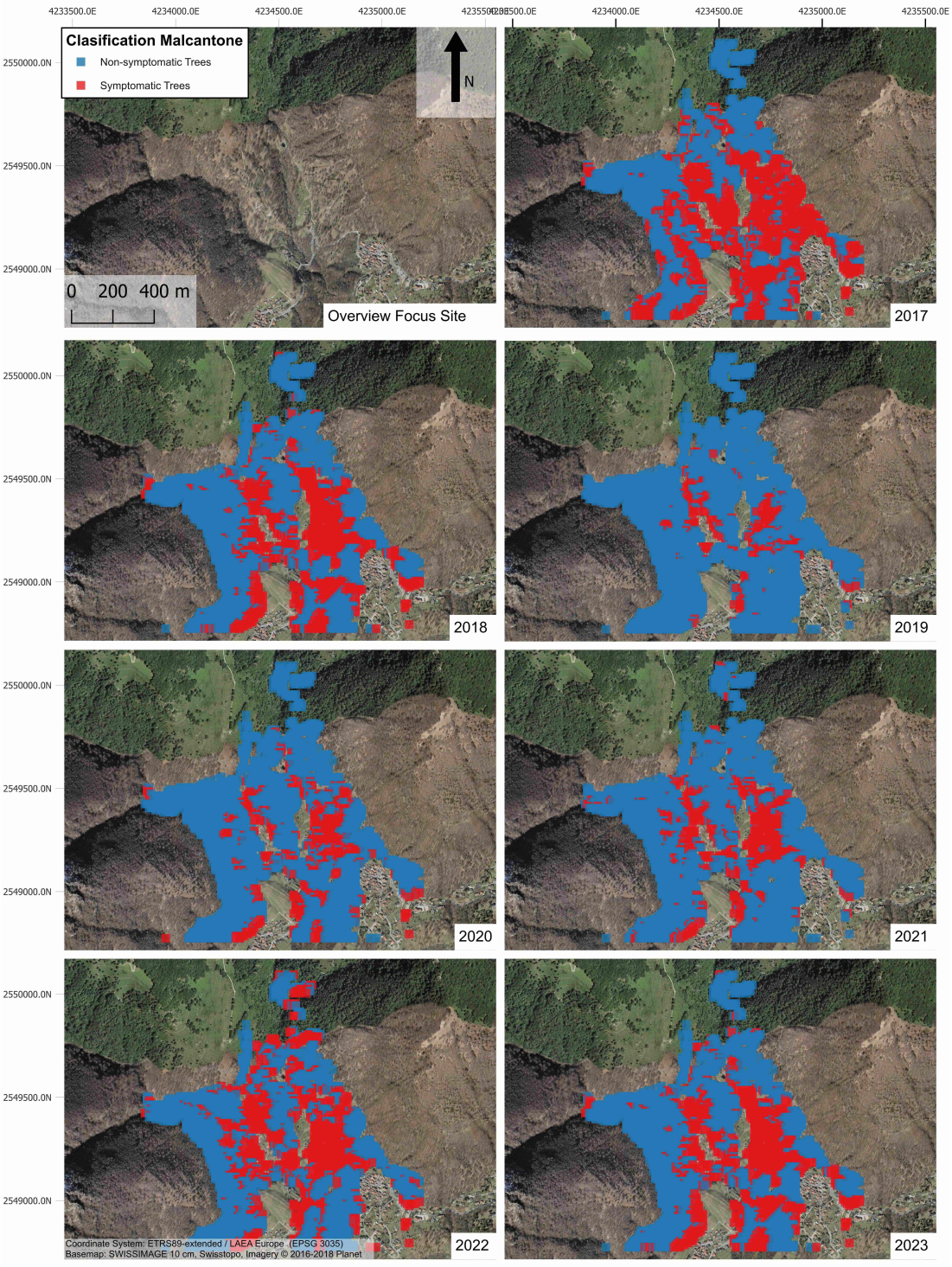

Figure 5.14: **Classification of sweet chestnut for the focus site Malcantone.** Selected pixels from the focus site of Malcantone were classified as either symptomatic (red) or non-symptomatic (blue) for each year from 2017 to 2023. Pixels in the valleys and the south-western facing slope were mostly classified as symptomatic, while the eastern facing slope was mainly classified as non-symptomatic over all seven years.

Chapter 6

Discussion

6.1 General Aspects of the Approach

The final approach of this thesis included the following steps: By using preprocessed Sentinel-2 data from 2017 to 2023 and sampled tree data, a RF model was trained to classify selected pixels covered by sweet chestnut into symptomatic or non-symptomatic classes regarding ink disease. This classification was conducted across three selected focus sites. The process included a complex approach using RFE and LLO CV to select the optimal number and combination of input features. Parallel to the ML approach, Sentinel-2 bands and VIs were analysed both visually and statistically over time to gain insights into the data and its characteristics.

The final results included annual classification maps from 2017 to 2023 for the three focus areas, with pixels categorized as either symptomatic or non-symptomatic in relation to ink disease. An in-depth analysis of bands and VIs revealed distinct features that were useful for identifying symptomatic trees. Key factors in this process were the high-quality Sentinel-2 data (exceeding the standard 2A-level) from Koch et al. (2024b), the thorough generation of training areas from sampled tree data including rigorous refinement procedure and a systematic, computationally optimised approach to find the optimal feature combination for training the RF model. The following sections provide a detailed description of these results.

6.1.1 Visual Analysis

The consistent plotted difference between the monthly medians from 2017 to 2023 of non-symptomatic and symptomatic classes of sweet chestnut trees for each band and VI is in general positive regarding the chosen RF approach. Nevertheless, in literature either a short death of a tree within five to 15 years or a general state of declining vitality over many years is found in the course of ink disease (Prospero et al., 2023). Against expectation, most of the visualised time series over seven years did not exhibit any decreasing VI medians or increasing band medians for symptomatic trees, which would have indicated a rapid decline. A possible explanation for the absence of such a progression in the measured values is that trees showing larger phytosanitary deficiencies may result in compensatory branch production (epicormic shoots) or in a richer growth of vegetation on the ground because of the larger amount of light passing through the damaged crown, resulting in spectral mixing

(see Guzmán Q. et al., 2023; Prospero et al., 2023). To conclude, a distinct signal about the course of a symptomatic tree in terms of the time series cannot be taken.

In contrast to the behaviour observed in all the other spectral bands, the NIR and RE3 band showed lower spectral DN values for symptomatic trees than non-symptomatic trees. This difference of the bands confirm reports in the literature. For example, Pádua et al. (2020) who assessed ink disease by using UAV-based data, observed lower reflectance values (DN = 10,000 * Reflectance, see ESA (2024)) for the wavelength regions starting from approximately 720 nm for trees having nutrient deficiencies (see fig. 6.1). These observed differences were explained by the changes in optical properties of the trees due to their reduced vitality (Pádua et al., 2020). While lower chlorophyll content in the leaves of diseased trees leads to higher reflectance values in the visible range, the NIR range (700–1,100 nm) is sensitive to changes in leaf structure, such as the thickness of intercellular space or cell membrane. Such structural changes in the leaves of symptomatic trees result in lower reflectance in the NIR band (Wong, 2023). Furthermore, the lower RE3 values for symptomatic trees result from reduced water content within the leaves. Since the SWIR range (1,100–2,500 nm) is sensitive to changes in water content, the observed lower DNs in the RE3 band indicates reduced water within the leaves of diseased trees (Wong, 2023).

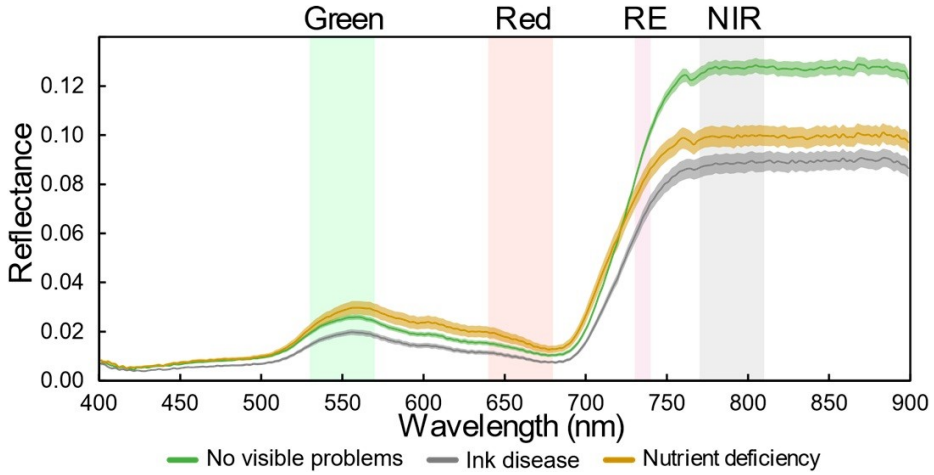

Figure 6.1: **Reflectance spectra of trees in varying health conditions.** "No visible problems" (green), "Ink Disease" (grey) and "Nutrient deficiency" (yellow). Lower reflectance values can be observed for trees with nutrient deficiencies, as well as those affected by ink disease, in the wavelength regions starting from approximately 720 nm (RE and NIR range). In the visible range, trees with nutrient deficiencies exhibit higher reflectance values compared to both non-symptomatic trees and those with proven ink disease. Image source: Pádua et al. (2020).

In general, the visual analysis contributed substantially to making preliminary decisions regarding the data processing between the raw DN values (bands) and ratios (VIs) to its use as input features for the RF model. The outliers, identified through plots of monthly

means, led to the decision of using median values for aggregating data on a monthly basis. As demonstrated in section 5.1, the median proved to be a robust statistical measure that effectively reduced the impact of extreme values and outliers. Furthermore, the decision to consider only data monitored between June and September of each year was consolidated by the visual assessment as the measurements during winter months showed to be less reliable and differences between classes became less distinct (see fig. 5.4). Especially in context of spatial dependence, differences between spatial folds became more pronounced between December and February. The boxplots provided valuable insights to prepare the RF classification and further feature selection applications. The visualised distribution of the data made apparent the difficulty in achieving a clear classification, as samples from both classes mostly showed only slightly differing spectral responses. This finding supported the decision to apply LLO CV and RFE as a method for selecting the most relevant input features for training the RF model to enhance the availability to clearly distinguish between the two defined classes.

6.1.2 Important Features

A comparison of the results from the statistical pre-evaluation of features and the results of the evaluation of feature combinations by LLO CV mainly showed that the two different approaches to measuring a feature's relevance for classification led to distinct, but nonetheless insightful results. The statistical analysis using Cliff's Delta for effect sizes showed that the monthly medians of NDWI occurred most frequently, followed by CIre, NDVIre, the SW2 band, NDVI, SAVI and CCI (see section 5.2). Surprisingly, the seven final features selected by using RFE, LLO CV and RF were exactly a combination of the top four VIs having the most occurrences of large effect sizes. Therefore, both evaluation methods identified similar key parameters, namely the NDWI, CIre, NDVIre, and the SW2-band.

While this evaluation is not without its uncertainties, it provided fundamental insights into the classification of sweet chestnut trees showing visual symptoms of ink disease. The high ranking of NDWI, especially within the statistical analysis, suggests that variations in leaf water content are a particularly strong signal for distinguishing trees affected by visual phytosanitary issues (Gao, 1996). Furthermore, as expected from the literature, chlorophyll-based VIs generally showed large effect sizes and significant differences between non-symptomatic and symptomatic classes. The expected importance of the SW2 band was also confirmed in both the statistical pre-analysis and the RF feature importance analysis. When compared to the findings of Sebastiani et al. (2024), which also aimed to detect ink disease and identify sweet chestnut trees with phytosanitary issues, the importance of VIs based on RE bands is highlighted. This is consistent with the results of this thesis, where both the NDVIre and CIre appear among the four most important features in the RF model, with the CIre even appearing twice. In contrast to Sebastiani et al. (2024), the NDWI was ranked higher in this thesis than the GNDVI, which was also included in the given set of VIs used in the compared study. These differences illustrate again that the selected features can vary depending on the specific circumstances and parameters of each study.

A general observation is that water and greenness VIs tend to achieve higher effect sizes

and feature importances than individual bands. Nevertheless, including the RE and SWIR bands further improved the classification model, as these bands were consistently selected across multiple months. The predominance of VIs in the feature selection process can be explained by the fact that VIs, calculated using original band values, target specific vegetation parameters (such as water or chlorophyll content) (Xue & Su, 2017), making them particularly suitable as input features for the RF model.

6.1.3 Leave-Location-Out Cross-Validation

In general, the specific LLO CV approach applied for the validation of feature combinations was chosen to reduce spatial influence. Subsetting the samples into folds based on their spatial distribution resulted in largely differing fold sizes, ranging from 17 to 135 samples. The decision to choose ten samples for each fold for testing helped to maintain an evenly distributed evaluation of the model's performance and with this to have a most possible generalised accuracy. Nevertheless, using the remaining samples for selecting the input features led to some issues to consider for the interpretation of the CV scores within the RFE-process. The training set of larger-sized folds has more impact on model training, as the amount of remaining data after the removal of test samples is higher. This becomes apparent when observing the accuracy scores during the validation of feature combinations in section 5.3. The high variance in scores again highlighted the spatial dependence of training data, which remains a crucial difficulty in the context of the diverse topographic characteristics of the study area.

6.1.4 Distinction of Non-symptomatic and Symptomatic Trees

The classification results across the three focus sites do not reveal an increase of symptomatic trees over the observed years. The proportion of symptomatic pixels shows irregular patterns in each area, making it difficult to state any clear trends. An in-depth analysis of the classification results is therefore not meaningful and would be based on too many assumptions. Nevertheless, some noteworthy observations can be made.

In general, most pixels were classified as non-symptomatic across all three focus sites. Except for 2017 and 2023 in Taverne, and 2023 in Malvaglia, the proportion of non-symptomatic pixels is higher than the proportion of symptomatic areas. This trend is particularly visible when analysing the class distribution over the seven-year periods, where non-symptomatic pixels are more frequently assigned to the same classification over the whole time, with proportions of at least 79.0%. This suggests that the RF model is particularly effective at identifying sweet chestnut that show no visible symptoms of phytosanitary deficiencies.

When focusing on the topographic conditions, it becomes apparent that symptomatic pixels are more frequently found in lower regions of steep slopes, while non-symptomatic pixels are predominantly found at higher elevations. This pattern is most prominent at the Malvaglia site but can also be observed to some extent in Malcantone. In contrast, the flatter site of Taverne, which has not as many differences in height as the other two

sites, shows a more even distribution of both non-symptomatic and symptomatic pixels. An enhanced occurrence of ink disease-affected trees in lower slope regions is consistent with existing literature, which analyses the dispersion pattern of *P. cinnamomi*. The pathogen's spread is influenced by water flow within the soil, which generally moves downslope. Given the condition that symptomatic chestnut trees are present uphill, water flows facilitate the accumulation of the pathogen in lower slope regions. These pixels tend to have higher soil moisture which favours the spread of the disease (Cardillo et al., 2018). The higher occurrence of symptomatic pixels at the foot of slopes may be influenced by topographical factors, such as proximity to streets and buildings where human activity could have introduced the pathogen (Vannini & Vettraino, 2001). Whether the observed tendency for symptomatic pixels to be concentrated in lower slope regions effectively stems from ink disease, or is due to abiotic factors, such as drought, hail, other diseases, can only be confirmed through isolation of the pathogens in the laboratory (Prospero et al., 2023).

A further observation concerns the presence of watercourses within the three focus sites. Particularly in Malvaglia, symptomatic classified pixels are often found near streams. Similarly, in Malcantone, the western-facing slope, which is traversed by multiple watercourses shows a higher proportion of symptomatic pixels compared to the eastern-facing slope, which has no streams on the slope, but only in the valley. As for the enhanced symptomatic classification in lower slopes, the observation aligns with the known spread of *Phytophthora* via watercourses, which increases the likelihood of symptomatic classified pixels being found near streams (Marzocchi et al., 2024). However, it is important to mention that other factors, such as shadows, stony subsoil, differing vegetation near the streams, or the aspect of slopes, may also influence the spectral signals and with this the classification results (Liu et al., 2024).

A general observation across all three focus sites is the persistence of core classified pixel areas over the whole analysis period, expanding more or less over distinct years. Especially the core areas classified as symptomatic are particularly valuable for planning further field sampling as they represent the most consistent sites for disease detection. The non-symptomatic core areas are valuable as well. As the examples of the eastern-facing slope in Malcantone shows, such consistent non-symptomatic core areas help to prioritise field sampling work by excluding these regions from testing. Additionally, the observation of sites with no apparent signs of reduced vitality contributes to the knowledge about potential future forest management, as these forest areas represent a high ecological value that could serve as example for maintaining forest health.

6.2 Limitations of the Approach

6.2.1 Topography of Ticino

The topographical challenges of the study area, in particular the presence of deep alpine valleys with steep slopes, are an issue that substantially impact classification outcomes. Discrepancies arise from non-representative measurements, as the angle at which the sensor's signal interacts with the Earth's surface can lead to distortions. Additional geometry

correction steps are therefore crucial to deal with effects such as light exposure and shadowing caused by a terrain's characteristics. Nevertheless, such corrections cannot fully compensate the topographical effects on the spectral signal. This leads to approximations of values which influence the pixel-based evaluation of a tree's health (Chen et al., 2023).

Moreover, classifying the whole of the Canton of Ticino presents considerable challenges due to the diverse patterns of the landscape and topography. Given the 10 m spatial resolution of Sentinel-2, it is difficult to achieve a precise detection of pure forest pixels. The use of auxiliary data sets such as the *VHM* or the *Tree Species Map of Switzerland* helped to refine the classification process and extract areas with higher probability of containing pure sweet chestnut populations. The existing studies, which were conducted in predominantly flat areas or even in sweet chestnut plantations, operate on terrain that allows for the extraction of pure, single pixels of sweet chestnut trees (see Pádua et al., 2020; Sebastiani et al., 2024). Compared with this thesis' given prerequisites, the extraction within mixed forests and changing sub-ground types is of different complexity and leads to higher levels of uncertainty in the classification.

6.2.2 Data Availability

The choice of data was limited by the availability of training samples. As discussed earlier in this thesis, the general set of sampled tree data collected was not optimal regarding the objectives of this thesis. Notably, over 50.0% of the samples were collected in 2013, which all had to be discarded, as the preprocessed Sentinel-2 imagery was only available since 2017 (Koch et al., 2024b). Initially, the use of PlanetScope data (PBC, 2024), which offers a higher spatial resolution of 3x3 m and includes imagery from 2013, was considered. However, as the given data set of Sentinel-2 time series is of very high processing quality and comparison studies showed that PlanetScope data did not significantly improve classification results (Rösch et al., 2022), Sentinel-2 images were ultimately selected as the preferred data source. In general, a joint use of different types of data, such as additional Synthetic Aperture Radar (SAR) data and high and mid-resolution multispectral data, has been shown to achieve best results in vegetation monitoring tasks but would have expanded the scope of this thesis (see Niculescu et al., 2018; Sebastiani et al., 2024; Wang et al., 2015). Moreover, PlanetScope would not have been freely available (Rösch et al., 2022), which is a further concern in regard to the research question. Also, alternative data sources, such as *SWISSIMAGE* or Light Detection and Ranging (LiDAR) data, were unsuitable for the task of performing annual classifications from 2017 to 2023. *SWISSIMAGE* data is only captured every three years, while LiDAR data is captured every six years, making both insufficient for the required temporal resolution (Swisstopo, 2022, 2023).

6.2.3 Scope of Optical Remote Sensing

A significant limitation of using optical RS data for monitoring forests is that it primarily allows to assess trees based on their visible condition, but the detection of the presence of pathogens itself, causing the ink disease, is not feasible (Sebastiani et al., 2024). Consequently,

a verification with field sampling and laboratory analyses is still necessary and the approach only detects trees that show signs of infection, while the actual presence of the disease remains uncertain. Other factors, such as drought or hail, also factor into diminished tree vitality that further complicates the interpretation of visual symptoms (Wong, 2023). Consequently, testing in site remains necessary for definitive diagnosis. Additionally, ink disease may show either a rapid or a slow progression depending probably on the vitality of a tree or the amount of inoculum present in the soil (Prospero et al., 2023). The time series of seven years used within this thesis did not reveal any distinct evidence of a rapid declining tree vitality or tree mortality based on the spectral data. Nevertheless, conducting a long-term analysis over more than seven years may provide further insights into patterns of tree decline and disease progression.

6.2.4 Training Areas

Having a very limited number of training samples was one of the main obstacles in this thesis and may be a common problem for invasive, still not widespread pathogens. The final training dataset consisted of a combined approach of using initial sampled data, extending and splitting up its area, and removing as well as adding some training areas by visual assessment of *SWISSIMAGE* data. This mixed approach is suboptimal but was necessary to ensure a training dataset accurately representing the two target classes of non-symptomatic and symptomatic trees. Furthermore, literature supports the effectiveness of visually selecting training areas, demonstrating that this approach can lead towards significant results and is a considerable method for sample refinement and expansion (see Guzmán Q. et al., 2023; Tan et al., 2024). Nevertheless, the described issue highlights the importance of a well-adapted tree sampling strategy that corresponds to the RF training process. Tree sampling in the real world is not only labour- and cost-intensive but also constrained by practical limitations. For example, in southern Switzerland, the distribution of ink disease is known to be patchy rather than uniform (Prospero et al., 2023). In general, ML applications always require more data, and their maximal feasibility is limited (Viana et al., 2019). To find a balance between the demands for the data analysts and the resources of the researchers in field is a general challenge that became clear over the course of this thesis.

Besides the already limited number of sampled tree data, the spatial distribution of tested trees presented another significant challenge. Invasive pathogens, particularly at the early stages of their spread, are rarely distributed evenly across the landscape. They typically spread from specific points of introduction, which are often linked to human activity and therefore need some time until they are distributed over a whole area (Cardillo et al., 2018). Additional to this biotic-driven challenge,the tree sampling involved a strategical approach of sampling in general 15 trees per test site, originating from three different types of starting positions (see section 3.1). While this approach is well-established for biological research, it does not entirely meet the requirements for optimal ML model training. Specifically, the samples are unevenly distributed in spatial clusters, making the dataset prone to overfitting (Belgiu & Drăguţ, 2016). The effect of spatial overfitting can be observed when analysing the results of the LLO CV. In this approach, each fold is used once for validation, and the

resulting accuracies of the RF classifier can be compared across all folds (Meyer et al., 2018). The large variation in CV-accuracies for each spatial fold of the final feature combination (e.g., Taverne, Brissago, or Tenero, all which had LLO CV scores above 90.0 %, compared to e.g., Calonico, Mugena (Malcantone), where LLO CV scores were below 60.0 %) shows that the spatial distribution and the spatial dependency of the training data makes it difficult to train a generalised model for the whole area of Ticino.

Due to spatial overfitting and clustered training samples, topographical input features were excluded from the classification approach. Although the literature highly recommends the use of terrain-related parameters (e.g., slope, terrain height, aspect) (see Rösch et al., 2022; Xiong et al., 2023), such input features were not considered within this thesis. This because preliminary analyses revealed that including such features was rather misleading and did not contribute to the model training. A deeper insight into the data revealed a significant bias in the tested samples, as no data was tested from slopes with a north exposure. Therefore, the use of such topographical variables would have led to a bias into the model and would have led to an overdependence of the classifier on local terrain features (Meyer et al., 2018).

Chapter 7

Impact of the Work

This Master's thesis evaluates the use of Sentinel-2 data combined with field sampled tree data for monitoring the spread of ink disease in sweet chestnut stands in the Canton of Ticino. Despite the challenges discussed above, particularly limited amounts of data and topographical factors, the thesis presents a straight-forward approach and in-depth analysis for monitoring tree disease in forests, with a customised processing pipeline for a direct application.

The selection of RF as the classification model is suitable for this task, given the diverse set of features derived from the Sentinel-2 time series. The characteristic will become even more significant in future applications, as time series will be available over longer time spans in respect to the ongoing Copernicus programme of ESA. Further, the implemented model generally demonstrates solid accuracy metrics and is a reliable base for future projects, particularly with new sampling data or in different study areas.

The products resulting from this work aim to support ongoing research on the occurrence and spread of ink disease in Switzerland. The derived classification maps can be used as a guideline to select potentially affected areas, which will then be validated through field sampling methods. The ground-truth data will serve as feedback to refine and improve the maps, approaching towards the aim of a comprehensive and accurate map identifying sweet chestnut trees affected by ink disease in Ticino.

This thesis highlights the significance of a joint effort between different fields of research and initiated the path for future collaborative projects. These efforts will contribute to an advanced progression of alternative methods for disease detection. Through the strengthened relationship between the WSL's Phytopathology and the RS research groups, future work will focus on advancing the integrated use of remote sensing and traditional biological methods to monitor forest health.

Chapter 8

Conclusions

This master's thesis aimed to develop an approach for monitoring sweet chestnut trees, with visual symptoms of ink disease in the Canton of Ticino by using Sentinel-2 data and sampled tree data. The thesis addressed two main questions:

RQ1: How can the current spatial distribution of diseased sweet chestnut (*Castanea sativa*) in Ticino be assessed by using freely available remote sensing data and sampled tree data?

RQ2: What features are indicative for such an assessment and how can they be extracted?

Regarding RQ1, the results of this thesis demonstrate that training a RF model using a combination of Sentinel-2 data and sampled tree data generally is an appropriate approach for assessing the spatial distribution of diseased sweet chestnut trees. The methodology is supported by a broad spectrum of literature, highlighting its potential for disease monitoring in forestry. Especially the aggregation of data into monthly medians proved to be valuable, as it enabled to consider inter-seasonal characteristics of both the non-symptomatic and symptomatic classes, and is highly recommended. The combined use of RFE and LLO CV, especially developed for this thesis' task, proved to enhance the performance of the final RF model. Furthermore, this method enabled to gain additional insight into the data and revealed specific features and months to be important for the classification. The final RF model achieved an OA of 86.7%, which is comparable to similar studies in the literature. Despite this solid metric, the resulting classification of this approach shows some inconsistencies in the identification of non-symptomatic and symptomatic areas and therefore must be interpreted with caution. These discrepancies result from several factors: As stated in the introduction, the challenging topography within the study area, characterised by steep slopes and diverse land cover, lead to unpure, mixed spectral signals which are difficult to interpret accurately. Additionally, the small number of sampled tree data available for this thesis required an artificial enhancement of training areas, which introduced another uncertainty in regards to the classification. Also, the spatial dependency of this task limited the performance of the model, as training samples were unevenly distributed within the diverse landscape the Canton of Ticino leading to a potential overfitting of the model.

Regarding RQ2, the combined application of RFE and LLO CV highlighted a set of seven features, including CIre, NDVIre and NDWI, and the SW2-band. These features are indicative of changes in water content or chlorophyll levels in vegetation and are consistent

with the current literature that states these parameters to be essential for monitoring diseased vegetation by using satellite data. Furthermore, these findings were consistent with the results of the preliminary visual and statistical analysis, emphasizing the importance of in-depth analysis of the data before model training.

To conclude, this thesis shows both the potential and the limitations of RS and ML techniques for monitoring diseased sweet chestnut trees in southern Switzerland. In general, it is not possible to directly detect ink disease through RS data, as this provides spectral information from the canopy and only is sensitive to visible symptoms of the disease. Field sampling and laboratory analyses are still a requirement for the definitive detection of the pathogen. Nevertheless, the RS approach gives valuable insights into areas areas where chestnut trees seem to have phytosanitary issues, encouraging for further validation in field. While the use of Sentinel-2 data was suitable for the scope of this thesis, future research could benefit from additional data sources, such as SAR- or LiDAR-derived values to obtain additional parameters targeting the textural structure of trees. Moreover, monitoring over longer time periods than the seven years of this thesis could provide further insights into the progression of tree health. This is particularly important given the complex nature of ink disease, which can follow multiple pathways of development. Despite the given limitations, the thesis contributed to a better understanding between biologists and RS experts, showing their specialised requirements and potential applications. This encourages further collaboration aimed at enhancing the understanding of ink disease distribution and progression in Switzerland, or, more generally, to monitor tree health over time using RS techniques.

References

Alonso, L., Armesto, J., & Picos, J. (2020). Chestnut Cover Automatic Classification Through LiDAR and Sentinel-2 Multi-Temporal Data. *ISPRS Annals of the Photogrammetry, Remote Sensing and Spatial Information Sciences*, *V-3-2020*, 425–430. https://doi.org/10.5194/isprs-annals-V-3-2020-425-2020

Belgiu, M., & Drăguţ, L. (2016). Random forest in remote sensing: A review of applications and future directions. *ISPRS Journal of Photogrammetry and Remote Sensing*, *114*, 24–31. https://doi.org/10.1016/j.isprsjprs.2016.01.011

Boiarskii, B., & Hasegawa, H. (2019). Comparison of NDVI and NDRE Indices to Detect Differences in Vegetation and Chlorophyll Content. *JOURNAL OF MECHANICS OF CONTINUA AND MATHEMATICAL SCIENCES*, *spl*(4). https://doi.org/10.26782/jmcms.spl.4/2019.11.00003

Breiman, L. (2001). Random Forests. *Machine Learning*, *45*(1), 5–32. https://doi.org/10.1023/A:1010933404324

Brungard, C. W., Boettinger, J. L., Duniway, M. C., Wills, S. A., & Edwards, T. C. (2015). Machine learning for predicting soil classes in three semi-arid landscapes. *Geoderma*, *239-240*, 68–83. https://doi.org/10.1016/j.geoderma.2014.09.019

Cardillo, E., Acedo, A., & Abad, E. (2018). Topographic effects on dispersal patterns of Phytophthora cinnamomi at a stand scale in a Spanish heathland (K. O. Reinhart, Ed.). *PLOS ONE*, *13*(3), n.s. https://doi.org/10.1371/journal.pone.0195060

Chen, R., Yin, G., Xu, B., & Liu, G. (2023). Topographic Effects on Optical Remote Sensing: Simulations by PLC Model. *IEEE Journal of Selected Topics in Applied Earth Observations and Remote Sensing*, *16*, 9977–9988. https://doi.org/10.1109/JSTARS.2023.3326228

Conedera, M., Krebs, P., Gehring, E., Wunder, J., Hülsmann, L., Abegg, M., & Maringer, J. (2021). How future-proof is Sweet chestnut (Castanea sativa) in a global change context? *Forest Ecology and Management*, *494*, 119320. https://doi.org/10.1016/j.foreco.2021.119320

De Angelis, A., Ricotta, C., Conedera, M., & Pezzatti, G. B. (2015). Modelling the Meteorological Forest Fire Niche in Heterogeneous Pyrologic Conditions. *PLOS ONE*, *10*(2), n.s. https://doi.org/10.1371/journal.pone.0116875

Dobrinić, D., Gašparović, M., & Medak, D. (2022). Evaluation of Feature Selection Methods for Vegetation Mapping Using Multitemporal Sentinel Imagery. *The International Archives of the Photogrammetry, Remote Sensing and Spatial Information Sciences*, *XLIII-B3-2022*, 485–491. https://doi.org/10.5194/isprs-archives-XLIII-B3-2022-485-2022

Ernst, N. (2021). Cliffs-delta. https://pypi.org/project/cliffs-delta/

ESA, E. S. A. (2024, May). N° 47–2024: Sentinel-2C wird Teil der Copernicus-Familie in der Umlaufbahn. Retrieved November 29, 2024, from https://www.esa.int/Newsroom/Press_Releases/Sentinel-2C_wird_Teil_der_Copernicus-Familie_in_der_Umlaufbahn

ESRI, E. S. R. I. (1998). ESRI Shapefile Technical Description. An ESRI White Paper. July 1998.

EU, C. (2022). Documentation - Sentinel-2 L2A. Retrieved January 2, 2025, from https://documentation.dataspace.copernicus.eu/APIs/SentinelHub/Data/S2L2A.html

Frantz, D. (2019). FORCE—Landsat + Sentinel-2 Analysis Ready Data and Beyond. *Remote Sensing*, *11*(9), 1124. https://doi.org/10.3390/rs11091124

Frascella, A., Sarrocco, S., Mello, A., Venice, F., Salvatici, C., Danti, R., Emiliani, G., Barberini, S., & Della Rocca, G. (2022). Biocontrol of Phytophthora xcambivora on Castanea sativa: Selection of Local Trichoderma spp. Isolates for the Management of Ink Disease. *Forests*, *13*(7), 1065. https://doi.org/10.3390/f13071065

Freitas, T. R., Santos, J. A., Silva, A. P., & Fraga, H. (2021). Influence of Climate Change on Chestnut Trees: A Review. *Plants*, *10*(7), 1463. https://doi.org/10.3390/plants10071463

Fu, Y., Zhu, Z., Liu, L., Zhan, W., He, T., Shen, H., Zhao, J., Liu, Y., Zhang, H., Liu, Z., Xue, Y., & Ao, Z. (2024). Remote Sensing Time Series Analysis: A Review of Data and Applications. *Journal of Remote Sensing*, *4*, 0285. https://doi.org/10.34133/remotesensing.0285

Galfetti, M. (2020). *La trasformaione del territorio in Ticino* (Analisi). Ufficio di statistica (Ustat). Giubasco.

Gamon, J. A., Huemmrich, K. F., Wong, C. Y. S., Ensminger, I., Garrity, S., Hollinger, D. Y., Noormets, A., & Peñuelas, J. (2016). A remotely sensed pigment index reveals photosynthetic phenology in evergreen conifers. *Proceedings of the National Academy of Sciences*, *113*(46), 13087–13092. https://doi.org/10.1073/pnas.1606162113

Gao, B. (1996). NDWI—A normalized difference water index for remote sensing of vegetation liquid water from space. *Remote Sensing of Environment*, *58*(3), 257–266. https://doi.org/10.1016/S0034-4257(96)00067-3

Ginzler, C. (2021). Vegetation Height Model NFI. https://doi.org/10.16904/1000001.1

Gitelson, A. A., & Merzlyak, M. N. (1997). Remote estimation of chlorophyll content in higher plant leaves. *International Journal of Remote Sensing*, *18*(12), 2691–2697. https://doi.org/10.1080/014311697217558

Gitelson, A., & Merzlyak, M. N. (1994). Spectral Reflectance Changes Associated with Autumn Senescence of Aesculus hippocastanum L. and Acer platanoides L. Leaves. Spectral Features and Relation to Chlorophyll Estimation. *Journal of Plant Physiology*, *143*(3), 286–292. https://doi.org/10.1016/S0176-1617(11)81633-0

Gitelson, A. A., Gritz, Y., & Merzlyak, M. N. (2003). Relationships between leaf chlorophyll content and spectral reflectance and algorithms for non-destructive chlorophyll assessment in higher plant leaves. *Journal of Plant Physiology*, *160*(3), 271–282. https://doi.org/10.1078/0176-1617-00887

Granitto, P. M., Furlanello, C., Biasioli, F., & Gasperi, F. (2006). Recursive feature elimination with random forest for PTR-MS analysis of agroindustrial products. *Chemometrics and Intelligent Laboratory Systems*, *83*(2), 83–90. https://doi.org/10.1016/j.chemolab.2006.01.007

Guzmán Q., J. A., Pinto-Ledezma, J. N., Frantz, D., Townsend, P. A., Juzwik, J., & Cavender-Bares, J. (2023). Mapping oak wilt disease from space using land surface phenology. *Remote Sensing of Environment*, *298*, 113794. https://doi.org/10.1016/j.rse.2023.113794

Heiniger, U., & Conedera, M. (1994). Chestnut Forests and Chestnut Cultivation in Switzerland. *Proceedings of the international chestnut conference*, 175–178.

Helfenstein, I. S., Schneider, F. D., Schaepman, M. E., & Morsdorf, F. (2022). Assessing biodiversity from space: Impact of spatial and spectral resolution on trait-based functional diversity. *Remote Sensing of Environment*, *275*, 113024. https://doi.org/10.1016/j.rse.2022.113024

Huete, A., Didan, K., Miura, T., Rodriguez, E., Gao, X., & Ferreira, L. (2002). Overview of the radiometric and biophysical performance of the MODIS vegetation indices. *Remote Sensing of Environment*, *83*(1-2), 195–213. https://doi.org/10.1016/S0034-4257(02)00096-2

Huete, A. (1988). A soil-adjusted vegetation index (SAVI). *Remote Sensing of Environment*, *25*(3), 295–309. https://doi.org/10.1016/0034-4257(88)90106-X

Jung, T., Pérez-Sierra, A., Durán, A., Jung, M. H., Balci, Y., & Scanu, B. (2018). Canker and decline diseases caused by soil- and airborne *Phytophthora* species in forests and woodlands. *Persoonia - Molecular Phylogeny and Evolution of Fungi*, *40*(1), 182–220. https://doi.org/10.3767/persoonia.2018.40.08

Jutz, S., & Milagro-Pérez, M. (2020). Copernicus: The European Earth Observation programme. *Revista de Teledetección*, (56), 5–11. https://doi.org/10.4995/raet.2020.14346

Kälin, M., Stauffacher, J., Schnyder, K., & Matzinger, D. (2005). *Portraits einheimischer Waldgehölzarten. Edelkastanie* (tech. rep.). ZHAW, Wädenswil. Studiengang Umweltingenieurswissenschaften. Wädenswil.

Karasiak, N., Dejoux, J.-F., Monteil, C., & Sheeren, D. (2021). Spatial dependence between training and test sets: Another pitfall of classification accuracy assessment in remote sensing. *Machine Learning*, *111*(7), 2715–2740. https://doi.org/10.1007/s10994-021-05972-1

Koch, T. (2023). 011_extract_s2_nfi_tss.

Koch, T., Hobi, M., Morsdorf, F., & Waser, L. (2024a). Tree species map of Switzerland. https://doi.org/10.16904/ENVIDAT.506

Koch, T., Weber, D., & Waser, L. (2024b). Sentinel-2 imagery of Switzerland. https://doi.org/10.16904/ENVIDAT.510

Krebs, P., Koutsias, N., & Conedera, M. (2012). Modelling the eco-cultural niche of giant chestnut trees: New insights into land use history in southern Switzerland through distribution analysis of a living heritage. *Journal of Historical Geography*, *38*(4), 372–386. https://doi.org/10.1016/j.jhg.2012.01.018

Liu, P., Ren, C., Wang, Z., Jia, M., Yu, W., Ren, H., & Xia, C. (2024). Evaluating the Potential of Sentinel-2 Time Series Imagery and Machine Learning for Tree Species Classification in a Mountainous Forest. *Remote Sensing*, *16*(2), 293. https://doi.org/10.3390/rs16020293

Macbeth, G., Razumiejczyk, E., & Ledesma, R. D. (2010). Cliff´s Delta Calculator: A non-parametric effect size program for two groups of observations. *Universitas Psychologica*, *10*(2), 545–555. https://doi.org/10.11144/Javeriana.upsy10-2.cdcp

Marques, P., Pádua, L., Adão, T., Hruška, J., Peres, E., Sousa, A., & Sousa, J. J. (2019). UAV-Based Automatic Detection and Monitoring of Chestnut Trees. *Remote Sensing*, *11*(7), 855. https://doi.org/10.3390/rs11070855

Marzocchi, G., Maresi, G., Luchi, N., Pecori, F., Gionni, A., Longa, C. M. O., Pezzi, G., & Ferretti, F. (2024). 85 years counteracting an invasion: Chestnut ecosystems and landscapes survival against ink disease. *Biological Invasions*, *26*(7), 2049–2062. https://doi.org/10.1007/s10530-024-03292-8

Matyukira, C., & Mhangara, P. (2024). Advances in vegetation mapping through remote sensing and machine learning techniques: A scientometric review. *European Journal of Remote Sensing*, *57*(1), 2422330. https://doi.org/10.1080/22797254.2024.2422330

Meissel, K., & Yao, E. (2024). Using Cliff's Delta as a Non-Parametric Effect Size Measure: An Accessible Web App and R Tutorial. *29*(2). https://doi.org/10.7275/PARE.1977

MeteoSwiss. (2024). *Climate normals* (tech. rep.). MeteoSwiss. Zürich. Retrieved November 12, 2024, from https://www.meteoswiss.admin.ch/climate/the-climate-of-switzerland/climate-normals/normal-values-per-measured-parameter.html

Meyer, H., Reudenbach, C., Hengl, T., Katurji, M., & Nauss, T. (2018). Improving performance of spatio-temporal machine learning models using forward feature selection and target-oriented validation. *Environmental Modelling & Software*, *101*, 1–9. https://doi.org/10.1016/j.envsoft.2017.12.001

Mohammadpour, P., Viegas, D. X., & Viegas, C. (2022). Vegetation Mapping with Random Forest Using Sentinel 2 and GLCM Texture Feature—A Case Study for Lousã Region, Portugal. *Remote Sensing*, *14*(18), 4585. https://doi.org/10.3390/rs14184585

Molnár, T., & Király, G. (2024). Forest Disturbance Monitoring Using Cloud-Based Sentinel-2 Satellite Imagery and Machine Learning. *Journal of Imaging*, *10*(1), 14. https://doi.org/10.3390/jimaging10010014

Nachar, N. (2008). The Mann-Whitney U: A Test for Assessing Whether Two Independent Samples Come from the Same Distribution. *Tutorials in Quantitative Methods for Psychology*, *4*(1), 13–20. https://doi.org/10.20982/tqmp.04.1.p013

Niculescu, S., Talab Ou Ali, H., & Billey, A. (2018). Random forest classification using Sentinel-1 and Sentinel-2 series for vegetation monitoring in the Pays de Brest (France). In C. M. Neale & A. Maltese (Eds.), *Remote Sensing for Agriculture, Ecosystems, and Hydrology XX* (p. 6). SPIE. https://doi.org/10.1117/12.2325546

Pádua, L., Marques, P., Martins, L., Sousa, A., Peres, E., & Sousa, J. J. (2020). Monitoring of Chestnut Trees Using Machine Learning Techniques Applied to UAV-Based Multispectral Data. *Remote Sensing*, *12*(18), 3032. https://doi.org/10.3390/rs12183032

PBC, P. L. (2024). Planet. Retrieved December 18, 2024, from https://www.planet.com/

Phiri, D., Simwanda, M., Salekin, S., Nyirenda, V., Murayama, Y., & Ranagalage, M. (2020). Sentinel-2 Data for Land Cover/Use Mapping: A Review. *Remote Sensing*, *12*(14), 2291. https://doi.org/10.3390/rs12142291

Pohjankukka, J., Pahikkala, T., Nevalainen, P., & Heikkonen, J. (2020). Estimating the Prediction Performance of Spatial Models via Spatial k-Fold Cross Validation. *International Journal of Geographical Information Science*, *31*(10), 2001–2019. https://doi.org/10.1080/13658816.2017.1346255

Prospero, S. (2022). *Tintenkrankheit der Edelkastanie: Schlussbericht. Pilotprogramm Anpassung an den Klimawandel: Projekt E.03* (tech. rep.). Eidgenössische Forschungsanstalt für Wald, Schnee und Landschaft (WSL). Birmensdorf.

Prospero, S., Heinz, M., Augustiny, E., Chen, Y.-Y., Engelbrecht, J., Fonti, M., Hoste, A., Ruffner, B., Sigrist, R., Van Den Berg, N., & Fonti, P. (2023). Distribution, causal agents, and infection dynamic of emerging ink disease of sweet chestnut in Southern Switzerland. *Environmental Microbiology*, *25*(11), 2250–2265. https://doi.org/10.1111/1462-2920.16455

Prospero, S., Vannini, A., & Vettraino, A. M. (2013). Phytophthora on Castanea sativa Mill. (sweet chestnut). *JKI Data Sheets Plant Pests and Diagnosis; 2013/81; 3-14*. https://doi.org/10.5073/JKIDSPDD.2013.081

Pudjihartono, N., Fadason, T., Kempa-Liehr, A. W., & O'Sullivan, J. M. (2022). A Review of Feature Selection Methods for Machine Learning-Based Disease Risk Prediction. *Frontiers in Bioinformatics*, *2*, 927312. https://doi.org/10.3389/fbinf.2022.927312

Rösch, M., Sonnenschein, R., Buchelt, S., & Ullmann, T. (2022). Comparing PlanetScope and Sentinel-2 Imagery for Mapping Mountain Pines in the Sarntal Alps, Italy. *Remote Sensing*, *14*(13), 3190. https://doi.org/10.3390/rs14133190

Scapozza, C., & Ambrosi, C. (2021). Between Glaciers, Rivers and Lakes: The Geomorphological Landscapes of Ticino. In E. Reynard (Ed.), *Landscapes and Landforms of Switzerland* (pp. 325–336). Springer International Publishing. Retrieved August 7, 2024, from http://link.springer.com/10.1007/978-3-030-43203-4_22

Sebastiani, A., Bertozzi, M., Vannini, A., Morales-Rodriguez, C., Calfapietra, C., & Vaglio Laurin, G. (2024). Monitoring ink disease epidemics in chestnut and cork oak forests in central Italy with remote sensing. *Remote Sensing Applications: Society and Environment*, *36*, 101329. https://doi.org/10.1016/j.rsase.2024.101329

Shapiro, S. S., & Wilk, M. B. (1965). An Analysis of Variance Test for Normality (Complete Samples). *Biometrika*, *52*(3/4), 591. https://doi.org/10.2307/2333709

Swisstopo, B. f. L. (2022). SWISSIMAGE. Das digitale Orthofotomosaik der Schweiz. Retrieved December 18, 2024, from https://www.swisstopo.admin.ch/de/orthobilder-swissimage-10-cm

Swisstopo, B. f. L. (2023). swissSURFACE3D. Die klassifizierte Punktwolke der Schweiz. Retrieved December 18, 2024, from https://www.swisstopo.admin.ch/de/hoehenmodell-swisssurface3d

Swisstopo, B. f. L. (2024a). swissBOUNDARIES3D. https://www.swisstopo.admin.ch/de/landschaftsmodell-swissboundaries3d

Swisstopo, B. f. L. (2024b). SWISSIMAGE 10 cm. https://www.swisstopo.admin.ch/de/geodata/landscape/tlm3d.html

Swisstopo, B. f. L. (2024c). swissTLM3D. https://www.swisstopo.admin.ch/de/geodata/landscape/tlm3d.html

Tan, C., Lin, Q., Du, H., Chen, C., Hu, M., Chen, J., Huang, Z., & Xu, Y. (2024). Detection of the Infection Stage of Pine Wilt Disease and Spread Distance Using Monthly UAV-Based Imagery and a Deep Learning Approach. *Remote Sensing*, *16*(2), 364. https://doi.org/10.3390/rs16020364

Tatbul, N., Lee, T. J., Zdonik, S., Alam, M., & Gottschlich, J. (2018). Precision and Recall for Time Series. *32nd Conference on Neural Information Processing Systems (NeurIPS 2018)*, 1–11. https://doi.org/10.48550/ARXIV.1803.03639

Torres, P., Rodes-Blanco, M., Viana-Soto, A., Nieto, H., & García, M. (2021). The Role of Remote Sensing for the Assessment and Monitoring of Forest Health: A Systematic Evidence Synthesis. *Forests*, *12*(8), 1134. https://doi.org/10.3390/f12081134

Tucker, C. (1979). Red and Photographic Infrared Linear Combinations for Monitoring Vegetation. *Remote Sensing of Environment*, *8*, 127–150.

Turchetti, T., & Maresi, G. (2000). Effects of diseases on chestnut orchards and forest ecosystems. *Ecologia mediterranea*, *26*(1), 113–121. https://doi.org/10.3406/ecmed.2000.1895

Ustat, U. d. s. d. C. T. (2024). *Territorio e Ambiente. Panoramica del Tema.* (tech. rep.). Ufficio di statistica del Cantone Ticino (Ustat). Bellinzona.

Valavi, R., Elith, J., Lahoz-Monfort, J. J., & Guillera-Arroita, G. (2018). BlockCV: An R Package for Generating Spatially or Environmentally Separated Folds for k-Fold Cross-Validation of Species Distribution Models. *Methods in Ecology and Evolution*, *10*(2), 225–232. https://doi.org/10.1111/2041-210X.13107

Vannini, A., & Vettraino, A. M. (2001). Ink disease in chestnuts: Impact on the European chestnut. *Forest Snow and Landscape Research*, *76*(3), 345–350.

Viana, C. M., Girão, I., & Rocha, J. (2019). Long-Term Satellite Image Time-Series for Land Use/Land Cover Change Detection Using Refined Open Source Data in a Rural Region. *Remote Sensing*, *11*(9), 1104. https://doi.org/10.3390/rs11091104

Wang, H., Zhao, Y., Pu, R., & Zhang, Z. (2015). Mapping Robinia Pseudoacacia Forest Health Conditions by Using Combined Spectral, Spatial, and Textural Information Extracted from IKONOS Imagery and Random Forest Classifier. *Remote Sensing*, *7*(7), 9020–9044. https://doi.org/10.3390/rs70709020

Wong, C. Y. S. (2023). Plant optics: Underlying mechanisms in remotely sensed signals for phenotyping applications. *AoB PLANTS*, *15*(4), plad039. https://doi.org/10.1093/aobpla/plad039

Xiong, N., Chen, H., Li, R., Su, H., Dai, S., & Wang, J. (2023). A Method of Chestnut Forest Identification Based on Time Series and Key Phenology from Sentinel-2. *Remote Sensing*, *15*(22), 5374. https://doi.org/10.3390/rs15225374

Xue, J., & Su, B. (2017). Significant Remote Sensing Vegetation Indices: A Review of Developments and Applications. *Journal of Sensors*, *2017*, 1–17. https://doi.org/10.1155/2017/1353691

Yu, R., Luo, Y., Zhou, Q., Zhang, X., Wu, D., & Ren, L. (2021). A machine learning algorithm to detect pine wilt disease using UAV-based hyperspectral imagery and LiDAR data at the tree level. *International Journal of Applied Earth Observation and Geoinformation*, *101*, 102363. https://doi.org/10.1016/j.jag.2021.102363

Zumbrunn, L. (2025). Assessing Potential Ink Disease Distribution in Sweet Chestnut Forests in Switzerland. A Remote Sensing Approach. Main Script. https://github.com/wombateer/Thesis_main

Personal declaration

I hereby declare that the submitted thesis is the result of my own, independent work. All external sources are explicitly acknowledged in the thesis

Zurich, 17.01.2025 Lisa Zumbrunn

Appendix A

Sampled Tree Data

A.1 Sampled Tree Data I-V

Original Sampled Tree Data from the Phytopathology Group of theSwiss Federal Institute for Forest, Snow and Landscape Research (WSL), Recieved in June 2024

Name Site	Year of Testing	Tree Code	Visual Condition	P. cinnamomi / P. cambivora	Latitude	Longitude	Accuracy [m]
Verscio Bartegna	2013	B1	non-symptomatic	positiv	46.19006	8.73404	3
Verscio Bartegna	2013	B4	non-symptomatic	positiv	46.18986	8.73347	3
Verscio Bartegna	2013	B6	non-symptomatic	positiv	46.18993	8.73626	3
Verscio Bartegna	2013	B11	symptomatic	positiv	46.19001	8.73583	3
Verscio Bartegna	2013	B12	symptomatic	positiv	46.19023	8.73572	5
Verscio Bartegna	2013	B14	symptomatic	positiv	46.19044	8.73590	4
Verscio Bartegna	2013	B15	symptomatic	positiv	46.19029	8.73570	4
Orselina Eco	2013	B3	non-symptomatic	positiv	46.18060	8.79241	7
Orselina Eco	2013	B4	non-symptomatic	positiv	46.18063	8.79236	8
Orselina Eco	2013	B6	non-symptomatic	positiv	46.17874	8.78651	8
Orselina Eco	2013	B8	non-symptomatic	positiv	46.17987	8.78755	10
Orselina Eco	2013	B9	non-symptomatic	positiv	46.17999	8.78941	6
Orselina Eco	2013	B10	non-symptomatic	positiv	46.17981	8.79016	8
Orselina Eco	2013	B11	symptomatic	positiv	46.17898	8.78600	6
Orselina Eco	2013	B13	symptomatic	positiv	46.17987	8.78757	5
Orselina Eco	2013	B14	symptomatic	positiv	46.17962	8.78750	7
Orselina Fassa	2013	B7	non-symptomatic	positiv	46.18232	8.79041	6
Orselina Fassa	2013	B8	non-symptomatic	positiv	46.18192	8.79029	4
Orselina Fassa	2013	B9	non-symptomatic	positiv	46.18208	8.79035	3
Orselina Fassa	2013	B10	non-symptomatic	positiv	46.18189	8.79073	4
Orselina Fassa	2013	B11	symptomatic	positiv	46.18222	8.79049	6
Orselina Fassa	2013	B12	symptomatic	positiv	46.18187	8.79035	3
Orselina Fassa	2013	B13	symptomatic	positiv	46.18207	8.79035	3
Orselina Fassa	2013	B14	symptomatic	positiv	46.18231	8.79036	13
Orselina Fassa	2013	B15	symptomatic	positiv	46.18224	8.79043	5
Ronco	2013	B6	non-symptomatic	positiv	46.15200	8.73348	3
Ronco	2013	B8	non-symptomatic	positiv	46.15237	8.73419	6
Ronco	2013	B11	symptomatic	positiv	46.15202	8.73355	5
Ronco	2013	B14	symptomatic	positiv	46.15252	8.73431	5
Ronco	2013	B15	symptomatic	positiv	46.15239	8.73464	4
Biasca	2013	B3	non-symptomatic	positiv	46.35337	8.97717	3
Biasca	2013	B13	symptomatic	positiv	46.35875	8.97370	-
Biasca	2013	B15	symptomatic	positiv	46.35753	8.97445	3
Solduno	2013	B3	non-symptomatic	positiv	46.17466	8.77349	3
Solduno	2013	B6	non-symptomatic	positiv	46.17501	8.77238	9
Solduno	2013	B8	non-symptomatic	positiv	46.17488	8.77213	4
Solduno	2013	B9	non-symptomatic	positiv	46.17482	8.77223	3
Solduno	2013	B11	symptomatic	positiv	46.17495	8.77224	7
Solduno	2013	B12	symptomatic	positiv	46.17488	8.77242	3
Solduno	2013	B13	symptomatic	positiv	46.17500	8.77220	3
Solduno	2013	B15	symptomatic	positiv	46.17491	8.77210	4
Brione	2013	B6	non-symptomatic	positiv	46.18655	8.81860	8
Brione	2013	B11	symptomatic	positiv	46.18638	8.81849	6
Brione	2013	B12	symptomatic	positiv	46.18657	8.81846	5
Brione	2013	B13	symptomatic	positiv	46.18685	8.81839	-
Arcegno	2013	B6	non-symptomatic	positiv	46.16686	8.73632	9
Arcegno	2013	B10	non-symptomatic	positiv	46.16804	8.73588	3
Arcegno	2013	B13	symptomatic	positiv	46.16716	8.73595	8
Arcegno	2013	B14	symptomatic	positiv	46.16747	8.73587	10
Arcegno	2013	B15	symptomatic	positiv	46.16811	8.73635	5
Losone Arbigo	2013	B1	non-symptomatic	positiv	46.17440	8.74570	4
Losone Arbigo	2013	B5	non-symptomatic	positiv	46.17406	8.74565	8
Losone Arbigo	2013	B8	non-symptomatic	positiv	46.17412	8.74445	6
Losone Arbigo	2013	B9	non-symptomatic	positiv	46.17439	8.74419	3
Losone Arbigo	2013	B10	non-symptomatic	positiv	46.17476	8.74422	11
Losone Arbigo	2013	B11	symptomatic	positiv	46.17416	8.74530	3
Losone Arbigo	2013	B13	symptomatic	positiv	46.17405	8.74432	6
Losone Arbigo	2013	B14	symptomatic	positiv	46.17441	8.74412	4
Losone Arbigo	2013	B15	symptomatic	positiv	46.17469	8.74402	3

Name Site	Year of Testing	Tree Code	Visual Condition	P. cinnamomi / P. cambivora	Latitude	Longitude	Accuracy [m]
Tegna Selvapiana	2013	B3	non-symptomatic	positiv	46.18903	8.73601	5
Tegna Selvapiana	2013	B6	non-symptomatic	positiv	46.18872	8.74052	5
Tegna Selvapiana	2013	B7	non-symptomatic	positiv	46.18857	8.74066	3
Tegna Selvapiana	2013	B8	non-symptomatic	positiv	46.18924	8.74017	5
Tegna Selvapiana	2013	B9	non-symptomatic	positiv	46.18911	8.74033	4
Tegna Selvapiana	2013	B10	non-symptomatic	positiv	46.18900	8.74069	3
Tegna Selvapiana	2013	B11	symptomatic	positiv	46.18878	8.74052	3
Tegna Selvapiana	2013	B12	symptomatic	positiv	46.18863	8.74012	4
Tegna Selvapiana	2013	B13	symptomatic	positiv	46.18915	8.74015	4
Tegna Selvapiana	2013	B14	symptomatic	positiv	46.18916	8.74024	5
Tegna Selvapiana	2013	B15	symptomatic	positiv	46.18897	8.74075	-
Arbedo	2019	B3	non-symptomatic	positiv	46.216778	9.054128	-
Arbedo	2019	B6	non-symptomatic	positiv	46.217288	9.054324	-
Arbedo	2019	B7	non-symptomatic	positiv	46.217554	9.054547	-
Arbedo	2019	B8	non-symptomatic	positiv	46.217370	9.054724	-
Arbedo	2019	B9	non-symptomatic	positiv	46.217252	9.054215	-
Arbedo	2019	B10	non-symptomatic	positiv	46.217299	9.054244	-
Arbedo	2019	B11	symptomatic	positiv	46.217129	9.054317	-
Arbedo	2019	B12	symptomatic	positiv	46.217283	9.054566	-
Arbedo	2019	B14	symptomatic	positiv	46.216916	9.054655	-
Arbedo	2019	B15	symptomatic	positiv	46.217185	9.054528	-
Locarno Pureta	2019	B1	non-symptomatic	positiv	46.173953	8.779544	-
Locarno Pureta	2019	B2	non-symptomatic	positiv	46.173853	8.779844	-
Locarno Pureta	2019	B3	non-symptomatic	positiv	46.173959	8.780198	-
Locarno Pureta	2019	B6	non-symptomatic	positiv	46.173842	8.778808	-
Locarno Pureta	2019	B7	non-symptomatic	positiv	46.173819	8.778852	-
Locarno Pureta	2019	B8	non-symptomatic	positiv	46.174033	8.778495	-
Locarno Pureta	2019	B9	non-symptomatic	positiv	46.174586	8.778493	-
Locarno Pureta	2019	B11	symptomatic	positiv	46.173785	8.779640	-
Locarno Pureta	2019	B12	symptomatic	positiv	46.174125	8.778499	-
Locarno Pureta	2019	B13	symptomatic	positiv	46.174299	8.778212	-
Locarno Verigana	2019	B1	non-symptomatic	positiv	46.177612	8.786775	-
Locarno Verigana	2019	B2	non-symptomatic	positiv	46.177070	8.786274	-
Locarno Verigana	2019	B6	non-symptomatic	positiv	46.177979	8.787259	-
Locarno Verigana	2019	B7	non-symptomatic	positiv	46.178269	8.786540	-
Locarno Verigana	2019	B11	symptomatic	positiv	46.176438	8.786695	-
Locarno Verigana	2019	B12	symptomatic	positiv	46.177678	8.786555	-
Locarno Verigana	2019	B13	symptomatic	positiv	46.177828	8.786819	-
Locarno Verigana	2019	B14	symptomatic	positiv	46.177844	8.786843	-
Brissago Motto	2019	B1	non-symptomatic	positiv	46.130435	8.710391	-
Brissago Motto	2019	B2	non-symptomatic	positiv	46.130996	8.711313	-
Brissago Motto	2019	B3	non-symptomatic	positiv	46.130825	8.711179	-
Brissago Motto	2019	B4	non-symptomatic	positiv	46.130929	8.71104	-
Brissago Motto	2019	B5	non-symptomatic	positiv	46.130887	8.7108	-
Brissago Motto	2019	B6	non-symptomatic	positiv	46.130664	8.710611	-
Brissago Motto	2019	B8	non-symptomatic	positiv	46.130849	8.710397	-
Brissago Motto	2019	B9	non-symptomatic	positiv	46.130874	8.710102	-
Brissago Motto	2019	B11	symptomatic	positiv	46.130832	8.71079	-
Brissago Motto	2019	B12	symptomatic	positiv	46.130875	8.71011	-
Brissago Motto	2019	B13	symptomatic	positiv	46.130651	8.710314	-
Brissago Motto	2019	B14	symptomatic	positiv	46.130607	8.710104	-
Tenero	2019	B3	non-symptomatic	positiv	46.192853	8.827177	-
Tenero	2019	B6	non-symptomatic	positiv	46.192922	8.827927	-
Tenero	2019	B8	non-symptomatic	positiv	46.193664	8.827351	-
Taverne	2019	B1	non-symptomatic	positiv	46.058998	8.934479	-
Taverne	2019	B2	non-symptomatic	positiv	46.059337	8.934813	-
Taverne	2019	B4	non-symptomatic	positiv	46.059419	8.935015	-
Taverne	2019	B9	non-symptomatic	positiv	46.060044	8.934007	-
Taverne	2019	B13	symptomatic	positiv	46.059226	8.933918	-
Taverne	2019	B14	symptomatic	positiv	46.060020	8.933875	-
Taverne	2019	B15	symptomatic	positiv	46.060627	8.934624	-
Origlio	2019	B11	symptomatic	positiv	46.056108	8.952123	-
Origlio	2019	B12	symptomatic	positiv	46.056177	8.952023	-

Name Site	Year of Testing	Tree Code	Visual Condition	P. cinnamomi / P. cambivora	Latitude	Longitude	Accuracy [m]
Mugena	2019	B11	symptomatic	positiv	46.051072	8.883259	-
Mugena	2019	B12	symptomatic	positiv	46.051572	8.883240	-
Mugena	2019	B13	symptomatic	positiv	46.051599	8.882990	-
Calonico	2019	B11	symptomatic	negative	46.444612	8.845151	-
Calonico	2019	B12	symptomatic	negative	46.444115	8.845155	-
Calonico	2019	B13	symptomatic	negative	46.444397	8.845372	-
Calonico	2019	B14	symptomatic	negative	46.445186	8.845858	-
Calonico	2019	B15	symptomatic	negative	46.445419	8.991886	-
Monte Carasso	2023	MC1	symptomatic	positiv	46.19400079	8.991886427	-
Monte Carasso	2023	MC2	symptomatic	positiv	46.19412599	8.991941823	-
Monte Carasso	2023	MC3	symptomatic	positiv	46.1941032	8.992290991	-
Monte Carasso	2023	MC5	symptomatic	positiv	46.19340542	8.991999008	-
Brissago Barcone	2020	3_D_T1	symptomatic	positiv	46.132849	8.712841	-
Brissago Barcone	2020	3_D_T4	symptomatic	positiv	46.133125	8.712623	-
Brissago Barcone	2020	3_D_T5	symptomatic	positiv	46.133037	8.712547	-
Brissago Barcone	2020	3_D_T6	symptomatic	positiv	46.133603	8.712603	-
Brissago Barcone	2020	3_D_T7	symptomatic	positiv	46.133793	8.712176	-
Brissago Barcone	2020	3_D_T8	symptomatic	positiv	46.13373	8.712083	-
Brissago Barcone	2020	3_H_T5	non-symptomatic	positiv	46.137052	8.715194	-
Brissago Barcone	2020	3_S_T4	non-symptomatic	positiv	46.13307	8.71225	-
Brissago Barcone	2020	3_S_T5	non-symptomatic	positiv	46.133156	8.712358	-
Brissago Barcone	2020	3_S_T6	non-symptomatic	positiv	46.133783	8.712296	-
Brissago Barcone	2020	3_S_T7	non-symptomatic	positiv	46.133973	8.712088	-
Brissago Barcone	2020	3_S_T8	non-symptomatic	positiv	46.13373	8.712083	-
Mezzovico	2020	1_D_T1	symptomatic	positiv	46.106744	8.930328	-
Mezzovico	2020	1_D_T2	symptomatic	positiv	46.107136	8.929689	-
Mezzovico	2020	1_D_T3	symptomatic	positiv	46.107387	8.92941	-
Mezzovico	2020	1_D_T4	symptomatic	positiv	46.107627	8.929381	-
Mezzovico	2020	1_D_T5	symptomatic	positiv	46.107807	8.929528	-
Mezzovico	2020	1_S_T1	non-symptomatic	positiv	46.106744	8.930328	-
Mezzovico	2020	1_S_T2	non-symptomatic	positiv	46.106997	8.929604	-
Mezzovico	2020	1_S_T3	non-symptomatic	positiv	46.107387	8.92941	-
Mezzovico	2020	1_S_T4	non-symptomatic	positiv	46.107626	8.929504	-
Mezzovico	2020	1_S_T5	non-symptomatic	positiv	46.107735	8.92943	-
Bironico			symptomatic	?	46.125926	8.928975	-
Biasca	2013	B1	non-symptomatic	negative	46.35240	8.97752	5
Biasca	2013	B2	non-symptomatic	negative	46.35144	8.97821	4
Biasca	2013	B4	non-symptomatic	negative	46.35351	8.97727	3
Biasca	2013	B5	non-symptomatic	negative	46.35379	8.97758	3
Biasca	2013	B6	non-symptomatic	negative	46.35734	8.97484	3
Biasca	2013	B7	non-symptomatic	negative	46.35783	8.97456	3
Biasca	2013	B8	non-symptomatic	negative	46.35912	8.97423	3
Biasca	2013	B9	non-symptomatic	negative	46.35886	8.97405	3
Biasca	2013	B10	non-symptomatic	negative	46.35748	8.97451	3
Claro	2013	B1	non-symptomatic	negative	46.27945	9.01894	6
Claro	2013	B2	non-symptomatic	negative	46.27977	9.01855	4
Claro	2013	B3	non-symptomatic	negative	46.27996	9.0186	4
Claro	2013	B4	non-symptomatic	negative	46.27982	9.01895	4
Claro	2013	B5	non-symptomatic	negative	46.27978	9.0194	6
Claro	2013	B6	non-symptomatic	negative	46.27556	9.02173	4
Claro	2013	B7	non-symptomatic	negative	46.27451	9.0226	11
Claro	2013	B8	non-symptomatic	negative	46.27423	9.02352	7
Claro	2013	B9	non-symptomatic	negative	46.27466	9.02359	4
Claro	2013	B10	non-symptomatic	negative	46.27468	9.02556	7
Cademario	2013	B1	non-symptomatic	negative	46.02392	8.89168	-
Cademario	2013	B2	non-symptomatic	negative	46.02383	8.89263	5
Cademario	2013	B3	non-symptomatic	negative	46.02401	8.89244	5
Cademario	2013	B4	non-symptomatic	negative	46.02443	8.89239	6
Cademario	2013	B5	non-symptomatic	negative	46.02459	8.89256	5
Cademario	2013	B6	non-symptomatic	negative	46.02381	8.89109	3
Cademario	2013	B7	non-symptomatic	negative	46.02401	8.89045	4
Cademario	2013	B8	non-symptomatic	negative	46.02397	8.88969	5
Solduno	2013	B1	non-symptomatic	negative	46.17483	8.77282	9

Name Site	Year of Testing	Tree Code	Visual Condition	P. cinnamomi / P. cambivora	Latitude	Longitude	Accuracy [m]
Solduno	2013	B2	non-symptomatic	negative	46.17471	8.77303	5
Solduno	2013	B4	non-symptomatic	negative	46.17473	8.77349	4
Solduno	2013	B5	non-symptomatic	negative	46.17498	8.77324	7
Bodio	2013	B1	non-symptomatic	negative	46.38208	8.90943	3
Bodio	2013	B2	non-symptomatic	negative	46.38190	8.90938	4
Bodio	2013	B3	non-symptomatic	negative	46.38177	8.90919	3
Bodio	2013	B4	non-symptomatic	negative	46.38135	8.90963	5
Bodio	2013	B5	non-symptomatic	negative	46.38125	8.90969	4
Bodio	2013	B6	non-symptomatic	negative	46.38259	8.90741	4
Bodio	2013	B7	non-symptomatic	negative	46.38252	8.90773	4
Bodio	2013	B8	non-symptomatic	negative	46.38241	8.90815	3
Bodio	2013	B9	non-symptomatic	negative	46.38265	8.90872	3
Bodio	2013	B10	non-symptomatic	negative	46.38256	8.90897	3
Calonico	2019	B1	non-symptomatic	negative	46.44637	8.84509	3
Calonico	2019	B2	non-symptomatic	negative	46.44654	8.84528	3
Calonico	2019	B3	non-symptomatic	negative	46.44649	8.84490	11
Calonico	2019	B4	non-symptomatic	negative	46.44626	8.84489	4
Arcegno	2013	B1	non-symptomatic	negative	46.16628	8.73683	5
Arcegno	2013	B2	non-symptomatic	negative	46.16628	8.73662	5
Arcegno	2013	B3	non-symptomatic	negative	46.16640	8.73702	3
Arcegno	2013	B4	non-symptomatic	negative	46.16647	8.73725	5
Arcegno	2013	B5	non-symptomatic	negative	46.16661	8.73733	4
Arcegno	2013	B7	non-symptomatic	negative	46.16703	8.73617	7
Arcegno	2013	B8	non-symptomatic	negative	46.16718	8.73640	11
Arcegno	2013	B9	non-symptomatic	negative	46.16726	8.73590	5
Losone Arbigo	2013	B2	non-symptomatic	negative	46.17431	8.74597	6
Losone Arbigo	2013	B3	non-symptomatic	negative	46.17437	8.74634	6
Losone Arbigo	2013	B4	non-symptomatic	negative	46.174	8.74576	5
Losone Arbigo	2013	B6	non-symptomatic	negative	46.17412	8.74513	3
Losone Arbigo	2013	B7	non-symptomatic	negative	46.17387	8.74431	12
Verscio Bartegna	2013	B7	non-symptomatic	negative	46.19005	8.73621	3
Verscio Bartegna	2013	B8	non-symptomatic	negative	46.19045	8.73601	4
Verscio Bartegna	2013	B9	non-symptomatic	negative	46.19062	8.7363	10
Verscio Bartegna	2013	B10	non-symptomatic	negative	46.19009	8.73506	3
Orselina Eco	2013	B1	non-symptomatic	negative	46.18064	8.79258	8
Orselina Eco	2013	B2	non-symptomatic	negative	46.18066	8.79259	8
Orselina Fassa	2013	B1	non-symptomatic	negative	46.18261	8.78896	3
Orselina Fassa	2013	B2	non-symptomatic	negative	46.18256	8.78914	13
Orselina Fassa	2013	B3	non-symptomatic	negative	46.18248	8.78895	3
Orselina Fassa	2013	B4	non-symptomatic	negative	46.18256	8.78813	3
Orselina Fassa	2013	B5	non-symptomatic	negative	46.18244	8.78859	5
Orselina Fassa	2013	B6	non-symptomatic	negative	46.18224	8.78958	4
Ronco	2013	B1	non-symptomatic	negative	46.15287	8.73498	16
Ronco	2013	B2	non-symptomatic	negative	46.15262	8.73498	5
Ronco	2013	B3	non-symptomatic	negative	46.15273	8.73508	7
Ronco	2013	B4	non-symptomatic	negative	46.15265	8.73479	3
Ronco	2013	B5	non-symptomatic	negative	46.15265	8.73522	4
Ronco	2013	B9	non-symptomatic	negative	46.15299	8.73435	11
Ronco	2013	B10	non-symptomatic	negative	46.1524	8.73461	3
Brissago Gadero	2013	B2	non-symptomatic	negative	46.12864	8.70633	5
Brissago Gadero	2013	B3	non-symptomatic	negative	46.12864	8.70614	8
Brissago Gadero	2013	B4	non-symptomatic	negative	46.12877	8.70605	3
Brissago Gadero	2013	B5	non-symptomatic	negative	46.12884	8.70607	3
Brissago Gadero	2013	B6	non-symptomatic	negative	46.12603	8.70418	15
Brissago Gadero	2013	B7	non-symptomatic	negative	46.12621	8.70428	5
Brissago Gadero	2013	B8	non-symptomatic	negative	46.126	8.7044	6
Brissago Gadero	2013	B9	non-symptomatic	negative	46.12606	8.70472	7
Brissago Gadero	2013	B10	non-symptomatic	negative	46.12592	8.70441	8
Tegna Selvapiana	2013	B1	non-symptomatic	negative	46.18903	8.7363	4
Tegna Selvapiana	2013	B2	non-symptomatic	negative	46.18908	8.73641	3
Tegna Selvapiana	2013	B4	non-symptomatic	negative	46.18884	8.73634	4
Tegna Selvapiana	2013	B5	non-symptomatic	negative	46.18885	8.73645	4
Arbedo	2019	B1	non-symptomatic	negative	46.217051	9.054064	-

Name Site	Year of Testing	Tree Code	Visual Condition	P. cinnamomi / P. cambivora	Latitude	Longitude	Accuracy [m]
Arbedo	2019	B2	non-symptomatic	negative	46.216928	9.054138	-
Arbedo	2019	B4	non-symptomatic	negative	46.216849	9.054233	-
Arbedo	2019	B5	non-symptomatic	negative	46.216722	9.054362	-

Appendix B

Monthly Aggregated Sentinel-2 Values

B.1 Monthly Mean Values of Non-symptomatic Sweet Chestnut Tree Samples (2017-2023)

Year	Month	Median Values of Bands [DN]								Median Values of Vegetation Indices [-]							
		BLU	GRN	RED	RE1	RE3	NIR	SW1	SW2	CCI	CIre	NDWI	NDVI	EVI	SAVI	GNDVI	NDVIre
2017	3	334	449	563	773	1277	1520	1763	1120	-0.109	0.068	-0.072	0.466	0.193	0.299	0.549	0.328
2017	4	321	510	473	838	1753	1984	1701	991	0.064	0.114	0.075	0.611	0.304	0.516	0.586	0.401
2017	5	236	528	278	876	3692	3967	1836	804	0.316	0.327	0.367	0.869	0.664	0.903	0.765	0.638
2017	6	245	504	323	846	3889	4209	1869	798	0.226	0.365	0.384	0.856	0.678	0.885	0.786	0.665
2017	7	229	450	273	757	3636	3966	1810	756	0.253	0.386	0.372	0.870	0.663	0.905	0.795	0.678
2017	8	242	437	287	712	3137	3473	1679	702	0.214	0.349	0.347	0.848	0.594	0.871	0.777	0.660
2017	9	212	383	258	681	2638	2965	1473	625	0.201	0.293	0.336	0.841	0.522	0.861	0.772	0.627
2017	10	267	432	355	753	2137	2477	1458	675	0.104	0.189	0.259	0.750	0.419	0.725	0.704	0.534
2017	11	237	361	425	709	1321	1624	1395	755	-0.075	0.089	0.073	0.587	0.240	0.480	0.638	0.393
2017	12	296	369	495	678	1103	1360	1410	851	-0.189	0.076	-0.029	0.518	0.142	0.377	0.640	0.366
2018	1	241	319	439	581	928	1127	1135	733	-0.164	0.066	0.007	0.457	0.143	0.285	0.577	0.330
2018	2	318	378	505	672	1053	1275	1464	936	-0.136	0.061	-0.063	0.444	0.161	0.266	0.549	0.317
2018	3	322	412	561	752	1182	1434	1720	1115	-0.148	0.062	-0.084	0.448	0.176	0.272	0.561	0.317
2018	4	339	521	588	884	1586	1847	1905	1180	-0.054	0.081	-0.018	0.515	0.246	0.373	0.560	0.350
2018	5	248	553	303	898	3461	3741	1776	806	0.303	0.295	0.352	0.847	0.624	0.870	0.740	0.610
2018	6	229	473	284	779	3792	4122	1794	751	0.259	0.394	0.393	0.872	0.678	0.907	0.795	0.683
2018	7	217	435	260	734	3677	4015	1819	751	0.259	0.408	0.374	0.878	0.671	0.916	0.804	0.691
2018	8	231	428	270	691	3232	3567	1676	685	0.234	0.374	0.359	0.858	0.611	0.887	0.785	0.675
2018	9	199	372	242	642	2734	3062	1516	634	0.219	0.332	0.336	0.854	0.539	0.881	0.784	0.653
2018	10	233	387	305	678	2135	2472	1418	628	0.129	0.222	0.269	0.783	0.429	0.774	0.731	0.571
2018	11	280	380	446	701	1156	1413	1563	924	-0.081	0.065	-0.051	0.524	0.201	0.386	0.581	0.338
2018	12	200	278	383	540	910	1138	1347	820	-0.153	0.076	-0.084	0.515	0.157	0.376	0.622	0.367
2019	1	194	273	383	530	876	1096	1380	876	-0.165	0.071	-0.113	0.494	0.148	0.340	0.608	0.354
2019	2	274	361	474	631	998	1211	1467	947	-0.126	0.064	-0.091	0.450	0.153	0.275	0.546	0.322
2019	3	311	411	543	733	1179	1425	1760	1142	-0.131	0.065	-0.104	0.455	0.178	0.283	0.555	0.324
2019	4	329	491	578	883	1573	1848	1974	1220	-0.073	0.082	-0.032	0.527	0.247	0.390	0.581	0.354
2019	5	189	466	262	844	3070	3319	1718	827	0.308	0.278	0.311	0.848	0.564	0.871	0.749	0.588
2019	6	259	502	311	801	3448	3745	1778	785	0.246	0.337	0.355	0.846	0.627	0.869	0.763	0.647
2019	7	247	452	296	725	3434	3755	1788	758	0.219	0.384	0.354	0.853	0.630	0.879	0.784	0.675
2019	8	217	392	248	636	3069	3380	1609	670	0.231	0.390	0.355	0.862	0.589	0.892	0.791	0.682
2019	9	216	385	252	642	2857	3165	1548	654	0.215	0.352	0.342	0.852	0.556	0.878	0.783	0.662
2019	10	222	365	278	623	2117	2415	1288	579	0.143	0.249	0.299	0.792	0.427	0.788	0.737	0.588
2019	11	260	377	333	676	1454	1692	1285	662	0.067	0.117	0.135	0.671	0.287	0.606	0.635	0.429
2019	12	224	287	376	519	871	1088	1245	762	-0.130	0.072	-0.065	0.496	0.152	0.344	0.589	0.359
2020	1	244	309	416	571	936	1156	1402	869	-0.146	0.069	-0.094	0.482	0.156	0.323	0.586	0.344
2020	2	317	394	502	674	1081	1305	1537	962	-0.117	0.066	-0.078	0.457	0.168	0.285	0.546	0.326
2020	3	331	440	582	775	1249	1512	1741	1118	-0.135	0.065	-0.070	0.451	0.185	0.276	0.554	0.326
2020	4	344	500	558	838	1535	1787	1827	1125	-0.044	0.085	-0.017	0.517	0.244	0.375	0.558	0.355
2020	5	239	529	277	872	3702	3980	1787	806	0.320	0.330	0.377	0.868	0.665	0.902	0.764	0.638
2020	6	239	493	295	826	3739	4047	1788	763	0.258	0.357	0.386	0.864	0.667	0.897	0.783	0.661
2020	7	230	446	275	746	3522	3870	1801	749	0.247	0.381	0.364	0.867	0.650	0.901	0.793	0.677
2020	8	206	395	245	685	3155	3514	1702	699	0.241	0.368	0.346	0.869	0.606	0.904	0.798	0.673
2020	9	219	391	260	665	2730	3072	1538	645	0.208	0.317	0.331	0.844	0.539	0.865	0.774	0.644
2020	10	209	369	306	693	1964	2297	1405	653	0.104	0.190	0.234	0.761	0.393	0.741	0.722	0.532
2020	11	242	331	413	616	1090	1361	1352	758	-0.105	0.080	0.006	0.539	0.195	0.409	0.611	0.379
2021	1	274	338	445	607	994	1212	1315	820	-0.130	0.069	-0.037	0.474	0.161	0.311	0.570	0.340
2021	2	308	437	561	731	1142	1364	1549	985	-0.117	0.061	-0.060	0.432	0.162	0.247	0.524	0.310
2021	3	341	438	571	762	1212	1463	1744	1120	-0.126	0.063	-0.085	0.446	0.181	0.269	0.543	0.319
2021	4	314	469	568	846	1473	1749	1878	1173	-0.089	0.076	-0.036	0.509	0.231	0.364	0.578	0.347
2021	5	208	523	258	881	3645	3944	1825	834	0.354	0.322	0.362	0.873	0.658	0.910	0.762	0.629
2021	6	201	467	251	795	4079	4406	1844	778	0.311	0.421	0.409	0.893	0.719	0.939	0.809	0.695
2021	7	221	425	257	683	3557	3895	1735	722	0.258	0.432	0.386	0.878	0.657	0.916	0.804	0.703
2021	8	220	398	249	661	3169	3493	1631	671	0.234	0.383	0.363	0.867	0.606	0.900	0.796	0.681
2021	9	220	385	249	638	2765	3101	1476	607	0.222	0.341	0.355	0.853	0.549	0.879	0.781	0.660
2021	10	202	351	272	654	2069	2406	1356	607	0.136	0.224	0.277	0.796	0.423	0.793	0.744	0.571
2021	11	199	317	368	639	1203	1492	1319	710	-0.067	0.093	0.054	0.606	0.228	0.508	0.652	0.405
2021	12	253	314	406	563	956	1181	1311	797	-0.145	0.078	-0.055	0.511	0.165	0.366	0.609	0.368
2022	1	217	293	401	559	949	1176	1428	882	-0.152	0.076	-0.092	0.504	0.161	0.355	0.610	0.363
2022	2	284	357	470	640	1064	1304	1559	970	-0.128	0.072	-0.085	0.480	0.174	0.320	0.575	0.347
2022	3	385	483	606	795	1274	1527	1796	1148	-0.108	0.064	-0.077	0.438	0.188	0.257	0.523	0.319
2022	4	364	534	600	908	1644	1928	1930	1190	-0.049	0.083	-0.005	0.520	0.258	0.380	0.563	0.355
2022	5	237	555	275	912	3818	4098	1883	840	0.343	0.329	0.367	0.870	0.680	0.905	0.757	0.631
2022	6	247	501	294	811	3981	4303	1884	802	0.270	0.396	0.389	0.871	0.703	0.907	0.791	0.682
2022	7	228	449	267	758	3773	4127	1907	797	0.262	0.405	0.365	0.877	0.686	0.916	0.803	0.688
2022	8	244	448	282	754	3371	3717	1762	740	0.233	0.352	0.355	0.858	0.630	0.887	0.784	0.661
2022	9	187	367	227	667	2853	3187	1535	645	0.239	0.333	0.347	0.866	0.560	0.899	0.793	0.653
2022	10	243	407	313	703	2153	2489	1400	625	0.138	0.213	0.275	0.773	0.430	0.759	0.716	0.556
2022	11	189	319	355	645	1245	1514	1298	688	-0.044	0.096	0.071	0.621	0.235	0.531	0.654	0.403
2022	12	227	301	415	576	961	1226	1381	838	-0.154	0.073	-0.060	0.509	0.168	0.363	0.615	0.369
2023	1	293	352	459	611	968	1191	1475	931	-0.127	0.063	-0.101	0.454	0.155	0.280	0.549	0.327
2023	2	298	370	479	640	1026	1253	1538	969	-0.120	0.066	-0.097	0.457	0.162	0.285	0.549	0.330
2023	3	343	431	563	744	1197	1460	1765	1124	-0.129	0.066	-0.090	0.455	0.183	0.282	0.553	0.331
2023	4	310	474	528	849	1607	1863	1882	1155	-0.039	0.092	-0.009	0.555	0.263	0.432	0.593	0.370
2023	5	258	586	316	964	3845	4114	1886	851	0.313	0.306	0.365	0.850	0.671	0.875	0.745	0.613
2023	6	254	531	307	857	3934	4263	1798	756	0.269	0.362	0.406	0.862	0.692	0.893	0.776	0.663
2023	7	239	456	273	744	3802	4172	1837	751	0.259	0.418	0.387	0.877	0.693	0.915	0.802	0.696
2023	8	241	435	283	720	3220	3594	1669	681	0.219	0.354	0.364	0.853	0.612	0.880	0.784	0.665
2023	9	249	419	337	727	2398	2765	1665	777	0.124	0.241	0.243	0.778	0.467	0.767	0.733	0.579
2023	10	286	443	368	730	2109	2452	1570	729	0.097	0.192	0.216	0.735	0.413	0.702	0.690	0.537
2023	11	266	374	406	682	1340	1616	1513	852	-0.025	0.102	0.036	0.607	0.250	0.510	0.628	0.410
2023	12	194	308	406	607	1057	1320	1446	869	-0.131	0.080	-0.045	0.539	0.185	0.409	0.628	0.377

B.2 Monthly Mean Values of Symptomatic Sweet Chestnut Tree Samples (2017-2023)

Year	Month	Median Values of Bands [DN]								Median Values of Vegetation Indices [-]							
		BLU	GRN	RED	RE1	RE3	NIR	SW1	SW2	CCI	CIre	NDWI	NDVI	EVI	SAVI	GNDVI	NDVIre
2017	3	362	480	604	810	1282	1526	1828	1162	-0.114	0.059	-0.090	0.433	0.185	0.249	0.522	0.306
2017	4	344	528	521	865	1694	1934	1790	1063	0.025	0.099	0.036	0.569	0.283	0.453	0.565	0.376
2017	5	251	530	315	884	3370	3637	1886	871	0.260	0.285	0.315	0.839	0.607	0.859	0.745	0.608
2017	6	272	519	349	867	3639	3953	1921	861	0.201	0.322	0.345	0.836	0.642	0.854	0.767	0.639
2017	7	253	472	308	795	3428	3757	1869	821	0.216	0.335	0.334	0.847	0.627	0.871	0.776	0.650
2017	8	262	454	317	742	2960	3288	1733	762	0.183	0.303	0.308	0.824	0.560	0.836	0.758	0.632
2017	9	240	409	298	719	2516	2838	1538	688	0.160	0.253	0.295	0.808	0.494	0.813	0.748	0.595
2017	10	283	439	390	770	1993	2337	1527	742	0.064	0.162	0.208	0.713	0.387	0.670	0.684	0.503
2017	11	266	388	477	742	1313	1620	1510	841	-0.100	0.077	0.032	0.541	0.228	0.412	0.611	0.369
2017	12	362	435	578	759	1169	1434	1519	925	-0.187	0.064	-0.043	0.472	0.128	0.308	0.603	0.338
2018	1	296	372	498	629	942	1152	1230	792	-0.158	0.053	-0.023	0.409	0.137	0.213	0.529	0.301
2018	2	350	419	570	732	1087	1312	1563	1005	-0.150	0.051	-0.087	0.400	0.153	0.199	0.519	0.288
2018	3	351	448	623	805	1209	1465	1804	1177	-0.163	0.052	-0.100	0.406	0.167	0.209	0.534	0.293
2018	4	358	546	649	925	1554	1823	1993	1252	-0.084	0.068	-0.048	0.470	0.226	0.305	0.537	0.324
2018	5	273	566	355	924	3224	3504	1860	891	0.242	0.256	0.300	0.810	0.577	0.815	0.717	0.578
2018	6	235	470	290	782	3577	3893	1842	809	0.242	0.362	0.356	0.861	0.647	0.891	0.785	0.666
2018	7	237	455	289	766	3450	3784	1867	811	0.228	0.355	0.337	0.857	0.634	0.885	0.785	0.663
2018	8	256	450	306	732	3004	3331	1720	744	0.196	0.315	0.317	0.831	0.569	0.846	0.762	0.639
2018	9	222	391	280	682	2564	2887	1594	707	0.173	0.280	0.287	0.823	0.504	0.834	0.761	0.617
2018	10	252	401	344	717	2026	2365	1507	701	0.084	0.187	0.220	0.746	0.401	0.719	0.710	0.535
2018	11	278	378	446	701	1225	1481	1588	927	-0.081	0.074	-0.038	0.536	0.213	0.403	0.592	0.356
2018	12	226	314	438	598	970	1211	1457	889	-0.163	0.064	-0.094	0.472	0.159	0.308	0.590	0.341
2019	1	222	311	443	595	945	1179	1511	949	-0.175	0.061	-0.122	0.457	0.151	0.285	0.584	0.331
2019	2	306	404	545	707	1062	1292	1620	1035	-0.145	0.052	-0.111	0.410	0.152	0.215	0.525	0.295
2019	3	352	462	620	814	1246	1504	1895	1221	-0.142	0.054	-0.115	0.418	0.175	0.226	0.530	0.298
2019	4	359	525	640	935	1586	1871	2067	1279	-0.093	0.071	-0.049	0.490	0.236	0.335	0.561	0.333
2019	5	225	500	316	897	2921	3175	1840	922	0.244	0.236	0.262	0.814	0.532	0.821	0.725	0.557
2019	6	282	520	341	828	3293	3588	1861	858	0.216	0.301	0.314	0.824	0.599	0.837	0.746	0.624
2019	7	278	483	335	770	3282	3602	1867	829	0.190	0.332	0.316	0.829	0.602	0.844	0.763	0.648
2019	8	241	416	280	677	2922	3231	1672	732	0.200	0.335	0.319	0.838	0.560	0.857	0.769	0.652
2019	9	244	412	290	687	2737	3044	1629	724	0.179	0.302	0.301	0.825	0.529	0.837	0.760	0.631
2019	10	249	395	317	674	2082	2385	1385	649	0.114	0.213	0.259	0.762	0.414	0.743	0.714	0.556
2019	11	277	398	383	715	1459	1707	1385	736	0.024	0.105	0.101	0.632	0.277	0.548	0.620	0.409
2019	12	233	310	417	563	917	1149	1367	840	-0.148	0.064	-0.088	0.468	0.153	0.301	0.575	0.342
2020	1	256	335	463	623	990	1225	1538	956	-0.160	0.060	-0.115	0.452	0.157	0.278	0.571	0.326
2020	2	342	428	558	727	1115	1347	1637	1027	-0.132	0.055	-0.097	0.418	0.162	0.226	0.521	0.301
2020	3	353	474	641	828	1276	1546	1864	1200	-0.146	0.055	-0.094	0.415	0.177	0.223	0.530	0.303
2020	4	375	533	616	882	1520	1776	1929	1194	-0.065	0.073	-0.046	0.477	0.229	0.316	0.533	0.330
2020	5	257	533	317	885	3366	3645	1858	886	0.264	0.284	0.319	0.835	0.608	0.852	0.741	0.604
2020	6	261	498	316	837	3472	3781	1847	830	0.229	0.318	0.341	0.844	0.629	0.867	0.766	0.637
2020	7	256	468	313	773	3246	3591	1847	815	0.205	0.324	0.319	0.839	0.603	0.858	0.769	0.645
2020	8	236	419	292	725	2879	3227	1768	777	0.186	0.303	0.291	0.833	0.554	0.850	0.770	0.633
2020	9	248	414	310	705	2521	2855	1628	733	0.151	0.261	0.271	0.803	0.494	0.804	0.746	0.603
2020	10	233	379	350	716	1808	2137	1493	737	0.048	0.156	0.171	0.712	0.356	0.669	0.695	0.494
2020	11	274	372	471	676	1160	1448	1500	853	-0.115	0.073	-0.016	0.508	0.199	0.363	0.590	0.363
2021	1	328	403	535	698	1074	1307	1461	917	-0.138	0.057	-0.056	0.427	0.159	0.240	0.534	0.308
2021	2	345	486	631	797	1192	1422	1671	1072	-0.128	0.052	-0.079	0.393	0.157	0.190	0.497	0.287
2021	3	376	487	647	830	1254	1513	1884	1224	-0.138	0.053	-0.109	0.404	0.172	0.206	0.514	0.293
2021	4	357	514	638	902	1491	1771	2001	1263	-0.103	0.066	-0.062	0.468	0.219	0.302	0.548	0.323
2021	5	243	535	338	909	3220	3523	1955	965	0.244	0.262	0.280	0.818	0.579	0.826	0.731	0.583
2021	6	239	494	297	829	3776	4099	1941	873	0.259	0.361	0.356	0.864	0.673	0.895	0.785	0.663
2021	7	255	464	306	746	3404	3751	1858	818	0.211	0.360	0.336	0.848	0.628	0.872	0.779	0.668
2021	8	246	419	287	701	2953	3271	1699	746	0.191	0.324	0.315	0.838	0.566	0.856	0.772	0.646
2021	9	248	410	295	686	2603	2947	1579	692	0.171	0.285	0.301	0.818	0.514	0.827	0.756	0.622
2021	10	226	368	314	683	1950	2286	1451	689	0.087	0.191	0.223	0.756	0.393	0.734	0.721	0.538
2021	11	231	353	423	695	1263	1563	1478	815	-0.086	0.083	0.022	0.571	0.230	0.456	0.630	0.385
2021	12	270	342	459	621	1020	1261	1462	895	-0.157	0.068	-0.076	0.476	0.167	0.315	0.589	0.346
2022	1	257	343	475	634	1023	1267	1588	987	-0.159	0.064	-0.112	0.458	0.162	0.287	0.576	0.334
2022	2	324	407	549	718	1127	1381	1726	1084	-0.145	0.059	-0.109	0.434	0.170	0.250	0.545	0.317
2022	3	415	527	683	869	1315	1583	1962	1262	-0.126	0.053	-0.106	0.399	0.179	0.199	0.501	0.292
2022	4	413	586	672	971	1684	1973	2051	1273	-0.061	0.074	-0.023	0.487	0.251	0.330	0.538	0.336
2022	5	280	573	345	945	3543	3850	2018	956	0.259	0.285	0.305	0.828	0.631	0.843	0.735	0.599
2022	6	279	524	329	836	3750	4070	1948	869	0.238	0.354	0.352	0.850	0.669	0.875	0.772	0.659
2022	7	271	491	335	818	3517	3882	2004	893	0.203	0.338	0.317	0.839	0.639	0.858	0.774	0.650
2022	8	281	483	349	819	3143	3500	1876	842	0.175	0.291	0.300	0.816	0.583	0.825	0.756	0.619
2022	9	226	402	295	724	2646	2981	1654	746	0.166	0.270	0.284	0.818	0.513	0.826	0.761	0.607
2022	10	273	431	374	748	2023	2365	1537	734	0.079	0.175	0.208	0.723	0.395	0.684	0.689	0.516
2022	11	234	362	424	704	1306	1586	1484	817	-0.073	0.086	0.030	0.575	0.234	0.462	0.626	0.382
2022	12	272	349	478	643	1058	1338	1518	917	-0.150	0.067	-0.063	0.476	0.176	0.314	0.586	0.352
2023	1	316	389	525	679	1045	1284	1639	1043	-0.146	0.056	-0.119	0.422	0.157	0.232	0.535	0.309
2023	2	344	432	571	733	1124	1371	1734	1106	-0.134	0.056	-0.115	0.416	0.164	0.223	0.522	0.305
2023	3	381	481	640	819	1267	1544	1933	1241	-0.140	0.057	-0.110	0.418	0.181	0.227	0.528	0.309
2023	4	379	544	631	936	1658	1923	2047	1282	-0.065	0.078	-0.036	0.500	0.251	0.350	0.555	0.341
2023	5	316	626	410	1015	3481	3751	2025	996	0.230	0.251	0.291	0.793	0.601	0.789	0.706	0.565
2023	6	286	561	344	898	3789	4116	1926	862	0.246	0.325	0.361	0.843	0.669	0.864	0.758	0.640
2023	7	280	501	330	808	3623	3992	1937	849	0.212	0.353	0.345	0.846	0.658	0.869	0.776	0.663
2023	8	274	469	329	776	3088	3459	1763	767	0.183	0.304	0.324	0.825	0.583	0.838	0.760	0.633
2023	9	280	448	398	782	2362	2744	1802	881	0.087	0.214	0.206	0.745	0.450	0.717	0.716	0.554
2023	10	316	466	426	772	2016	2369	1707	842	0.055	0.165	0.164	0.693	0.385	0.639	0.668	0.506
2023	11	310	433	489	775	1454	1757	1707	972	-0.053	0.090	0.013	0.564	0.256	0.446	0.603	0.386
2023	12	235	362	487	688	1166	1450	1629	996	-0.140	0.073	-0.059	0.502	0.191	0.352	0.601	0.358

B.3 Monthly Standard Deviation Values of Non-symptomatic Sweet Chestnut Tree Samples (2017-2023)

Year	Month	Median Values of Bands [DN]								Median Values of Vegetation Indices [-]							
		BLU	GRN	RED	RE1	RE3	NIR	SW1	SW2	CCI	CIre	NDWI	NDVI	EVI	SAVI	GNDVI	NDVIre
2017	3	96	119	159	153	212	235	300	210	0.066	0.029	0.075	0.085	0.036	0.128	0.064	0.057
2017	4	114	113	177	142	372	377	303	236	0.130	0.054	0.128	0.141	0.087	0.211	0.086	0.088
2017	5	63	89	71	123	394	413	191	117	0.077	0.056	0.048	0.034	0.062	0.051	0.032	0.040
2017	6	60	89	91	128	499	529	236	117	0.072	0.059	0.043	0.042	0.077	0.063	0.033	0.038
2017	7	56	82	72	118	501	531	216	101	0.067	0.067	0.038	0.037	0.076	0.055	0.032	0.038
2017	8	70	94	88	126	413	428	197	102	0.061	0.064	0.039	0.042	0.063	0.063	0.036	0.041
2017	9	59	84	72	121	369	401	204	109	0.056	0.052	0.041	0.037	0.059	0.055	0.034	0.038
2017	10	91	114	109	169	444	492	294	165	0.062	0.048	0.059	0.058	0.076	0.088	0.047	0.056
2017	11	72	102	136	184	360	418	321	194	0.086	0.031	0.089	0.090	0.065	0.135	0.053	0.056
2017	12	737	630	586	562	526	510	318	213	0.071	0.031	0.094	0.115	0.261	0.173	0.118	0.079
2018	1	113	141	188	206	262	316	387	232	0.092	0.032	0.081	0.095	0.033	0.143	0.087	0.072
2018	2	106	118	172	188	239	278	364	242	0.061	0.028	0.092	0.088	0.031	0.132	0.064	0.061
2018	3	100	121	171	173	206	236	364	262	0.058	0.029	0.074	0.092	0.029	0.138	0.068	0.061
2018	4	94	118	158	154	347	347	295	230	0.109	0.035	0.106	0.111	0.073	0.166	0.058	0.066
2018	5	81	117	111	177	610	636	257	176	0.092	0.081	0.075	0.058	0.099	0.088	0.053	0.068
2018	6	73	106	92	142	525	550	227	115	0.074	0.059	0.038	0.036	0.073	0.054	0.031	0.033
2018	7	51	81	78	125	522	538	209	120	0.069	0.067	0.044	0.035	0.075	0.053	0.028	0.038
2018	8	61	84	78	112	463	494	195	104	0.066	0.068	0.044	0.040	0.073	0.061	0.035	0.040
2018	9	55	84	72	126	464	504	230	121	0.062	0.062	0.049	0.037	0.074	0.055	0.031	0.040
2018	10	85	110	107	165	429	486	271	146	0.062	0.055	0.065	0.055	0.071	0.082	0.046	0.053
2018	11	106	107	118	146	242	272	277	199	0.054	0.014	0.055	0.057	0.038	0.086	0.044	0.028
2018	12	97	116	163	182	253	303	353	215	0.075	0.035	0.070	0.100	0.034	0.159	0.081	0.067
2019	1	94	105	152	167	236	284	354	226	0.070	0.033	0.084	0.097	0.035	0.145	0.082	0.067
2019	2	96	117	171	185	235	278	366	244	0.065	0.033	0.097	0.101	0.033	0.151	0.077	0.070
2019	3	89	112	166	174	245	278	346	243	0.058	0.033	0.083	0.097	0.040	0.146	0.067	0.067
2019	4	118	127	172	172	302	322	332	238	0.076	0.036	0.093	0.107	0.056	0.160	0.073	0.069
2019	5	75	102	121	155	541	555	222	165	0.130	0.101	0.099	0.080	0.100	0.121	0.065	0.092
2019	6	68	86	89	114	405	412	195	125	0.084	0.067	0.054	0.043	0.063	0.064	0.036	0.044
2019	7	77	98	93	129	468	490	231	132	0.062	0.085	0.048	0.047	0.073	0.070	0.044	0.048
2019	8	56	82	69	117	509	539	249	122	0.058	0.080	0.051	0.038	0.082	0.058	0.038	0.043
2019	9	62	84	68	113	442	468	214	108	0.054	0.069	0.044	0.037	0.069	0.056	0.037	0.042
2019	10	70	108	98	158	497	534	231	133	0.064	0.077	0.066	0.061	0.083	0.091	0.052	0.067
2019	11	63	94	100	163	339	391	280	161	0.057	0.027	0.063	0.061	0.062	0.091	0.042	0.045
2019	12	98	107	143	168	259	314	359	226	0.071	0.029	0.080	0.088	0.041	0.132	0.070	0.059
2020	1	102	108	146	162	232	276	335	216	0.070	0.031	0.075	0.096	0.035	0.144	0.080	0.064
2020	2	129	136	170	180	225	259	336	227	0.057	0.033	0.072	0.103	0.032	0.154	0.089	0.070
2020	3	104	130	181	193	272	307	336	242	0.057	0.031	0.081	0.095	0.041	0.142	0.073	0.066
2020	4	85	102	157	142	406	412	290	227	0.114	0.044	0.125	0.128	0.090	0.192	0.068	0.080
2020	5	77	109	85	143	607	632	224	123	0.077	0.068	0.060	0.043	0.091	0.065	0.041	0.052
2020	6	64	94	81	126	455	481	194	102	0.065	0.054	0.042	0.032	0.061	0.048	0.030	0.033
2020	7	63	87	79	123	443	462	192	109	0.059	0.072	0.040	0.036	0.063	0.053	0.033	0.041
2020	8	52	77	65	116	425	456	193	107	0.052	0.072	0.043	0.031	0.065	0.047	0.031	0.041
2020	9	64	90	74	121	438	470	201	104	0.056	0.064	0.045	0.039	0.068	0.059	0.039	0.042
2020	10	77	109	110	176	535	594	287	156	0.091	0.066	0.081	0.082	0.099	0.124	0.055	0.079
2020	11	83	102	138	172	294	356	365	221	0.066	0.027	0.097	0.081	0.049	0.121	0.060	0.052
2021	1	99	117	158	183	246	284	325	209	0.068	0.032	0.098	0.093	0.035	0.139	0.071	0.069
2021	2	100	145	199	206	252	280	346	241	0.054	0.029	0.084	0.100	0.033	0.150	0.074	0.068
2021	3	104	120	167	171	231	265	330	237	0.056	0.030	0.078	0.095	0.039	0.143	0.070	0.065
2021	4	78	98	141	147	291	303	286	215	0.091	0.033	0.100	0.100	0.059	0.150	0.055	0.063
2021	5	80	104	104	146	652	668	242	161	0.096	0.087	0.083	0.062	0.105	0.094	0.055	0.074
2021	6	65	100	81	135	501	517	204	115	0.074	0.068	0.039	0.031	0.064	0.047	0.030	0.035
2021	7	66	98	81	142	584	640	313	160	0.066	0.074	0.039	0.032	0.087	0.047	0.030	0.033
2021	8	52	71	56	101	422	451	202	97	0.046	0.053	0.036	0.024	0.060	0.036	0.025	0.030
2021	9	68	96	76	137	455	493	245	127	0.051	0.059	0.043	0.033	0.069	0.049	0.033	0.039
2021	10	58	94	91	161	511	561	290	156	0.073	0.068	0.074	0.056	0.088	0.084	0.043	0.064
2021	11	63	104	135	205	370	431	308	179	0.090	0.034	0.105	0.095	0.066	0.142	0.055	0.058
2021	12	327	285	261	265	315	339	344	212	0.082	0.035	0.140	0.108	0.041	0.163	0.107	0.077
2022	1	84	97	139	154	219	260	345	228	0.072	0.037	0.088	0.101	0.034	0.152	0.078	0.070
2022	2	94	103	147	162	216	252	347	236	0.064	0.035	0.087	0.097	0.035	0.146	0.070	0.071
2022	3	106	119	159	165	213	241	332	238	0.061	0.031	0.084	0.091	0.039	0.136	0.066	0.067
2022	4	104	109	159	148	407	418	278	218	0.103	0.038	0.113	0.120	0.083	0.180	0.067	0.071
2022	5	52	97	78	153	646	685	254	151	0.082	0.095	0.076	0.049	0.101	0.073	0.050	0.070
2022	6	73	96	89	121	507	534	190	104	0.082	0.064	0.041	0.039	0.072	0.059	0.032	0.036
2022	7	60	80	74	115	523	547	197	116	0.071	0.078	0.049	0.038	0.079	0.056	0.031	0.043
2022	8	56	76	70	112	489	523	223	125	0.062	0.064	0.050	0.036	0.075	0.054	0.029	0.041
2022	9	47	77	59	115	472	503	208	106	0.058	0.060	0.047	0.032	0.073	0.049	0.030	0.039
2022	10	76	106	98	164	527	581	279	148	0.066	0.066	0.080	0.068	0.092	0.102	0.056	0.068
2022	11	61	101	127	182	364	416	292	178	0.102	0.037	0.107	0.102	0.068	0.153	0.060	0.065
2022	12	91	105	156	174	246	305	340	216	0.077	0.034	0.082	0.104	0.040	0.156	0.074	0.067
2023	1	103	107	147	161	214	254	352	236	0.068	0.030	0.079	0.091	0.033	0.136	0.074	0.063
2023	2	90	104	151	164	208	247	345	238	0.066	0.031	0.081	0.090	0.032	0.135	0.063	0.064
2023	3	125	141	181	182	228	257	356	254	0.063	0.034	0.079	0.101	0.037	0.151	0.077	0.071
2023	4	89	115	175	169	412	412	317	244	0.128	0.043	0.117	0.134	0.089	0.201	0.065	0.079
2023	5	70	104	121	139	672	689	224	174	0.101	0.083	0.093	0.080	0.117	0.120	0.064	0.079
2023	6	56	97	72	148	696	734	305	145	0.069	0.057	0.044	0.041	0.100	0.061	0.039	0.037
2023	7	71	90	77	118	508	546	217	114	0.059	0.076	0.038	0.034	0.074	0.051	0.033	0.038
2023	8	63	83	78	120	459	489	205	109	0.062	0.071	0.045	0.040	0.070	0.059	0.034	0.043
2023	9	67	98	131	166	552	593	300	239	0.092	0.083	0.108	0.081	0.101	0.122	0.055	0.084
2023	10	73	96	95	146	494	554	310	175	0.060	0.053	0.087	0.063	0.089	0.095	0.051	0.062
2023	11	98	113	155	178	324	360	369	235	0.084	0.039	0.087	0.103	0.058	0.155	0.061	0.067
2023	12	80	100	144	171	256	297	335	220	0.078	0.037	0.084	0.102	0.044	0.153	0.069	0.067

B.4 Monthly Standard Deviation Values of Symptomatic Sweet Chestnut Tree Samples (2017-2023)

Year	Month	Median Values of Bands [DN]								Median Values of Vegetation Indices [-]							
		BLU	GRN	RED	RE1	RE3	NIR	SW1	SW2	CCI	CIre	NDWI	NDVI	EVI	SAVI	GNDVI	NDVIre
2017	3	76	89	106	107	204	216	222	160	0.059	0.021	0.062	0.070	0.040	0.105	0.057	0.046
2017	4	103	86	153	107	338	336	266	216	0.116	0.047	0.116	0.135	0.084	0.203	0.082	0.081
2017	5	80	85	78	111	413	423	181	112	0.082	0.048	0.054	0.042	0.068	0.063	0.035	0.040
2017	6	59	78	77	113	454	489	213	105	0.060	0.047	0.041	0.042	0.073	0.062	0.034	0.035
2017	7	62	75	74	105	412	433	189	99	0.063	0.053	0.042	0.037	0.063	0.055	0.030	0.033
2017	8	66	86	77	113	403	413	175	92	0.053	0.051	0.041	0.039	0.061	0.058	0.033	0.036
2017	9	57	71	64	95	354	369	163	83	0.059	0.045	0.052	0.042	0.060	0.063	0.035	0.037
2017	10	85	98	101	140	368	400	250	151	0.065	0.040	0.068	0.062	0.068	0.093	0.044	0.052
2017	11	57	73	99	125	280	319	238	162	0.069	0.025	0.084	0.079	0.056	0.118	0.043	0.049
2017	12	839	712	650	621	572	539	258	191	0.057	0.024	0.103	0.105	0.295	0.157	0.118	0.074
2018	1	122	155	180	188	239	277	356	212	0.079	0.021	0.086	0.079	0.030	0.118	0.089	0.055
2018	2	117	120	159	179	221	252	288	194	0.049	0.019	0.077	0.070	0.031	0.105	0.062	0.048
2018	3	87	96	129	138	186	217	317	231	0.054	0.018	0.061	0.067	0.031	0.101	0.058	0.044
2018	4	97	93	124	122	314	317	244	199	0.099	0.027	0.090	0.098	0.068	0.146	0.056	0.055
2018	5	95	111	135	169	633	643	237	189	0.103	0.077	0.091	0.075	0.108	0.112	0.059	0.075
2018	6	62	86	74	125	473	497	211	110	0.068	0.050	0.043	0.033	0.068	0.049	0.027	0.030
2018	7	52	72	68	115	473	491	194	112	0.061	0.054	0.046	0.033	0.069	0.049	0.027	0.034
2018	8	66	82	77	112	398	423	181	102	0.058	0.053	0.046	0.040	0.064	0.060	0.034	0.037
2018	9	55	75	74	118	391	414	208	122	0.064	0.052	0.055	0.043	0.064	0.065	0.034	0.041
2018	10	76	89	100	138	335	380	239	140	0.064	0.043	0.066	0.058	0.059	0.086	0.043	0.048
2018	11	66	78	93	134	291	324	259	168	0.048	0.015	0.060	0.055	0.046	0.082	0.036	0.030
2018	12	80	85	117	144	228	262	269	171	0.055	0.024	0.071	0.070	0.036	0.105	0.054	0.049
2019	1	81	81	112	131	201	236	287	191	0.057	0.024	0.075	0.076	0.033	0.113	0.065	0.052
2019	2	76	87	125	151	198	224	281	192	0.050	0.020	0.072	0.070	0.030	0.105	0.055	0.049
2019	3	66	82	126	136	210	235	285	205	0.044	0.020	0.061	0.071	0.036	0.107	0.050	0.046
2019	4	95	90	138	135	272	286	296	211	0.074	0.026	0.073	0.088	0.052	0.132	0.057	0.052
2019	5	89	99	118	164	452	452	201	156	0.125	0.076	0.086	0.080	0.084	0.120	0.059	0.077
2019	6	73	82	89	111	436	441	179	118	0.084	0.055	0.057	0.047	0.070	0.071	0.037	0.040
2019	7	82	97	95	126	447	470	217	126	0.061	0.059	0.048	0.047	0.071	0.070	0.039	0.041
2019	8	58	77	68	119	517	555	280	140	0.057	0.058	0.057	0.039	0.084	0.058	0.037	0.036
2019	9	67	79	71	108	418	442	212	111	0.059	0.053	0.046	0.041	0.067	0.062	0.037	0.038
2019	10	60	85	84	123	427	452	170	111	0.064	0.059	0.070	0.061	0.075	0.091	0.046	0.060
2019	11	67	76	102	144	317	348	225	147	0.074	0.026	0.071	0.069	0.060	0.103	0.042	0.049
2019	12	90	89	115	146	255	302	316	206	0.060	0.024	0.075	0.070	0.043	0.105	0.060	0.050
2020	1	88	86	118	142	237	278	292	196	0.058	0.023	0.068	0.074	0.039	0.110	0.064	0.049
2020	2	101	110	139	161	217	245	304	208	0.046	0.022	0.069	0.075	0.033	0.113	0.067	0.051
2020	3	71	101	155	172	262	299	309	229	0.051	0.021	0.065	0.073	0.040	0.109	0.055	0.048
2020	4	67	76	130	116	346	351	251	198	0.098	0.035	0.107	0.112	0.079	0.168	0.056	0.067
2020	5	79	90	97	125	616	635	211	127	0.100	0.068	0.079	0.064	0.104	0.097	0.047	0.062
2020	6	61	79	70	113	459	479	185	101	0.065	0.045	0.051	0.036	0.069	0.053	0.029	0.032
2020	7	66	78	80	110	392	403	169	100	0.063	0.054	0.044	0.040	0.060	0.061	0.033	0.036
2020	8	57	71	75	117	369	386	194	117	0.064	0.059	0.049	0.039	0.059	0.059	0.030	0.041
2020	9	64	81	79	109	374	392	182	107	0.063	0.052	0.056	0.049	0.062	0.073	0.041	0.042
2020	10	62	79	94	137	410	445	222	133	0.087	0.054	0.084	0.083	0.081	0.124	0.050	0.072
2020	11	72	82	114	138	261	307	313	200	0.057	0.022	0.087	0.069	0.046	0.104	0.047	0.044
2021	1	134	150	186	209	279	315	305	198	0.052	0.024	0.099	0.085	0.040	0.128	0.072	0.059
2021	2	131	156	193	193	235	258	307	221	0.048	0.022	0.077	0.082	0.035	0.123	0.069	0.056
2021	3	87	102	147	151	212	241	287	213	0.050	0.021	0.065	0.075	0.037	0.113	0.058	0.049
2021	4	69	83	126	133	280	294	272	207	0.078	0.024	0.086	0.087	0.055	0.130	0.048	0.051
2021	5	84	84	129	138	615	614	261	207	0.122	0.084	0.106	0.086	0.115	0.129	0.060	0.084
2021	6	76	92	94	122	463	472	186	112	0.084	0.059	0.043	0.043	0.068	0.065	0.036	0.036
2021	7	58	72	73	96	404	431	188	119	0.058	0.052	0.039	0.035	0.061	0.053	0.030	0.030
2021	8	56	68	67	98	383	404	200	106	0.056	0.051	0.045	0.035	0.061	0.053	0.030	0.033
2021	9	65	82	80	115	372	404	203	113	0.063	0.054	0.051	0.044	0.063	0.066	0.036	0.041
2021	10	52	75	86	131	390	422	255	147	0.077	0.056	0.081	0.061	0.073	0.091	0.042	0.059
2021	11	69	88	119	165	317	357	243	159	0.076	0.026	0.100	0.086	0.060	0.129	0.047	0.049
2021	12	287	246	222	228	290	307	303	188	0.070	0.030	0.129	0.093	0.042	0.139	0.092	0.067
2022	1	76	85	123	136	212	246	296	203	0.052	0.027	0.076	0.081	0.036	0.121	0.063	0.056
2022	2	79	84	123	136	197	224	288	205	0.048	0.025	0.072	0.076	0.035	0.114	0.057	0.054
2022	3	86	97	134	139	205	227	280	207	0.049	0.021	0.067	0.073	0.039	0.109	0.054	0.050
2022	4	100	96	151	126	360	369	252	202	0.089	0.032	0.098	0.112	0.078	0.168	0.065	0.064
2022	5	61	84	101	133	611	642	174	135	0.090	0.094	0.090	0.068	0.108	0.103	0.059	0.083
2022	6	76	89	90	114	383	394	174	98	0.071	0.053	0.037	0.040	0.057	0.060	0.034	0.033
2022	7	72	82	111	120	426	426	179	130	0.089	0.076	0.062	0.058	0.078	0.088	0.040	0.053
2022	8	70	80	112	115	401	412	195	134	0.086	0.068	0.063	0.064	0.077	0.095	0.043	0.054
2022	9	59	77	95	105	384	399	191	120	0.084	0.060	0.066	0.062	0.072	0.093	0.044	0.050
2022	10	76	94	104	134	399	436	232	139	0.071	0.056	0.089	0.080	0.079	0.119	0.059	0.068
2022	11	53	72	100	124	285	314	231	170	0.084	0.030	0.103	0.089	0.059	0.133	0.048	0.055
2022	12	61	79	122	139	218	265	282	180	0.046	0.028	0.071	0.079	0.037	0.118	0.052	0.056
2023	1	85	84	119	130	197	233	303	213	0.056	0.023	0.070	0.076	0.037	0.114	0.062	0.052
2023	2	79	94	138	151	210	242	309	223	0.048	0.024	0.075	0.077	0.037	0.116	0.056	0.055
2023	3	106	122	163	164	228	251	318	235	0.052	0.026	0.073	0.084	0.041	0.125	0.063	0.057
2023	4	87	109	173	163	409	412	315	250	0.101	0.037	0.107	0.123	0.087	0.185	0.063	0.073
2023	5	85	103	163	135	649	644	215	207	0.117	0.085	0.109	0.106	0.127	0.160	0.077	0.093
2023	6	67	94	85	133	562	592	249	129	0.075	0.052	0.045	0.046	0.086	0.068	0.041	0.037
2023	7	72	85	83	109	416	442	174	104	0.062	0.059	0.041	0.040	0.066	0.061	0.035	0.037
2023	8	66	82	85	119	367	390	191	110	0.061	0.058	0.045	0.045	0.060	0.067	0.037	0.041
2023	9	89	106	182	173	416	435	336	274	0.106	0.078	0.116	0.110	0.092	0.165	0.067	0.090
2023	10	84	102	130	153	409	453	356	230	0.068	0.049	0.091	0.083	0.081	0.124	0.061	0.067
2023	11	79	87	128	138	293	323	280	182	0.070	0.031	0.081	0.089	0.057	0.134	0.052	0.058
2023	12	76	96	149	161	256	296	307	219	0.062	0.032	0.076	0.092	0.045	0.137	0.063	0.061

B.5 Monthly Median Values of Non-symptomatic Sweet Chestnut Tree Samples (2017-2023)

Year	Month	Median Values of Bands [DN]								Median Values of Vegetation Indices [-]							
		BLU	GRN	RED	RE1	RE3	NIR	SW1	SW2	CCI	CIre	NDWI	NDVI	EVI	SAVI	GNDVI	NDVIre
2017	3	319	433	553	769	1227	1478	1792	1134	-0.119	0.060	-0.092	0.454	0.189	0.280	0.550	0.314
2017	4	330	504	478	840	1714	1947	1688	966	0.043	0.095	0.060	0.593	0.288	0.490	0.569	0.378
2017	5	236	522	267	884	3696	3966	1838	796	0.317	0.327	0.372	0.876	0.669	0.915	0.767	0.643
2017	6	249	502	312	834	3900	4229	1883	785	0.235	0.365	0.394	0.865	0.685	0.898	0.789	0.668
2017	7	224	448	264	755	3647	4013	1814	749	0.255	0.386	0.378	0.877	0.671	0.916	0.798	0.683
2017	8	230	432	274	717	3138	3484	1685	693	0.219	0.346	0.354	0.857	0.597	0.886	0.783	0.664
2017	9	205	388	249	693	2626	2961	1472	613	0.205	0.291	0.342	0.846	0.521	0.869	0.774	0.629
2017	10	265	430	348	754	2104	2453	1461	667	0.108	0.186	0.266	0.755	0.417	0.732	0.704	0.537
2017	11	240	363	428	723	1297	1590	1413	748	-0.084	0.081	0.071	0.579	0.231	0.468	0.635	0.382
2017	12	201	284	425	616	1021	1286	1450	845	-0.193	0.068	-0.041	0.514	0.177	0.370	0.643	0.359
2018	1	244	325	445	602	937	1135	1100	746	-0.151	0.056	0.016	0.437	0.145	0.256	0.554	0.309
2018	2	304	364	504	672	1034	1258	1508	953	-0.145	0.051	-0.088	0.426	0.158	0.239	0.549	0.303
2018	3	324	405	564	756	1159	1415	1757	1138	-0.155	0.051	-0.101	0.424	0.172	0.235	0.550	0.297
2018	4	344	517	590	887	1518	1784	1929	1199	-0.079	0.071	-0.044	0.500	0.227	0.350	0.551	0.335
2018	5	239	547	287	884	3471	3760	1770	779	0.304	0.295	0.365	0.858	0.628	0.887	0.744	0.620
2018	6	219	466	267	773	3840	4168	1805	743	0.261	0.394	0.400	0.878	0.687	0.917	0.799	0.685
2018	7	211	431	245	728	3686	4026	1814	741	0.263	0.411	0.381	0.886	0.675	0.929	0.808	0.696
2018	8	226	426	260	687	3235	3577	1668	667	0.236	0.374	0.365	0.865	0.614	0.897	0.787	0.680
2018	9	195	369	232	643	2718	3047	1504	614	0.227	0.328	0.344	0.862	0.537	0.893	0.786	0.655
2018	10	216	378	290	665	2089	2427	1400	610	0.133	0.217	0.274	0.791	0.421	0.786	0.735	0.572
2018	11	257	358	427	676	1119	1371	1544	924	-0.080	0.064	-0.059	0.516	0.189	0.374	0.580	0.336
2018	12	198	274	380	552	897	1127	1383	836	-0.164	0.062	-0.091	0.491	0.156	0.337	0.608	0.344
2019	1	193	267	376	537	873	1095	1401	880	-0.168	0.058	-0.126	0.475	0.150	0.312	0.595	0.332
2019	2	273	355	471	644	996	1216	1488	957	-0.134	0.051	-0.112	0.424	0.152	0.236	0.536	0.298
2019	3	311	408	549	750	1173	1426	1793	1159	-0.139	0.052	-0.120	0.429	0.175	0.243	0.541	0.301
2019	4	333	488	581	892	1554	1829	2025	1247	-0.079	0.072	-0.040	0.508	0.241	0.361	0.566	0.337
2019	5	166	459	219	829	3167	3432	1698	793	0.317	0.278	0.341	0.872	0.582	0.907	0.760	0.606
2019	6	251	494	303	794	3467	3760	1767	768	0.234	0.335	0.362	0.846	0.629	0.869	0.765	0.650
2019	7	234	445	284	717	3464	3767	1778	743	0.217	0.383	0.359	0.858	0.638	0.887	0.788	0.681
2019	8	210	384	241	638	3099	3412	1588	656	0.233	0.385	0.356	0.869	0.599	0.903	0.796	0.684
2019	9	208	379	246	641	2878	3196	1538	638	0.214	0.353	0.351	0.856	0.565	0.884	0.785	0.668
2019	10	214	352	264	603	2074	2359	1264	557	0.143	0.236	0.306	0.797	0.428	0.794	0.739	0.588
2019	11	255	372	327	675	1415	1647	1249	639	0.070	0.118	0.147	0.677	0.279	0.615	0.641	0.436
2019	12	231	287	370	526	858	1077	1263	770	-0.131	0.065	-0.072	0.482	0.153	0.323	0.582	0.346
2020	1	240	303	417	573	911	1126	1417	879	-0.147	0.059	-0.102	0.465	0.156	0.297	0.579	0.327
2020	2	299	382	507	670	1063	1285	1545	970	-0.124	0.056	-0.086	0.437	0.166	0.256	0.542	0.313
2020	3	325	421	567	754	1218	1473	1745	1111	-0.141	0.055	-0.086	0.430	0.184	0.245	0.546	0.307
2020	4	344	496	574	840	1423	1684	1854	1152	-0.077	0.069	-0.043	0.484	0.219	0.325	0.545	0.331
2020	5	233	517	263	861	3684	3959	1784	795	0.327	0.331	0.387	0.876	0.670	0.914	0.769	0.647
2020	6	229	488	286	816	3706	4022	1786	750	0.257	0.352	0.389	0.868	0.665	0.902	0.784	0.661
2020	7	222	442	262	745	3511	3851	1797	740	0.249	0.375	0.365	0.871	0.646	0.907	0.793	0.678
2020	8	196	392	233	684	3146	3503	1700	683	0.244	0.361	0.346	0.875	0.604	0.913	0.801	0.675
2020	9	213	388	253	657	2718	3052	1525	634	0.204	0.309	0.333	0.847	0.538	0.870	0.775	0.643
2020	10	197	361	291	678	1894	2214	1373	630	0.117	0.192	0.254	0.779	0.390	0.768	0.723	0.545
2020	11	236	328	417	624	1077	1354	1391	772	-0.112	0.074	0.002	0.534	0.191	0.400	0.612	0.371
2021	1	262	322	438	598	967	1185	1365	848	-0.139	0.058	-0.056	0.456	0.160	0.284	0.573	0.323
2021	2	304	430	556	721	1121	1331	1579	1000	-0.125	0.052	-0.080	0.412	0.156	0.218	0.517	0.295
2021	3	338	436	578	764	1192	1441	1788	1145	-0.133	0.052	-0.103	0.419	0.175	0.229	0.531	0.299
2021	4	319	466	582	846	1430	1702	1906	1191	-0.113	0.067	-0.054	0.490	0.219	0.335	0.571	0.332
2021	5	194	519	232	863	3762	4063	1800	801	0.371	0.333	0.380	0.893	0.676	0.939	0.773	0.645
2021	6	189	459	235	785	4082	4409	1828	759	0.315	0.418	0.412	0.898	0.724	0.946	0.811	0.697
2021	7	216	425	249	687	3593	3948	1734	701	0.259	0.424	0.390	0.882	0.669	0.922	0.806	0.702
2021	8	215	394	244	649	3163	3481	1612	657	0.235	0.383	0.367	0.868	0.607	0.902	0.797	0.683
2021	9	213	383	242	633	2739	3098	1442	587	0.224	0.342	0.362	0.857	0.551	0.886	0.783	0.664
2021	10	193	347	262	647	2028	2362	1342	597	0.142	0.219	0.283	0.806	0.418	0.808	0.748	0.575
2021	11	196	316	360	637	1185	1477	1326	696	-0.071	0.087	0.063	0.601	0.222	0.501	0.651	0.401
2021	12	209	278	380	545	911	1134	1325	790	-0.149	0.070	-0.068	0.511	0.161	0.366	0.612	0.358
2022	1	221	300	415	577	938	1167	1471	887	-0.158	0.064	-0.117	0.483	0.158	0.325	0.602	0.344
2022	2	285	363	483	649	1050	1290	1598	975	-0.139	0.060	-0.107	0.457	0.169	0.286	0.566	0.325
2022	3	379	478	621	814	1251	1508	1857	1169	-0.117	0.051	-0.096	0.414	0.181	0.221	0.519	0.295
2022	4	359	530	604	914	1556	1838	1956	1200	-0.072	0.072	-0.025	0.497	0.239	0.345	0.557	0.338
2022	5	240	562	262	921	3845	4110	1884	837	0.360	0.311	0.379	0.878	0.685	0.917	0.757	0.626
2022	6	236	495	281	819	4012	4325	1876	788	0.270	0.395	0.398	0.878	0.710	0.917	0.794	0.684
2022	7	223	446	256	751	3790	4146	1894	776	0.270	0.409	0.378	0.884	0.693	0.926	0.806	0.695
2022	8	239	448	275	756	3386	3732	1764	725	0.240	0.351	0.368	0.865	0.634	0.897	0.787	0.664
2022	9	183	366	220	669	2810	3149	1528	636	0.246	0.334	0.358	0.873	0.558	0.909	0.794	0.657
2022	10	240	398	308	695	2127	2460	1370	604	0.139	0.209	0.286	0.781	0.433	0.771	0.720	0.562
2022	11	187	320	351	656	1226	1499	1282	659	-0.049	0.090	0.076	0.625	0.228	0.537	0.649	0.394
2022	12	221	298	434	596	951	1226	1428	850	-0.158	0.060	-0.070	0.485	0.166	0.327	0.608	0.348
2023	1	292	351	465	637	969	1196	1513	930	-0.134	0.051	-0.123	0.429	0.151	0.243	0.545	0.305
2023	2	295	367	486	653	1019	1246	1572	975	-0.131	0.054	-0.104	0.438	0.159	0.256	0.545	0.313
2023	3	332	417	567	749	1171	1436	1812	1132	-0.139	0.052	-0.103	0.430	0.177	0.245	0.549	0.307
2023	4	312	468	526	857	1521	1786	1893	1136	-0.074	0.081	-0.027	0.537	0.238	0.405	0.588	0.359
2023	5	251	581	291	952	3994	4280	1841	822	0.330	0.332	0.392	0.874	0.705	0.911	0.766	0.643
2023	6	247	525	301	846	3966	4292	1821	745	0.269	0.362	0.415	0.870	0.702	0.905	0.782	0.667
2023	7	224	447	256	739	3799	4180	1831	738	0.267	0.418	0.395	0.885	0.697	0.928	0.808	0.700
2023	8	233	432	273	723	3207	3598	1661	672	0.221	0.349	0.372	0.859	0.613	0.888	0.784	0.669
2023	9	245	417	311	718	2347	2731	1657	731	0.134	0.259	0.264	0.806	0.470	0.809	0.748	0.610
2023	10	279	437	360	738	2035	2378	1588	727	0.098	0.188	0.220	0.740	0.405	0.710	0.691	0.545
2023	11	259	380	413	710	1329	1614	1551	855	-0.032	0.099	0.044	0.620	0.247	0.529	0.633	0.410
2023	12	199	316	414	626	1044	1308	1485	870	-0.143	0.068	-0.048	0.533	0.181	0.398	0.620	0.360

B.6 Monthly Median Values of Symptomatic Sweet Chestnut Tree Samples (2017-2023)

Year	Month	Median Values of Bands [DN]								Median Values of Vegetation Indices [-]							
		BLU	GRN	RED	RE1	RE3	NIR	SW1	SW2	CCI	CIre	NDWI	NDVI	EVI	SAVI	GNDVI	NDVIre
2017	3	348	470	607	807	1254	1499	1825	1152	-0.119	0.054	-0.102	0.416	0.177	0.224	0.523	0.299
2017	4	358	529	543	864	1667	1923	1791	1063	-0.003	0.081	0.011	0.539	0.270	0.409	0.554	0.356
2017	5	252	532	304	893	3358	3630	1907	862	0.251	0.286	0.322	0.845	0.612	0.868	0.748	0.612
2017	6	278	521	348	873	3699	4010	1950	857	0.200	0.320	0.347	0.841	0.650	0.862	0.770	0.640
2017	7	244	466	295	796	3459	3783	1888	816	0.215	0.332	0.336	0.853	0.628	0.879	0.779	0.652
2017	8	253	446	307	745	2932	3270	1748	763	0.182	0.303	0.312	0.830	0.557	0.845	0.762	0.635
2017	9	231	403	292	723	2510	2834	1542	679	0.160	0.248	0.303	0.814	0.492	0.821	0.752	0.594
2017	10	280	436	386	770	1976	2335	1530	732	0.065	0.162	0.219	0.717	0.390	0.676	0.684	0.508
2017	11	268	385	479	745	1290	1593	1479	824	-0.114	0.071	0.022	0.537	0.218	0.405	0.614	0.362
2017	12	228	320	474	649	1062	1355	1496	882	-0.197	0.060	-0.069	0.472	0.172	0.308	0.616	0.337
2018	1	299	379	509	643	943	1156	1293	835	-0.147	0.048	-0.008	0.403	0.136	0.204	0.517	0.299
2018	2	343	406	557	708	1062	1286	1562	987	-0.152	0.046	-0.107	0.384	0.149	0.176	0.514	0.279
2018	3	357	445	623	789	1188	1443	1781	1155	-0.161	0.048	-0.111	0.390	0.162	0.184	0.522	0.284
2018	4	375	546	656	918	1495	1775	1997	1243	-0.103	0.062	-0.071	0.455	0.209	0.283	0.530	0.319
2018	5	255	549	329	922	3201	3479	1860	857	0.244	0.262	0.315	0.827	0.584	0.841	0.729	0.593
2018	6	228	468	282	789	3575	3901	1877	813	0.235	0.361	0.360	0.864	0.646	0.895	0.787	0.667
2018	7	233	453	279	766	3435	3778	1881	803	0.227	0.354	0.341	0.862	0.633	0.893	0.788	0.665
2018	8	248	445	297	728	2988	3310	1717	734	0.195	0.314	0.324	0.835	0.567	0.852	0.764	0.642
2018	9	215	383	266	676	2552	2868	1581	682	0.176	0.283	0.293	0.831	0.501	0.847	0.764	0.624
2018	10	236	388	331	708	1993	2326	1495	681	0.083	0.181	0.227	0.748	0.398	0.722	0.714	0.533
2018	11	260	359	430	671	1152	1388	1547	873	-0.091	0.073	-0.047	0.530	0.201	0.396	0.591	0.354
2018	12	227	311	433	589	945	1181	1446	874	-0.165	0.057	-0.113	0.457	0.155	0.286	0.586	0.329
2019	1	224	310	445	593	924	1152	1488	930	-0.173	0.053	-0.143	0.440	0.148	0.260	0.576	0.317
2019	2	310	402	542	696	1051	1276	1605	1013	-0.149	0.046	-0.133	0.393	0.147	0.190	0.516	0.283
2019	3	353	458	620	809	1233	1489	1885	1203	-0.149	0.049	-0.129	0.405	0.170	0.207	0.523	0.289
2019	4	368	531	656	941	1548	1842	2070	1264	-0.100	0.065	-0.061	0.475	0.226	0.312	0.556	0.324
2019	5	216	495	286	895	2939	3209	1841	920	0.234	0.235	0.280	0.837	0.541	0.856	0.733	0.572
2019	6	274	514	333	829	3280	3574	1867	850	0.201	0.295	0.321	0.825	0.597	0.837	0.746	0.624
2019	7	264	471	323	756	3259	3593	1869	818	0.186	0.326	0.317	0.833	0.602	0.850	0.766	0.648
2019	8	231	408	270	673	2914	3239	1682	727	0.198	0.326	0.316	0.841	0.563	0.862	0.771	0.651
2019	9	233	409	287	687	2723	3047	1635	720	0.176	0.294	0.305	0.827	0.529	0.840	0.762	0.629
2019	10	239	382	306	661	2045	2336	1376	631	0.116	0.210	0.272	0.768	0.414	0.752	0.716	0.560
2019	11	274	383	366	686	1414	1656	1361	710	0.026	0.107	0.120	0.650	0.271	0.575	0.623	0.421
2019	12	251	318	424	565	902	1135	1383	834	-0.144	0.058	-0.101	0.463	0.150	0.295	0.571	0.335
2020	1	256	331	460	608	966	1197	1525	938	-0.157	0.055	-0.127	0.443	0.152	0.264	0.569	0.316
2020	2	324	413	547	713	1100	1317	1618	1004	-0.135	0.051	-0.107	0.407	0.158	0.210	0.518	0.295
2020	3	354	460	624	804	1241	1503	1858	1183	-0.151	0.051	-0.109	0.403	0.171	0.204	0.523	0.296
2020	4	376	526	635	877	1457	1719	1935	1191	-0.093	0.062	-0.072	0.451	0.205	0.277	0.526	0.317
2020	5	247	529	301	889	3414	3692	1874	882	0.275	0.293	0.339	0.854	0.621	0.880	0.749	0.617
2020	6	254	495	312	833	3486	3792	1879	833	0.224	0.313	0.345	0.848	0.632	0.871	0.768	0.637
2020	7	248	460	302	764	3274	3612	1864	817	0.200	0.319	0.324	0.842	0.604	0.863	0.773	0.646
2020	8	228	416	282	717	2874	3236	1773	772	0.187	0.297	0.296	0.838	0.554	0.856	0.770	0.634
2020	9	244	411	302	696	2494	2825	1618	720	0.148	0.255	0.280	0.806	0.491	0.808	0.748	0.602
2020	10	232	375	349	705	1765	2087	1480	719	0.047	0.154	0.179	0.718	0.353	0.678	0.694	0.500
2020	11	267	370	469	679	1140	1436	1524	857	-0.121	0.067	-0.027	0.505	0.193	0.357	0.590	0.355
2021	1	304	381	517	659	1021	1243	1456	902	-0.146	0.051	-0.086	0.417	0.154	0.225	0.533	0.300
2021	2	347	466	604	771	1175	1404	1655	1059	-0.128	0.047	-0.094	0.380	0.151	0.171	0.491	0.280
2021	3	374	477	642	825	1238	1500	1884	1204	-0.140	0.048	-0.126	0.391	0.166	0.186	0.509	0.283
2021	4	359	508	644	900	1455	1740	1991	1230	-0.120	0.061	-0.085	0.457	0.207	0.285	0.548	0.317
2021	5	238	535	293	900	3262	3576	1959	922	0.275	0.270	0.312	0.853	0.596	0.880	0.743	0.604
2021	6	223	484	278	826	3810	4132	1958	872	0.256	0.358	0.364	0.871	0.680	0.906	0.787	0.665
2021	7	248	460	295	746	3429	3782	1875	807	0.212	0.357	0.342	0.851	0.630	0.877	0.781	0.668
2021	8	239	415	278	692	2958	3280	1708	733	0.196	0.318	0.321	0.841	0.566	0.861	0.773	0.646
2021	9	242	403	285	676	2594	2937	1580	677	0.174	0.278	0.305	0.823	0.516	0.834	0.758	0.622
2021	10	221	362	310	684	1938	2275	1451	675	0.087	0.188	0.225	0.760	0.393	0.739	0.721	0.541
2021	11	234	345	419	680	1222	1510	1463	810	-0.092	0.079	0.028	0.572	0.222	0.458	0.630	0.380
2021	12	241	318	437	593	978	1225	1467	885	-0.158	0.061	-0.093	0.477	0.162	0.316	0.595	0.340
2022	1	263	344	477	631	994	1242	1586	975	-0.163	0.056	-0.136	0.449	0.156	0.273	0.570	0.321
2022	2	321	404	550	719	1115	1371	1731	1069	-0.149	0.051	-0.137	0.422	0.164	0.233	0.539	0.305
2022	3	409	518	681	858	1292	1564	1983	1264	-0.132	0.047	-0.128	0.384	0.172	0.175	0.497	0.281
2022	4	409	579	681	963	1616	1897	2062	1268	-0.086	0.064	-0.044	0.458	0.232	0.287	0.530	0.318
2022	5	277	585	323	955	3579	3891	2031	932	0.270	0.276	0.323	0.846	0.651	0.869	0.741	0.602
2022	6	269	520	320	839	3773	4111	1956	869	0.227	0.350	0.356	0.850	0.672	0.875	0.772	0.660
2022	7	264	486	311	810	3545	3908	2008	880	0.214	0.343	0.330	0.854	0.652	0.881	0.780	0.659
2022	8	272	477	329	810	3188	3536	1866	823	0.182	0.292	0.315	0.831	0.598	0.846	0.763	0.627
2022	9	215	395	276	719	2650	2985	1644	724	0.176	0.272	0.298	0.833	0.518	0.849	0.768	0.616
2022	10	278	434	369	755	2025	2374	1547	720	0.072	0.171	0.213	0.726	0.396	0.688	0.692	0.522
2022	11	236	366	430	718	1279	1562	1475	795	-0.088	0.080	0.031	0.573	0.227	0.460	0.627	0.375
2022	12	278	352	485	637	1027	1301	1522	914	-0.159	0.060	-0.062	0.468	0.176	0.301	0.583	0.338
2023	1	317	388	527	676	1031	1277	1646	1032	-0.147	0.049	-0.145	0.405	0.151	0.208	0.526	0.296
2023	2	339	425	567	723	1108	1356	1761	1105	-0.140	0.048	-0.129	0.399	0.157	0.199	0.518	0.290
2023	3	366	462	621	799	1240	1511	1936	1222	-0.148	0.049	-0.129	0.399	0.174	0.198	0.524	0.294
2023	4	374	530	629	911	1593	1860	2038	1238	-0.095	0.068	-0.055	0.481	0.226	0.321	0.551	0.326
2023	5	302	617	370	997	3549	3826	2018	952	0.244	0.272	0.315	0.826	0.632	0.839	0.732	0.603
2023	6	274	556	329	912	3837	4160	1949	864	0.242	0.326	0.365	0.851	0.677	0.876	0.766	0.645
2023	7	266	490	317	807	3632	4007	1945	844	0.212	0.351	0.348	0.852	0.661	0.879	0.782	0.666
2023	8	268	463	319	778	3082	3454	1762	758	0.180	0.296	0.325	0.829	0.584	0.843	0.763	0.633
2023	9	265	436	348	759	2337	2718	1715	811	0.091	0.212	0.219	0.771	0.454	0.756	0.728	0.565
2023	10	303	461	405	777	1987	2348	1685	803	0.059	0.162	0.174	0.705	0.388	0.657	0.674	0.513
2023	11	299	430	478	775	1437	1744	1691	952	-0.064	0.088	0.011	0.569	0.251	0.453	0.610	0.385
2023	12	238	357	472	679	1138	1408	1620	988	-0.145	0.064	-0.075	0.486	0.183	0.329	0.596	0.348